

JSCSEN 86(6)547–624(2021)

ISSN 1820-7421(Online)

Journal of the Serbian Chemical Society

Electronic
version

VOLUME 86

No 6

BELGRADE 2021

Available on line at



www.shd.org.rs/JSCS/

The full search of JSCS
is available through

DOAJ DIRECTORY OF
OPEN ACCESS
JOURNALS
www.doaj.org



CONTENTS*

Organic Chemistry

- A. Berjis, B. Mirza and H. Anaraki-Ardakani: Green and efficient synthesis of new β -amido-aryl carbonyl derivatives catalyzed by choline chloride/urea as a deep eutectic solvent 547

Biochemistry and Biotechnology

- M. R. Pantović Pavlović, M. M. Pavlović, J. N. Kovačina, B. P. Stanojević, J. S. Stevanović, V. V. Panić and N. L. Ignjatović: Cytotoxicity of amorphous calcium phosphate multifunctional composite coatings on titanium obtained by *in situ* anodization/anaphoretic deposition (Note)..... 555

Theoretical Chemistry

- S. Erić, I. Cvijetić and M. Zloh: 3D-QSAR study of adenosine 5'-phosphosulfate (APS) analogues as ligands for APS reductase 561

Physical Chemistry

- R. N. Sahoo, B. S. Satapathy and S. Mallick: Improved dissolution of ibuprofen after crystallization from polymeric solution: Correlation with crystal parameter 571

Electrochemistry

- B. M. Šmit, P. B. Stanić, Lj. G. Joksović, D. P. Ašanin and Z. Simić: Influence of electrochemical conditions on the regio- and stereoselectivity of selenocyclization of alkenyl hydantoin (Short communication) 585

Polymers

- M. S. Shakir, M. K. Khosa, K. M. Zia, M. J. Saif and T. H. Bokhari: Investigation of the thermal, mechanical and biological properties of PVC/ABS blends loaded with cobalt chloride for biomedical and electronics applications 591

Chemical Engineering

- T. Gagić, Ž. Knez and M. Škerget: Subcritical water extraction of horse chestnut (*Aesculus hippocastanum*) tree parts 603

Environmental

- T. H. Pham, V. B. Bui and H. A. Q. Than: CO oxidation over alumina monolith impregnated with oxides of copper and manganese 615

Published by the Serbian Chemical Society
Karnegijeva 4/III, P.O. Box 36, 11120 Belgrade, Serbia
Printed by the Faculty of Technology and Metallurgy
Karnegijeva 4, P.O. Box 35-03, 11120 Belgrade, Serbia

* For colored figures in this issue please see electronic version at the Journal Home Page:
<http://www.shd.org.rs/JSCS/>

The **Journal of the Serbian Chemical Society** (formerly Glasnik Hemijskog društva Beograd), one volume (12 issues) per year, publishes articles from the fields of chemistry. The **Journal** is financially supported by the **Ministry of Education, Science and Technological Development of the Republic of Serbia**.

Articles published in the **Journal** are indexed in **Clarivate Analytics products: Science Citation Index-Expanded™** – accessed via **Web of Science®** and **Journal Citation Reports®**.

Impact Factor announced 2020: **1.097**; **5-year Impact Factor**: **1.023**.

Articles appearing in the **Journal** are also abstracted by: **Scopus**, **Chemical Abstracts Plus (CAplusSM)**, **Directory of Open Access Journals**, **Referativnii Zhurnal (VINITI)**, **RSC Analytical Abstracts**, **EuroPub**, **Pro Quest** and **Asian Digital Library**.

Publisher:

Serbian Chemical Society, Karnegijeva 4/III, P. O. Box 36, 1120 Belgrade 35, Serbia
tel./fax: +381-11-3370-467, E-mails: **Society** – shd@shd.org.rs; **Journal** – jscs@shd.org.rs
Home Pages: **Society** – <http://www.shd.org.rs/>; **Journal** – <http://www.shd.org.rs/JSCS/>
Contents, Abstracts and full papers (from Vol 64, No. 1, 1999) are available in the electronic form at the Web Site of the **Journal** (<http://www.shd.org.rs/JSCS/>).

Internet Service:

Former Editors:

Nikola A. Pušin (1930–1947), **Aleksandar M. Leko** (1948–1954),
Panta S. Tutundžić (1955–1961), **Miloš K. Mladenović** (1962–1964),
Đorđe M. Dimitrijević (1965–1969), **Aleksandar R. Despić** (1969–1975),
Slobodan V. Ribnikar (1975–1985), **Dragutin M. Dražić** (1986–2006).

Editor-in-Chief:

BRANISLAV Ž. NIKOLIĆ, Serbian Chemical Society (E-mail: jscs-ed@shd.org.rs)

Deputy Editor:

DUŠAN SLADIĆ, Faculty of Chemistry, University of Belgrade

Sub editors:

Organic Chemistry

DEJAN OPSENICA, Institute of Chemistry, Technology and Metallurgy, University of Belgrade

Biochemistry and Biotechnology

JANOS CSANÁDI, Faculty of Science, University of Novi Sad

Inorganic Chemistry

OLGICA NEDIĆ, INEP – Institute for the Application of Nuclear Energy, University of Belgrade

Theoretical Chemistry

MILOŠ ĐURAN, Serbian Chemical Society

Physical Chemistry

IVAN JURANIĆ, Serbian Chemical Society

Electrochemistry

LJILJANA DAMJANOVIĆ-VASILJIĆ, Faculty of Physical Chemistry, University of Belgrade

Analytical Chemistry

SNEŽANA GOJKOVIĆ, Faculty of Technology and Metallurgy, University of Belgrade

Polymers

SLAVICA RAŽIĆ, Faculty of Pharmacy, University of Belgrade

Thermodynamics

BRANKO DUNJIĆ, Faculty of Technology and Metallurgy, University of Belgrade

Chemical Engineering

MIRJANA KIJEVCANIN, Faculty of Technology and Metallurgy, University of Belgrade

Materials

TATJANA KALUĐEROVIĆ RADOIČIĆ, Faculty of Technology and Metallurgy, University of Belgrade

Metallic Materials and Metallurgy

RADA PETROVIĆ, Faculty of Technology and Metallurgy, University of Belgrade

Environmental and Geochemistry

NENAD RADOVIĆ, Faculty of Technology and Metallurgy, University of Belgrade

History of and Education in Chemistry

VESNA ANTIĆ, Faculty of Agriculture, University of Belgrade

English Language

DRAGICA TRIVIĆ, Faculty of Chemistry, University of Belgrade

Editors:

LYNNE KATSIKAS, Serbian Chemical Society

VLATKA VAJS, Serbian Chemical Society

JASMINA NIKOLIĆ, Faculty of Technology and Metallurgy, University of Belgrade

Technical Editors:

VLADIMIR PANIĆ, ALEKSANDAR DEKANSKI, VUK FILIPOVIĆ, Institute of Chemistry, Technology and Metallurgy, University of Belgrade

ALEKSANDAR DEKANSKI, Institute of Chemistry, Technology and Metallurgy, University of Belgrade

Journal Manager & Web Master:

VERA ČUŠIĆ, Serbian Chemical Society

Office:

VERA ČUŠIĆ, Serbian Chemical Society

Editorial Board

From abroad: **R. Adžić**, Brookhaven National Laboratory (USA); **A. Casini**, University of Groningen (The Netherlands); **G. Cobb**, Baylor University (USA); **D. Douglas**, University of British Columbia (Canada); **G. Inzelt**, Etvos Lorand University (Hungary); **N. Katsaros**, NCSR “Demokritos”, Institute of Physical Chemistry (Greece); **J. Kenny**, University of Perugia (Italy); **Ya. I. Korenman**, Voronezh Academy of Technology (Russian Federation); **M. D. Lechner**, University of Osnabrueck (Germany); **S. Macura**, Mayo Clinic (USA); **M. Spiteller**, INFU, Technical University Dortmund (Germany); **M. Stratakis**, University of Crete (Greece); **M. Swart**, University de Girona (Cataluna, Spain); **G. Vunjak-Novaković**, Columbia University (USA); **P. Worsfold**, University of Plymouth (UK); **J. Zagal**, Universidad de Santiago de Chile (Chile).

From Serbia: **B. Abramović**, **V. Antić**, **V. Bešković**, **J. Csanádi**, **Lj. Damjanović-Vasiljić**, **A. Dekanski**, **V. Dondur**, **B. Dunjić**, **M. Đuran**, **S. Gojković**, **I. Gutman**, **B. Jovančičević**, **I. Juranić**, **L. Katsikas**, **M. Kijevcanin**, **V. Leovac**, **S. Milonjić**, **V.B. Mišković-Stanković**, **O. Nedić**, **B. Nikolić**, **J. Nikolić**, **D. Opsenica**, **V. Panić**, **M. Petkovska**, **R. Petrović**, **I. Popović**, **B. Radak**, **T. Kaluderović Radiočić**, **N. Radović**, **S. Ražić**, **D. Sladić**, **S. Sovilj**, **S. Šerbanović**, **B. Šolaja**, **Ž. Tešić**, **D. Trivić**, **V. Vajs**.

Subscription: The annual subscription rate is **150.00 €** including postage (surface mail) and handling. For Society members from abroad rate is **50.00 €**. For the proforma invoice with the instruction for bank payment contact the Society Office (E-mail: shd@shd.org.rs) or see JSCS Web Site: <http://www.shd.org.rs/JSCS/>, option Subscription.

Godišnja pretplata: Za članove SHD: **2.500,00 RSD**, za penzionere i studente: **1000,00 RSD**, a za ostale: **3.500,00 RSD**; za organizacije i ustanove: **16.000,00 RSD**. Uplate se vrše na tekući račun Društva: **205-13815-62**, poziv na broj **320**, sa naznakom “pretplata za JSCS”.

Nota: Radovi čiji su svi autori članovi SHD prioritarno se publikuju.

Odlukom Odbora za hemiju Republičkog fonda za nauku Srbije, br. 66788/1 od 22.11.1990. godine, koja je kasnije potvrđena odlukom Saveta Fonda, časopis je uvršten u kategoriju međunarodnih časopisa (**M-23**). Takođe, aktom Ministarstva za nauku i tehnologiju Republike Srbije, 413-00-247/2000-01 od 15.06.2000. godine, ovaj časopis je proglašen za publikaciju od posebnog interesa za nauku. **Impact Factor** časopisa objavljen 2020. godine iznosi **1,097**, a petogodišnji **Impact Factor 1,023**.

INSTRUCTIONS FOR AUTHORS (2021)

GENERAL

The *Journal of the Serbian Chemical Society* (the *Journal* in further text) is an international journal publishing papers from all fields of chemistry and related disciplines. Twelve issues are published annually. The Editorial Board expects the editors, reviewers, and authors to respect the well-known standard of professional ethics.

Types of Contributions

Original scientific papers	(up to 15 typewritten pages, including Figures, Tables and References) report original research which must not have been previously published.
Short communications	(up to 8 pages) report unpublished preliminary results of sufficient importance to merit rapid publication.
Notes	(up to 5 pages) report unpublished results of short, but complete, original research
Authors' reviews	(up to 40 pages) present an overview of the author's current research with comparison to data of other scientists working in the field
Reviews ^a	(up to 40 pages) present a concise and critical survey of a specific research area. Generally, these are prepared at the invitation of the Editor
Surveys	(about 25 pages) communicate a short review of a specific research area.
Book and Web site reviews	(1 - 2 pages)
Extended abstracts	(about 4 pages) of Lectures given at meetings of the Serbian Chemical Society Divisions
Letters to the Editor	report miscellaneous topics directed directly to the Editor

^aGenerally, Authors' reviews, Reviews and Surveys are prepared at the invitation of the Editor.

Submission of manuscripts

Manuscripts should be submitted using the **OnLine Submission Form**, available on the JSCS Web Site (<http://www.shd-pub.org.rs/index.php/JSCS>). The manuscript must be uploaded as a Word.doc or .rtf file, with tables and figures (including the corresponding captions – above Tables and below Figures), placed within the text to follow the paragraph in which they were mentioned for the first time.

Please note that **Full Names** (First Name, Last Name), **Full Affiliation** and **Country** (from drop down menu) of **ALL OF AUTHORS** (written in accordance with English spelling rules - the first letter capitalized) must be entered in the manuscript Submission Form (Step 3). Manuscript Title, authors' names and affiliations, as well as the Abstract, **WILL APPEAR** in the article listing, as well as in **BIBLIOGRAPHIC DATABASES (WoS, SCOPUS...)**, in the form and in the order entered in the author details

Graphical abstract

Graphical abstract is a one-image file containing the main depiction of the authors work and/or conclusion and must be supplied along with the manuscript. It must enable readers to quickly gain the main message of the paper and to encourage browsing, help readers identify which papers are most relevant to their research interests. Authors must provide an image that clearly represents the research described in the paper. The most relevant figure from the work, which summarizes the content, can also be submitted. The image should be submitted as a separate file in **Online Submission Form - Step 2**.

Specifications: The graphical abstract should have a clear start and end, reading from top to bottom or left to right. Please omit unnecessary distractions as much as possible.

- **Image size:** minimum of 500×800 pixels (W×H) and a minimum resolution of 300 dpi. If a larger image is sent, then please use the same ratio: 16 wide × 9 high. Please note that your image will be scaled proportionally to fit in the available window in TOC; a 150×240 pixel rectangle. Please be sure that the quality of an image cannot be increased by changing the resolution from lower to higher, but only by rescanning or exporting the image with a higher resolution, which can be set in usual "settings" option.
- **Font:** Please use Calibri and Symbol font with a large enough font size, so it is readable even from the image of a smaller size (150 × 240 px) in TOC.
- **File type:** JPG and PNG only.

No additional text, outline or synopsis should be included. Please do not use white space or any heading within the image.

Cover Letter

Manuscripts must be accompanied by a cover letter (strictly uploaded in **Online Submission Step 2**) in which the type of the submitted manuscript and a warranty as given below are given. The Author(s) has(have) to warranty that the manuscript submitted to the *Journal* for review is original, has been written by the stated author(s) and has not been published elsewhere; is currently not being considered for publication by any other journal and will not be submitted for such a review while under review by the *Journal*; the manuscript contains no libellous or other unlawful statements and does not contain any materials that violate any personal or proprietary rights of any other person or entity. All manuscripts will be acknowledged on receipt (by e-mail).

Illustrations

Illustrations (Figs, schemes, photos...) in TIF or EPS format (JPG format is acceptable for colour and greyscale photos, only), must be additionally uploaded (Online Submission Step 2) as a separate file or one archived (.zip, .rar or .arj) file. Figures and/or Schemes should be prepared according to the **Artwork Instructions** - http://www.shd.org.rs/JSCS/jscs-pdf/Artwork_Instructions.pdf!

For any difficulties and questions related to **OnLine Submission Form** - <https://www.shd-pub.org.rs/index.php/JSCS/submission/wizard>, please refer to **User Guide** - <https://openjournal-systems.com/ojs-3-user-guide/>, Chapter **Submitting an Article** - <https://openjournal-systems.com/ojs-3-user-guide/submitting-an-article/>. If difficulties still persist, please contact JSCS Editorial Office at JSCS@shd.org.rs

A manuscript not prepared according to these instructions will be returned for resubmission without being assigned a reference number.

Conflict-of-Interest Statement*: Public trust in the peer review process and the credibility of published articles depend in part on how well a conflict of interest is handled during writing, peer review, and editorial decision making. A conflict of interest exists when an author (or the author's institution), reviewer, or editor has financial or personal relationships that inappropriately influence (bias) his or her actions (such relationships are also known as dual commitments, competing interests, or competing loyalties). These relationships vary from those with negligible potential to those with great potential to influence judgment, and not all relationships represent true conflict of interest. The potential for a conflict of interest can exist whether or not an individual believes that the relationship affects his or her scientific judgment. Financial relationships (such as employment, consultancies, stock ownership, honoraria, paid expert testimony) are the most easily identifiable conflicts of interest and the most likely to undermine the credibility of the journal, the authors, and of science itself. However, conflicts can occur for other reasons, such as personal relationships, academic competition, and intellectual passion.

Informed Consent Statement*: Patients have a right to privacy that should not be infringed without informed consent. Identifying information, including patients' names, initials, or hospital numbers, should not be published in written descriptions, photographs, and pedigrees unless the information is essential for scientific purposes and the patient (or parent or guardian) gives written informed consent for publication. Informed consent for this purpose requires that a patient who is identifiable be shown the manuscript to be published. Authors should identify Individuals who provide writing assistance and disclose the funding source for this assistance. Identifying details should be omitted if they are not essential. Complete anonymity is difficult to achieve, however, and informed consent should be obtained if there is any doubt. For example, masking the eye region in photographs of patients is inadequate protection of anonymity. If identifying characteristics are altered to protect anonymity, such as in genetic pedigrees, authors should provide assurance that alterations do not distort scientific meaning and editors should so note. The requirement for informed consent should be included in the journal's instructions for authors. When informed consent has been obtained it should be indicated in the published article.

Human and Animal Rights Statement* When reporting experiments on human subjects, authors should indicate whether the procedures followed were in accordance with the ethical standards of the responsible committee on human experimentation (institutional and national) and with the Helsinki Declaration of 1975, as revised in 2000 (5). If doubt exists whether the research was conducted in accordance with the Helsinki Declaration, the authors must explain the rationale for their approach, and demonstrate that the institutional review body explicitly approved the doubtful aspects of the study. When reporting experiments on animals, authors should be asked to indicate whether the institutional and national guide for the care and use of laboratory animals was followed.

*International Committee of Medical Journal Editors ("Uniform Requirements for Manuscripts Submitted to Biomedical Journals"), February 2006

PROCEDURE

All contributions will be peer reviewed and only those deemed worthy and suitable will be accepted for publication. The Editor has the final decision. To facilitate the reviewing process, authors are encouraged to suggest up to three persons competent to review their manuscript. Such suggestions will be taken into consideration but not always accepted. If authors would prefer a specific person not be a reviewer, this should be announced. The Cover Letter must be accompanied by these suggestions. Manuscripts requiring revision should be returned according to the requirement of the Editor, within 60 days upon reception of the reviewing comments by e-mail.

The *Journal* maintains its policy and takes the liberty of correcting the English as well as false content of manuscripts **provisionally accepted** for publication in the first stage of reviewing process. In this second stage of manuscript preparation by JSCS Editorial Office, the author(s) may be required to supply some **additional clarifications and corrections**. This procedure will be executed during copyediting actions, with a demand to author(s) to perform corrections of unclear parts before the manuscript would be published OnLine as **finally accepted manuscript (OLF Section of the JSCS website)**. Please note that the manuscript can receive the status of **final rejection** if the author's corrections would not be satisfactory.

When finally accepted manuscript is ready for printing, the corresponding author will receive a request for proof reading, which should be performed within 2 days. Failure to do so will be taken as the authors agree with any alteration which may have occurred during the preparation of the manuscript for printing.

Accepted manuscripts of active members of the Serbian Chemical Society (all authors) have publishing priority.

MANUSCRIPT PRESENTATION

Manuscripts should be typed in English (either standard British or American English, but consistent throughout) with 1.5 spacing (12 points Times New Roman; Greek letters in the character font Symbol) in A4 format leaving 2.5 cm for margins. For Regional specific, non-standard characters that may appear in the text, save documents with Embed fonts Word option: *Save as -> (Tools) -> Save Options... -> Embed fonts in the text.*

The authors are requested to seek the assistance of competent English language expert, if necessary, to ensure their English is of a reasonable standard. The Serbian Chemical Society can provide this service in advance of submission of the manuscript. If this service is required, please contact the office of the Society by e-mail (jscs-info@shd.org.rs).

Tables, figures and/or schemes must be embedded in the main text of the manuscript and should follow the paragraph in which they are mentioned for the first time. **Tables** must be prepared with the aid of the **WORD table function**, without vertical lines. The minimum size of the font in the tables should be **10 pt**. Table columns must not be formatted using multiple spaces. Table rows must not be formatted using any returns (enter key; ↵ key) and are **limited to 12 cm width**. Tables should not be incorporated as graphical objects. **Footnotes to Tables** should follow them and are to be indicated consequently (in a single line) in superscript letters and separated by semi-column.

Table caption must be placed above corresponding Table, while **Captions of the Illustrations** (Figs. Schemes...) must follow the corresponding item. **The captions, either for Tables or Illustrations**, should make the items comprehensible without reading of the main text (but clearly referenced in), must follow numerical order (Roman for Tables, Arabic for Illustrations), and should not be provided on separate sheets or as separate files.

High resolution Illustrations (named as Fig. 1, Fig. 2... and/or Scheme 1, Scheme 2...) in **TIF or EPS format** (JPG format is acceptable for photos, only) **must be additionally uploaded as a separate files or one archived (.zip, .rar) file.**

Illustrations should be prepared according to the [ARTWORK INSTRUCTIONS](http://www.shd.org.rs/JSCS/jscs-pdf/Artwork_Instructions.pdf) - http://www.shd.org.rs/JSCS/jscs-pdf/Artwork_Instructions.pdf. !

All pages of the manuscript must be numbered continuously.

DESIGNATION OF PHYSICAL QUANTITIES AND UNITS

IUPAC recommendations for the naming of compounds should be followed. SI units, or other permissible units, should be employed. The designation of physical quantities must be in italic throughout the text (including figures, tables and equations), whereas the units and indexes (except for indexes having the meaning of physical quantities) are in upright letters. They should be in Times New Roman font. In graphs and tables, a slash should be used to separate the designation of a physical quantity from the unit

(example: p / kPa, j / mA cm², t / °C, T_0 / K, τ / h, $\ln(j$ / mA cm²)...). Designations such as: p (kPa), t [min]..., are not acceptable. However, if the full name of a physical quantity is unavoidable, it should be given in upright letters and separated from the unit by a comma (example: Pressure, kPa; Temperature, K; Current density, mA cm²...). Please do not use the axes of graphs for additional explanations; these should be mentioned in the figure captions and/or the manuscript (example: “pressure at the inlet of the system, kPa” should be avoided). The axis name should follow the direction of the axis (the name of y-axis should be rotated by 90°). Top and right axes should be avoided in diagrams, unless they are absolutely necessary.

Latin words, as well as the names of species, should be in *italic*, as for example: *i.e.*, *e.g.*, *in vivo*, *ibid*, *Calendula officinalis* L., *etc.* The branching of organic compound should also be indicated in *italic*, for example, *n*-butanol, *tert*-butanol, *etc.*

Decimal numbers must have decimal points and not commas in the text (except in the Serbian abstract), tables and axis labels in graphical presentations of results. Thousands are separated, if at all, by a comma and not a point.

Mathematical and chemical equations should be given in separate lines and must be numbered, Arabic numbers, consecutively in parenthesis at the end of the line. All equations should be embedded in the text. Complex equations (fractions, integrals, matrix...) should be prepared with the aid of the **Microsoft Equation 3.0** (or higher) or **MathType** (Do not use them to create simple equations and labels). **Using the Insert -> Equation option, integrated in MS Office 2010 and MS Office 2013, as well as insertion of equation objects within paragraph text IS NOT ALLOWED.**

ARTICLE STRUCTURE

- TITLE PAGE;
- MAIN TEXT – including Tables and Illustrations with corresponding captions;
- SUPPLEMENTARY MATERIAL (optional)

Title page

- **Title** in bold letters, should be clear and concise, preferably 12 words or less. The use of non-standard abbreviations, symbols and formulae is discouraged.
- **AUTHORS' NAMES** in capital letters with the full first name, initials of further names separated by a space and surname. Commas should separate the author's names except for the last two names when 'and' is to be used. In multi-affiliation manuscripts, the author's affiliation should be indicated by an Arabic number placed in superscript after the name and before the affiliation. Use * to denote the corresponding author(s).
- *Affiliations* should be written in *italic*. The e-mail address of the corresponding author should be given after the affiliation(s).
- *Abstract*: A one-paragraph abstract written of 150 – 200 words in an impersonal form indicating the aims of the work, the main results and conclusions should be given and clearly set off from the text. Domestic authors should also submit, on a separate page, an Abstract - Izvod, the author's name(s) and affiliation(s) in Serbian (Cyrillic letters). (Домаћи аутори морају доставити Извод (укључујући имена аутора и афилијацију) на српском језику, исписане ћирилицом, иза Захвалнице, а пре списка референци.) For authors outside Serbia, the Editorial Board will provide a Serbian translation of their English abstract.
- *Keywords*: Up to 6 keywords should be given. Do not use words appearing in the manuscript title
- **RUNNING TITLE**: A one line (maximum five words) short title in capital letters should be provided.

Main text – should have the form:

- **INTRODUCTION**,
- **EXPERIMENTAL (RESULTS AND DISCUSSION)**,
- **RESULTS AND DISCUSSION (EXPERIMENTAL)**,
- **CONCLUSIONS**,
- **NOMENCLATURE (optional) and**
- **Acknowledgements: If any.**
- **REFERENCES** (Citation of recent papers published in chemistry journals that highlight the significance of work to the general readership is encouraged.)

The sections should be arranged in a sequence generally accepted for publication in the respective fields. They subtitles should be in capital letters, centred and NOT numbered.

- The INTRODUCTION should include the aim of the research and a concise description of background information and related studies directly connected to the paper.
- The EXPERIMENTAL section should give the purity and source of all employed materials, as well as details of the instruments used. The employed methods should be described in sufficient detail to enable experienced persons to repeat them. Standard procedures should be referenced and only modifications described in detail. On no account should results be included in the experimental section.

Chemistry

Detailed information about instruments and general experimental techniques should be given in all necessary details. If special treatment for solvents or chemical purification were applied that must be emphasized.

Example: Melting points were determined on a Boetius PMHK or a Mel-Temp apparatus and were not corrected. Optical rotations were measured on a Rudolph Research Analytical automatic polarimeter, Autopol IV in dichloromethane (DCM) or methanol (MeOH) as solvent. IR spectra were recorded on a Perkin-Elmer spectrophotometer FT-IR 1725X. ¹H and ¹³C NMR spectra were recorded on a Varian Gemini-200 spectrometer (at 200 and 50 MHz, respectively), and on a Bruker Ultrashield Advance III spectrometer (at 500 and 125 MHz, respectively) employing indicated solvents (*vide infra*) using TMS as the internal standard. Chemical shifts are expressed in ppm (δ / ppm) values and coupling constants in Hz (J / Hz). ESI-MS spectra were recorded on Agilent Technologies 6210 Time-Of-Flight LC-MS instrument in positive ion mode with CH₃CN/H₂O 1/1 with 0.2 % HCOOH as the carrying solvent solution. Samples were dissolved in CH₃CN or MeOH (HPLC grade purity). The selected values were as follows: capillary voltage = 4 kV, gas temperature = 350 °C, drying gas flow 12 L min⁻¹, nebulizer pressure = 310 kPa, fragmentator voltage = 70 V. The elemental analysis was performed on the Vario EL III- C,H,N,S/O Elemental Analyzer (Elementar Analysensysteme GmbH, Hanau-Germany). Thin-layer chromatography (TLC) was performed on precoated Merck silica gel 60 F254 and RP-18 F254 plates. Column chromatography was performed on Lobar LichroPrep Si 60 (40-63 μ m), RP-18 (40-63 μ m) columns coupled to a Waters RI 401 detector, and on Biotage SP1 system with UV detector and FLASH 12+, FLASH 25+ or FLASH 40+ columns pre packed with KP-SIL [40-63 μ m, pore diameter 6 nm (60 Å)], KP-C18-HS (40-63 μ m, pore diameter 9 nm (90 Å) or KP-NH [40-63 μ m, pore diameter 10 nm (100 Å)] as adsorbent. Compounds were analyzed for purity (HPLC) using a Waters 1525 HPLC dual pump system equipped with an Alltech, Select degasser system, and dual λ 2487 UV-VIS detector. For data processing, Empower software was used (methods A and B). Methods C and D: Agilent Technologies 1260 Liquid Chromatograph equipped with Quat Pump (G1311B), Injector (G1329B) 1260 ALS, TCC 1260 (G1316A) and Detector 1260 DAD VL+ (G1315C). For data processing, LC OpenLab CDS ChemStation software was used. For details, see Supporting Information.

1. Synthesis experiments

Each paragraph describing a synthesis experiment should begin with the name of the product and any structure number assigned to the compound in the Results and Discussions section. Thereafter, the compound should be identified by its structure number. Use of standard abbreviations or unambiguous molecular formulas for reagents and solvents, and of structure numbers rather than chemical names to identify starting materials and intermediates, is encouraged.

When a new or improved synthetic method is described, the yields reported in key experimental examples, and yields used for comparison with existing methods, should represent amounts of isolated and purified products, rather than chromatographically or spectroscopically determined yields. Reactant quantities should be reported in weight and molar units and for product yields should be reported in weight units; percentage yields should only be reported for materials of demonstrated purity. When chromatography is used for product purification, both the support and solvent should be identified.

2. Microwave experiments

Reports of syntheses conducted in microwave reactors must clearly indicate whether sealed or open reaction vessels were used and must document the manufacturer and model of the reactor, the method of monitoring the reaction mixture temperature, and the temperature-time profile. Reporting a wattage rating or power setting is not an acceptable alternative to providing temperature data. Manuscripts describing work done with domestic (kitchen) microwave ovens will not be accepted except for studies where the unit is used for heating reaction mixtures at atmospheric pressure.

3. Compound characterization

The Journal upholds a high standard for compound characterization to ensure that substances being added to the chemical literature have been correctly identified and can be synthesized in known yield and purity by the reported preparation and isolation methods. For **all new** compounds, evidence adequate to establish both **identity** and **degree of purity** (homogeneity) must be provided.

Identity - Melting point. All homogeneous solid products (*e.g.* not mixtures of isomers) should be characterized by melting or decomposition points. The colors and morphologies of the products should also be noted.

Specific rotations. Specific rotations based on the equation $[\alpha]_D = (100 \alpha) / (l c)$ should be reported as unitless numbers as in the following example: $[\alpha]_D^{20}; D = -25.4$ (c 1.93, CHCl_3), where c / g mL^{-1} is concentration and l / dm is path length. The units of the specific rotation, $(\text{deg mL}) / (\text{g dm})$, are implicit and are not included with the reported value.

Spectra/Spectral Data. Important IR adsorptions should be given.

For all new diamagnetic substances, NMR data should be reported (^1H , ^{13}C , and relevant heteronuclei).

^1H NMR chemical shifts should be given with two digits after the decimal point. Include the number of protons represented by the signal, signal multiplicity, and coupling constants as needed (J italicized, reported with up to one digit after the decimal). The number of bonds through which the coupling is operative, nJ , may be specified by the author if known with a high degree of certainty. ^{13}C NMR signal shifts should be rounded to the nearest 0.01 ppm unless greater precision is needed to distinguish closely spaced signals. Field strength should be noted for each spectrum, not as a comment in the general experimental section. Hydrogen multiplicity (C, CH, CH_2 , CH_3) information obtained from routine DEPT spectra should be included. If detailed signal assignments are made, the type of NOESY or COSY methods used to establish atom connectivity and spatial relationships should be identified in the Supporting Information. Copies of spectra should also be included where structure assignments of complex molecules depend heavily on NMR interpretation. Numbering system used for assignments of signals should be given in the Supporting Information with corresponding general structural formula of named derivative.

HPLC/LCMS can be substituted for biochemistry papers where the main focus is not on compound synthesis.

HRMS/elemental analysis. To support the molecular formula assignment, HRMS data accurate within 5 ppm, or combustion elemental analysis [carbon and hydrogen (and nitrogen, if present)] data accurate within 0.5 %, should be reported for new compounds. HRMS data should be given in format as is usually given for combustion analysis: calculated mass for given formula following with observed mass: (+)ESI-HRMS m/z : [molecular formula + H]⁺ calculated mass, observed mass. Example: (+)ESI-HRMS m/z : calculated for $[\text{C}_{13}\text{H}_8\text{BrCl}_2\text{N} + \text{H}^+]$ 327.92899, observed 327.92792.

NOTE: in certain cases, a crystal structure may be an acceptable substitute for HRMS/elemental analysis.

Biomacromolecules. The structures of biomacromolecules may be established by providing evidence about sequence and mass. Sequences may be inferred from the experimental order of amino acid, saccharide, or nucleotide coupling, from known sequences of templates in enzyme-mediated syntheses, or through standard sequencing techniques. Typically, a sequence will be accompanied by MS data that establish the molecular weight.

Example: Product was isolated upon column chromatography [dry flash (SiO_2 , eluent EA, EA/MeOH gradient 95/5 \rightarrow 9/1, EA/MeOH/ NH_3 gradient 18/0.5/0.5 \rightarrow 9/1/1, and flash chromatography (Biotage SP1, RP column, eluent MeOH/ H_2O gradient 75/25 \rightarrow 95/5, N-H column, eluent EA/Hex gradient 6/3 \rightarrow EA). was obtained after flash column chromatography (Biotage SP NH column, eluent hexane/EA 4:6 \rightarrow 2:6). Yield 968.4 mg (95 %). Colorless foam softens at 96-101 °C. $[\alpha]_D^{20}; D = +0.163$ ($c = 2.0 \times 10^{-3}$ g/mL , CH_2Cl_2). IR (ATR): 3376w, 2949m, 2868w, 2802w, 1731s, 1611w, 1581s, 1528m, 1452m, 1374s, 1331w, 1246s, 1171m, 1063w, 1023m, 965w, 940w, 881w, 850w, 807w, cm^{-1} . ^1H NMR (500 MHz, CDCl_3 , δ): 8.46 (*d*, 1H, $J = 5.4$, H-2'), 7.89 (*s*, 1H, $J = 2.0$, H-8'), 7.71 (*d*, 1H, $J = 8.9$, H-5'), 7.30 (*dd*, 1H, $J_1 = 8.8$, $J_2 = 2.1$, H-6'), 6.33 (*d*, 1H, $J = 5.4$, H-3'), 6.07 (*s*, HN-Boc, exchangeable with D_2O), 5.06 (*s*, 1H, H-12), 4.92-4.88 (*m*, 1H, H-7), 4.42 (*bs*, H-3), 3.45 (*s*, CH_3 -N), 3.33 (*bs*, H-9'), 3.05-2.95 (*m*, 2H, H-11'), 2.70-2.43 (*m*, 2H, H-24) and HN, exchangeable with D_2O), 2.07 (*s*, CH_3COO), 2.04 (*s*, CH_3COO), 1.42 (*s*, 9H, $(\text{CH}_3)_3\text{C-N}(\text{Boc})$), 0.88 (*s*, 3H, CH_3 -10), 0.79 (*d*, 3H, $J = 6.6$, CH_3 -20), 0.68 (*s*, 3H, CH_3 -13). ^{13}C NMR (125 MHz, CDCl_3 , δ): 170.34, 170.27, 151.80, 149.92, 148.87, 134.77, 128.36, 125.11, 121.43, 117.29, 99.98, 75.41, 70.82, 50.43, 49.66, 47.60, 47.33, 44.97, 43.30, 41.83, 41.48, 37.65, 36.35, 35.44, 34.89,

34.19, 33.23, 31.24, 28.79, 28.35, 27.25, 26.45, 25.45, 22.74, 22.63, 21.57, 21.31, 17.85, 12.15. (+)ESI-HRMS (*m/z*): calculated for [C₄₅H₆₇CIN₄O₆ + H]⁺ 795.48219, observed 795.48185. Combustion analysis for C₄₅H₆₇CIN₄O₆: Calculated. C 67.94, H 8.49, N 7.04; found C 67.72, H 8.63, N 6.75. HPLC purity: method A: RT 1.994, area 99.12 %; method C: RT 9.936, area 98.20 %.

Purity - Evidence for documenting compound purity should include one or more of the following:

- Well-resolved high field 1D ¹H NMR spectrum showing at most only trace peaks not attributable to the assigned structure and a standard 1D proton-decoupled ¹³C NMR spectrum. Copies of the spectra should be included as figures in the Supporting Information.
- Quantitative gas chromatographic analytical data for distilled or vacuum-transferred samples, or quantitative HPLC analytical data for materials isolated by column chromatography or separation from a solid support. HPLC analyses should be performed in two diverse systems. The stationary phase, solvents (HPLC), detector type, and percentage of total chromatogram integration should be reported; a copy of the chromatograms may be included as a figure in the Supporting Information.
- Electrophoretic analytical data obtained under conditions that permit observing impurities present at the 5 % level.

HRMS data may be used to support a molecular formula assignment **but cannot be used as a criterion of purity.**

4. Biological Data

Quantitative biological data are required for all tested compounds. Biological test methods must be referenced or described in sufficient detail to permit the experiments to be repeated by others. Detailed descriptions of biological methods should be placed in the experimental section. Standard compounds or established drugs should be tested in the same system for comparison. Data may be presented as numerical expressions or in graphical form; biological data for extensive series of compounds should be presented in tabular form. Tables consisting primarily of negative data will not usually be accepted; however, for purposes of documentation they may be submitted as supporting information. Active compounds obtained from combinatorial syntheses should be resynthesized and retested to verify that the biology conforms to the initial observation.

Statistical limits (statistical significance) for the biological data are usually required. If statistical limits cannot be provided, the number of determinations and some indication of the variability and reliability of the results should be given. References to statistical methods of calculation should be included. Doses and concentrations should be expressed as molar quantities (*e.g.*, mol/kg, μmol/kg, M, mM). The routes of administration of test compounds and vehicles used should be indicated, and any salt forms used (hydrochlorides, sulfates, *etc.*) should be noted. The physical state of the compound dosed (crystalline, amorphous; solution, suspension) and the formulation for dosing (micronized, jet-milled, nanoparticles) should be indicated. For those compounds found to be inactive, the highest concentration (*in vitro*) or dose level (*in vivo*) tested should be indicated.

- The RESULTS AND DISCUSSION should include concisely presented results and their significance discussed and compared to relevant literature data. The results and discussion may be combined or kept separate.
- The inclusion of a CONCLUSION section, which briefly summarizes the principal conclusions, is recommended.
- NOMENCLATURE is optional but, if the authors wish, a list of employed symbols may be included.
- REFERENCES should be numbered sequentially as they appear in the text. Please note that any reference numbers appearing in the Illustrations and/or Tables and corresponding captions must follow the numbering sequence of the paragraph in which they appear for the first time. When cited, the reference number should be superscripted in Font 12, following any punctuation mark. In the reference list, they should be in normal position followed by a full stop. Reference entry must not be formatted using Carriage returns (enter key; ↵ key) or multiple space key. The formatting of references to published work should follow the *Journal's* style as follows:

- Journals^a: A. B. Surname1, C. D. Surname2, *J. Serb. Chem. Soc.* **Vol** (Year) first page Number
(<https://doi.org/doi>)^b
- Books: A. B. Surname1, C. D. Surname2, *Name of Book*, Publisher, City, Year, pp. 100-101
(<https://doi.org/doi>)^b
- Compilations: A. B. Surname1, C. D. Surname2, in *Name of Compilation*, A. Editor1, C. Editor2, Ed(s)., Publisher, City, Year, p. 100 (<https://doi.org/doi>)^b
- Proceedings: A. B. Surname1, C. D. Surname2, in *Proceedings of Name of the Conference or Symposium*, (Year), Place of the Conference, Country, *Title of the Proceeding*, Publisher, City, Year, p. or Abstract No. 100
- Patents: A. B. Inventor1, C. D. Inventor2, (Holder), Country Code and patent number (registration year)
- Chemical Abstracts: A. B. Surname1, C. D. Surname2, *Chem. Abstr.* CA 234 567a; For non-readily available literature, the Chemical Abstracts reference should be given in square brackets: [C.A. 139/2003 357348t] after the reference
- Standards: EN ISO 250: *Name of the Standard* (Year)
- Websites: Title of the website, URL in full (date accessed)
- ^a When citing Journals, the International Library Journal abbreviation is required. Please consult, e.g., https://images.wobofknowledge.com/WOK46/help/WOS/A_abrvjt.html
- ^b doi should be replaced by doi number of the Article, for example: <http://dx.doi.org/10.2298/JSC161212085B> (as active link). If doi do not exist, provide the link to the online version of the publication.

Only the last entry in the reference list should end with a full stop.

The names of all authors should be given in the list of references; the abbreviation *et al.* may only be used in the text. The original journal title is to be retained in the case of publications published in any language other than English (please denote the language in parenthesis after the reference). Titles of publications in non-Latin alphabets should be transliterated. Russian references are to be transliterated using the following transcriptions:

ж→zh, х→kh, ц→ts, ч→ch, ш→sh, щ→shch, ы→y, ю→yu, я→ya, э→e, й→i, ь→'.

Supplementary material

Authors are encouraged to present the information and results non-essential to the understanding of their paper as SUPPLEMENTARY MATERIAL (can be uploaded in Step 4 of Online Submission). This material may include as a rule, but is not limited to, the presentation of analytical and spectral data demonstrating the identity and purity of synthesized compounds, tables containing raw data on which calculations were based, series of figures where one example would remain in the main text, etc. The Editorial Board retain the right to assign such information and results to the Supplementary material when deemed fit. Supplementary material does not appear in printed form but can be downloaded from the web site of the JSCS.

Mathematical and chemical equations should be given in separate lines and must be numbered, Arabic numbers, consecutively in parenthesis at the end of the line. All equations should be embedded in the text. Complex equations (fractions, integrals, matrix...) should be prepared with the aid of the Microsoft Equation 3.0 (or higher) or MathType (Do not use them to create simple equations and labels). Using the Insert -> Equation option, integrated in MS Office 2010 and MS Office 2013, as well as insertion of equation objects within paragraph text IS NOT ALLOWED.

Deposition of crystallographic data

Prior to submission, the crystallographic data included in a manuscript presenting such data should be deposited at the appropriate database. Crystallographic data associated with organic and metal-organic structures should be deposited at the Cambridge Crystallographic Data Centre (CCDC) by e-mail to deposit@ccdc.cam.ac.uk

Crystallographic data associated with inorganic structures should be deposited with the Fachinformationszentrum Karlsruhe (FIZ) by e-mail to crysdata@fiz-karlsruhe.de. A deposition number will then be provided, which should be added to the reference section of the manuscript.

For detailed instructions please visit the JSCS website:
<https://www.shd-pub.org.rs/index.php/JSCS/Instructions>

ARTWORK INSTRUCTIONS

JSCS accepts only **TIFF** or **EPS** formats, as well as **JPEG** format (only for colour and greyscale photographs) for electronic artwork and graphic files. **MS files** (Word, PowerPoint, Excel, Visio) **NOT acceptable**. Generally, scanned instrument data sheets should be avoided. Authors are responsible for the quality of their submitted artwork. Every single Figure or Scheme, as well as any part of the Figure (A, B, C...) should be prepared according to following instructions (every part of the figure, A, B, C..., must be submitted as an independent single graphic file):

TIFF

Virtually all common artwork and graphic creation software is capable of saving files in TIFF format. This 'option' can normally be found under 'the 'Save As...' or 'Export...' commands in the 'File' menu.

TIFF (Tagged Image File Format) is the recommended file format for bitmap, greyscale and colour images.

- Colour images should be in the RGB mode
- When supplying TIFF files, please ensure that the files are supplied at the correct resolution:
 1. Line artwork: minimum of 1000 dpi
 2. RGB image: minimum of 300 dpi
 3. Greyscale image: minimum of 300 dpi
 4. Combination artwork (line/greyscale/RGB): minimum of 500 dpi
- Images should be tightly cropped, without frame and any caption.
- If applicable please re-label artwork with a font supported by JSCS (Arial, Helvetica, Times, Symbol) and ensure it is of an appropriate font size.
- Save an image in TIFF format with LZW compression applied.
- It is recommended to remove Alpha channels before submitting TIFF files.
- It is recommended to flatten layers before submitting TIFF files.

Please be sure that quality of an image cannot be increased by changing the resolution from lower to higher, but only by rescanning or exporting the image with higher resolution, which can be set in usual "settings" facilities.

EPS

Virtually all common artwork creation software, such as Canvas, ChemDraw, CorelDraw, SigmaPlot, Origin Lab..., are capable of saving files in EPS format. This 'option' can normally be found under the 'Save As...' or 'Export...' commands in the 'File' menu.

For vector graphics, EPS (Encapsulated PostScript) files are the preferred format as long as they are provided in accordance with the following conditions:

- when they contain bitmap images, the bitmaps should be of good resolution (see instructions for TIFF files)
- when colour is involved, it should be encoded as RGB
- an 8-bit preview/header at a resolution of 72 dpi should always be included
- embed fonts should always included and only the following fonts should be used in artwork: Arial, Helvetica, Times, Symbol
- the vertical space between the parts of an illustration should be limited to the bare necessity for visual clarity
- no data should be present outside the actual illustration area
- line weights should range from 0.35 pt to 1.5 pt
- when using layers, they should be reduced to one layer before saving the image (Flatten Artwork)

JPEG

Virtually all common artwork and graphic creation software is capable of saving files in JPEG format. This 'option' can normally be found under 'the 'Save As...' or 'Export...' commands in the 'File' menu.

JPEG (Joint Photographic Experts Group) is the acceptable file format **only for colour and greyscale photographs**. JPEG can be created with respect to photo quality (low, medium, high; from 1 to 10), ensuring file sizes are kept to a minimum to aid easy file transfer. Images should have a minimum resolution of 300 dpi. Image width: minimum 3.0 cm; maximum 12.0 cm.

Please be sure that quality of an image cannot be increased by changing the resolution from lower to higher, but only by rescanning or exporting the image with higher resolution, which can be set in usual "settings" facilities.

SIZING OF ARTWORK

- JSCS aspires to have a uniform look for all artwork contained in a single article. Hence, it is important to be aware of the style of the journal.
- Figures should be submitted in black and white or, if required, colour (charged). If coloured figures or photographs are required, this must be stated in the cover letter and arrangements made for payment through the office of the Serbian Chemical Society.
- As a general rule, the lettering on an artwork should have a finished, printed size of 11 pt for normal text and no smaller than 7 pt for subscript and superscript characters. Smaller lettering will yield a text that is barely legible. This is a rule-of-thumb rather than a strict rule. There are instances where other factors in the artwork, (for example, tints and shadings) dictate a finished size of perhaps 10 pt. Lines should be of at least 1 pt thickness.
- When deciding on the size of a line art graphic, in addition to the lettering, there are several other factors to address. These all have a bearing on the reproducibility/readability of the final artwork. Tints and shadings have to be printable at the finished size. All relevant detail in the illustration, the graph symbols (squares, triangles, circles, *etc.*) and a key to the diagram (to explain the explanation of the graph symbols used) must be discernible.
- The sizing of halftones (photographs, micrographs,...) normally causes more problems than line art. It is sometimes difficult to know what an author is trying to emphasize on a photograph, so you can help us by identifying the important parts of the image, perhaps by highlighting the relevant areas on a photocopy. The best advice that can be given to graphics suppliers is not to over-reduce halftones. Attention should also be paid to magnification factors or scale bars on the artwork and they should be compared with the details inside. If a set of artwork contains more than one halftone, again please ensure that there is consistency in size between similar diagrams.

General sizing of illustrations which can be used for the Journal of the Serbian Chemical Society:

- Minimum fig. size: 30 mm width
- Small fig. size - 60 mm width
- Large fig. size - 90 mm width
- Maximum fig. size - 120 mm width

Pixel requirements (width) per print size and resolution for bitmap images:

	Image width	A	B	C
Minimal size	30 mm	354	591	1181
Small size	60 mm	709	1181	2362
Large size	90 mm	1063	1772	3543
Maximal size	120 mm	1417	2362	4724

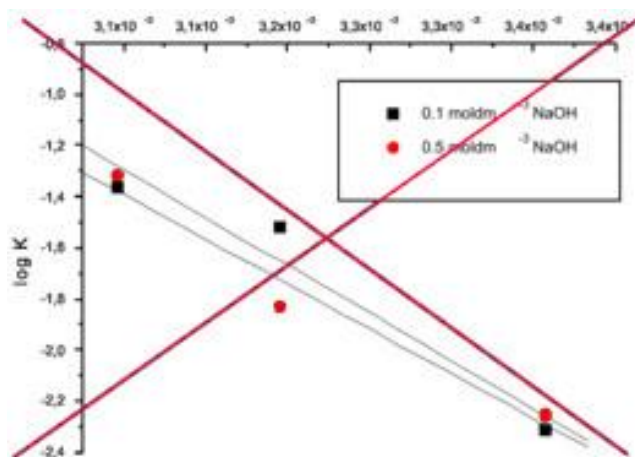
A: 300 dpi > RGB or Greyscale image

B: 500 dpi > Combination artwork (line/greyscale/RGB)

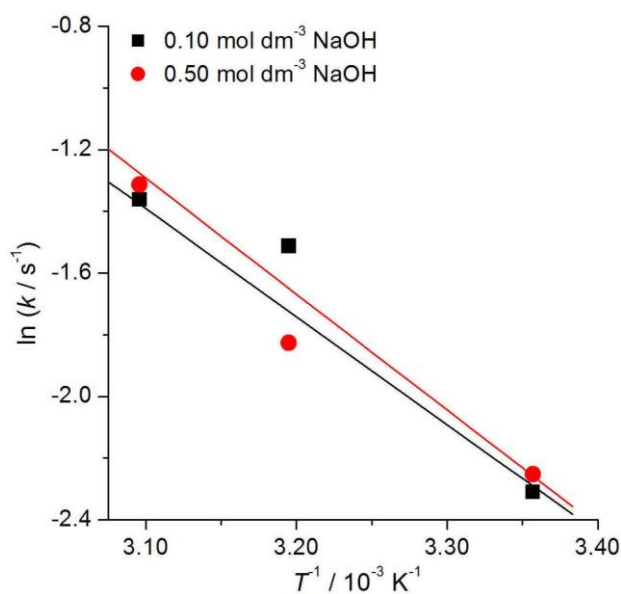
C: 1000 dpi > Line artwork

The designation of physical quantities and graphs formatting

The designation of physical quantities on figures must be in italic, whereas the units are in upright letters. They should be in Times New Roman font. In graphs a slash should be used to separate the designation of a physical quantity from the unit (example: p / kPa , $t / ^\circ\text{C}$, T_0 / K , τ / h , $\ln(j / \text{mA cm}^{-2})$...). Designations such as: p (kPa), t [min]..., are not acceptable. However, if the full name of a physical quantity is unavoidable, it should be given in upright letters and separated from the unit by a comma (example: Pressure, kPa, Temperature, K...). Please do not use the axes of graphs for additional explanations; these should be mentioned in the figure captions and/or the manuscript (example: “pressure at the inlet of the system, kPa” should be avoided). The axis name should follow the direction of the axis (the name of y-axis should be rotated by 90°). Top and right axes should be avoided in diagrams, unless they are absolutely necessary. Decimal numbers must have decimal points and not commas in the axis labels in graphical presentations of results. Thousands are separated, if at all, by a comma and not a point.



INCORRECT



CORRECT



J. Serb. Chem. Soc. 86 (6) 547–553 (2021)
JSCS–5441

Green and efficient synthesis of new β -amido-aroyl carbonyl derivatives catalyzed by choline chloride/urea as a deep eutectic solvent

ANITA BERJIS¹, BEHROOZ MIRZA^{1*} and HOSSEIN ANARAKI-ARDAKANI²

¹Department of Chemistry, Islamic Azad University, Karaj Branch, Karaj, Iran and

²Department of Chemistry, Mahshahr Branch, Islamic Azad University, Mahshahr, Iran

(Received 6 May 2020, revised 9 March, accepted 11 March 2021)

Abstract: A green and highly efficient synthesis of some new β -amido-aroyl carbonyl derivatives has been achieved through a one-pot, three-component reaction of dimedone/barbituric acid derivatives, arylglyoxals, and amides in choline chloride/urea as a deep eutectic solvent (DES). The use of biodegradable materials, short reaction time and high yields of products introduced this protocol as an efficient environmentally friendly method. The DES could be easily recovered and reused about four times with satisfied catalytic activity.

Keywords: deep eutectic solvents; green chemistry; multi-component reaction; β -amido-aroyl carbonyl compounds.

INTRODUCTION

Multicomponent reactions (MCRs) have been identified as one of the most efficient methods for the synthesis of heterocyclic compounds.^{1,2} MCRs provide a powerful synthetic method in which a wide range of raw materials could react through one-pot reactions to produce valuable compounds. In general, most of the atoms in the substrates are also found in the structure of the newly-formed products.³

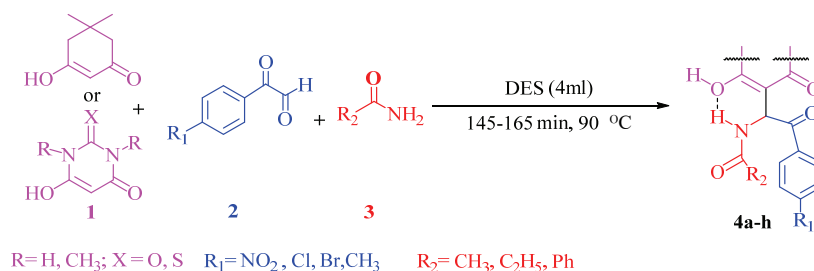
Green chemistry, as an essential and evolving research field, has focused on designing processes that reduce the consumption and production of environmentally harmful substances.⁴

Recently, deep eutectic solvents (DES) have been utilized as a new green solvent in research. DESs have received more attention due to their exciting properties, such as high thermal stability, high purity, high solubility, no water-reactivity, low cost, and simple preparation methods. Therefore, many valuable review articles examine the types and features of DES.⁵ A deep eutectic solvent (DES) is defined as a mixture of two or more components with effective hydro-

*Corresponding author. E-mail: b_mirza@azad.ac.ir
<https://doi.org/10.2298/JSC200506019B>

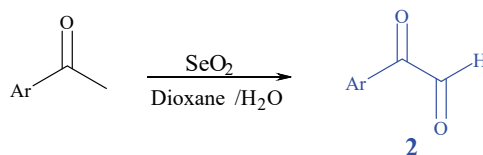
gen-bond interactions that result in the observed melting point being much lower than either of the individual components.^{6–10} Choline chloride (ChCl) is one of the most common materials utilized in the synthesis of DESs. This quaternary ammonium salt has received more attention due to its special properties, such as low cost, biodegradability, environmental friendliness, and reusability. In addition, choline chloride exhibits high thermal and chemical stability.¹¹ ChCl as hydrogen bond acceptor (HBA) could produce DES in reaction with hydrogen bond donors (HBD), such as acids,¹² alcohols,¹³ amines¹⁴ or amides.¹⁵

β -Acetamido carbonyl compounds have been identified as precursors of 1,3-amino alcohols and γ -lactams.^{16,17} They also exhibit biological and pharmaceutical activities¹⁸ and are used to prepare of antibiotic drugs, such as nikkomycin or neopolyoxins.¹⁹ The modified Dakin–West condensation of aromatic aldehyde, acetophenone and acetonitrile is highly recommended in the synthesis of β -acetamido carbonyl compounds.^{20,21} Moreover, several efficient methods have been reported for the synthesis of β -acetamido ketones through three-component reactions of acetophenone, an aryl aldehyde, and acetyl chloride in acetonitrile using CoCl_2 ,¹⁷ montmorillonite K-10 clay²² and heteropoly acids²³ as useful catalysts. Three-component reactions of 1,3-dicarbonyl compounds, arylglyoxals, and heteroaryl amines/2-aminobenzimidazoles were reported in order to synthesis of 6,7-dihydrobenzofuran-4(5*H*)-one²⁴/12-arylbenzimidazo[2,1-*b*]-quinazolin-1(2*H*)-one²⁵ derivatives. Moreover, some reports have been found on the synthesis of β -amido-aryl carbonyl derivatives through three-component reaction of 1,3-dicarbonyl compounds, arylglyoxal, and benzamide.^{26–28} Following previous works, herein an efficient approach is reported for the one-pot synthesis of β -amido-aryl carbonyl derivatives (**4**) using three-component reactions of dimedone, barbituric/thiobarbituric acid derivatives (**1**), arylglyoxals (**2**) and amides (**3**), in the presence of choline chloride/urea as a deep eutectic solvent (DES), Scheme 1.



Scheme 1. Synthesis of β -amido-aryl carbonyl derivatives in DES as solvent and catalyst.

Arylglyoxals **2** were synthesized by the reported reaction of the corresponding acetophenone and SeO_2 ²⁹ (Scheme 2).



Ar = 4-Nitrophenyl, 4-Chlorophenyl, 4-Bromophenyl, 4-CH₃-phenyl

Scheme 2. The synthesis of arylglyoxals.

EXPERIMENTAL

All used chemicals and solvents were purchased from Fluka (Buchs, Switzerland) and used without further purification. Melting points of the synthesized products were determined with an electrothermal 9100 apparatus. The IR spectra were recorded on a Shimadzu IR-470 spectrometer. ¹H- and ¹³C-NMR spectra were recorded on Bruker DRX-250 Avance spectrometer in DMSO-*d*₆ or CDCl₃ with TMS as the internal standard. In addition, elemental analyses were performed using a Heraeus CHN-O-Rapid analyzer.

General procedure for the synthesis of β -amido-aryl carbonyl derivatives

A mixture of dimedone/barbituric acid derivatives (1 mmol), arylglyoxals (1 mmol), and amides (1 mmol) were added to choline chloride/urea (1:2, 4 mL). The resulting mixture was stirred and heated 90 °C for 145–165 min (Scheme 1). After completion of the reaction (TLC, ethyl acetate/*n*-hexane, 2:1), the reaction mixture was washed with water (10 mL) and the solid residue recrystallized from ethanol to obtain the pure product.

The spectral and analytical data for the new compounds are presented in the Supplementary material to this paper.

RESULTS AND DISCUSSION

First, the reaction of dimedone, 4-nitrophenylglyoxal, and benzamide was selected as a model reaction. Then the model reaction was performed in various DESs based on choline chloride (ChCl), and the results are listed in Table I. The mixture of choline chloride:urea (1:2) was identified as the best DES. Next, the reaction was tested at different temperatures to find the most suitable conditions, whereby the best reaction result was observed in the presence of choline chloride:urea (1:2) at 90 °C. Performing the reaction at lower temperatures reduced the reaction yields (Table I, entries 9–11). Furthermore only 20 % yield of the product was detected in the absence of any DES (Table I, entry 8).

In order to prove the efficiency of the method, several cyclic 1,3-diketones (**1**), various substituted arylglyoxal (**2**, including electron-donating and electron-withdrawing groups), and different amides (**3**) were employed in presence of choline chloride:urea (1:2) at 90 °C (Table II). Excellent yields of products and short reaction times were found as the advantages of the method.

Novel synthesized products (**4a–h**) were characterized by IR, ¹H-NMR and ¹³C-NMR spectral data, as well as elemental analyses.

For example, the IR spectrum of **4a** showed absorptions at 3417 and 3258 cm⁻¹ for OH and NH groups and at 1710, 1610 cm⁻¹ for carbonyl groups, indi-

cating the presence of these functional groups in the proposed structure. The ^1H -NMR spectrum of **4a** exhibited two singlet signals at δ 0.63 and 0.99 ppm for methyl groups, and the methylene group was observed at δ 2.01 and 2.67 ppm. Additionally, a single signal was observed at δ 5.81 ppm for the methine group, and multiplet signals were observed at 7.50–8.27 ppm related to aromatic and NH hydrogens and finally a broad signals at δ 12.43 ppm related to the OH proton. The decoupled ^{13}C -NMR spectrum of **4a** showed 19 resonances that are consistent with the proposed structure. The elemental analysis confirmed the amounts of C, H and N in the final product.

TABLE I. Optimization of reaction in various choline chloride-based DESs; reaction conditions: dimedone (0.25 mmol), 4-nitrophenyl glyoxal (0.25 mmol) and benzamide (0.25 mmol) in DES (1 mL)

Entry	DES	$t / ^\circ\text{C}$	Time, min	Yield ^a , %
1	Choline chloride	90	200	20
2	Choline chloride:ZnCl ₂ (1:2)	90	200	40
3	Choline chloride:PTSA (1:1)	90	200	45
4	Choline chloride:malonic acid (1:1)	90	200	55
5	Choline chloride:succinic acid (1:1)	90	200	55
6	Choline chloride:citric acid (1:1)	90	200	50
7	Choline chloride:oxalic acid (1:1)	90	200	55
8	–	100	220	20
9	Choline chloride:urea (1:2)	70	150	70
10	Choline chloride:urea (1:2)	80	150	82
11	Choline chloride:urea (1:2)	90	150	90
12	Choline chloride:urea (1:2)	100	150	90

^aIsolated yield

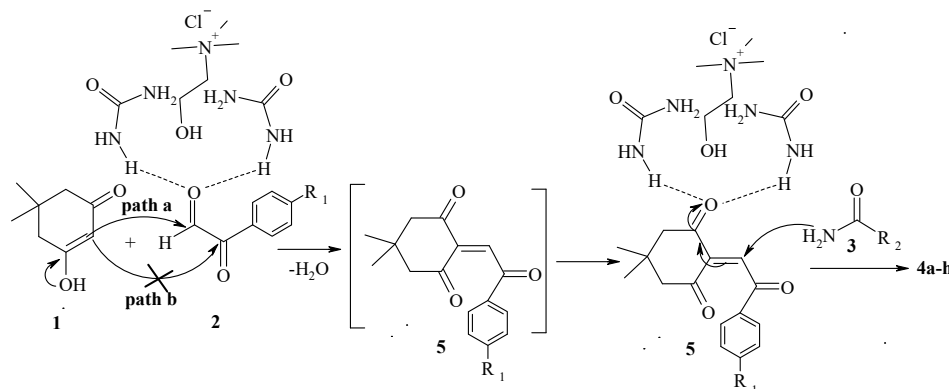
TABLE II. Three-component reaction of dimedone or barbituric acid derivatives, arylglyoxals, and amides in a deep eutectic solvent (DES); *MP* – melting point

Entry	Substrate	Ar	R ₂	Time, min	Yield ^a , %	<i>MP</i> / $^\circ\text{C}$
4a	Dimedone	4-NO ₂ -C ₆ H ₄	Ph	150	90	200
4b	Dimedone	4-Cl-C ₆ H ₄	Ph	160	89	205
4c	Dimedone	4-Br-C ₆ H ₄	Ph	160	85	225
4d	Dimedone	4-Br-C ₆ H ₄	CH ₃	155	90	210
4e	Dimedone	4-NO ₂ -C ₆ H ₄	CH ₃	145	88	215
4f	Dimedone	4-Br-C ₆ H ₄	C ₂ H ₅	150	85	210
4g	1,3-Dimethylbarbituric acid	4-CH ₃ -C ₆ H ₄	CH ₃	165	80	200–203
4h	Thiobarbituric acid	4-Cl-C ₆ H ₄	C ₂ H ₅	165	78	215–217

^aIsolated yield

A plausible mechanism for the synthesis of β -amido-aryl carbonyl derivatives based on the previously reported^{30,31} is presented in Scheme 3. First, a Knoevenagel condensation of enolic form of dimedone **1** with more electrophilic formyl group of the arylglyoxal **2** (path a) in the presence of DES is proposed to

give intermediate **5**.^{28,29} Then Michael addition of amide **3** to intermediate **5** forms the β -amido-aryl carbonyl derivatives products. DES activates all carbonyl groups *via* hydrogen bonding. (Scheme 3).



Scheme 3. Suggested pathway for the formation of compounds **4a-h**.

Finally, the reusability of the catalyst for the synthesis of *N*-[1-(2-hydroxy-4,4-dimethyl-6-oxo-cyclohex-1-enyl)-2-(4-nitro-phenyl)-2-oxo-ethyl]-benzamide (**4a**) was studied (Fig. 1). After completion of the reaction, the reaction mixture was washed with water and the solid residue recrystallized to obtain the pure product. The DES was recovered from the aqueous phase by evaporation at 80 °C under vacuum and prepared for the next run. It was applied for four runs without noticeable decrease in the catalyst activity (Fig. 1).

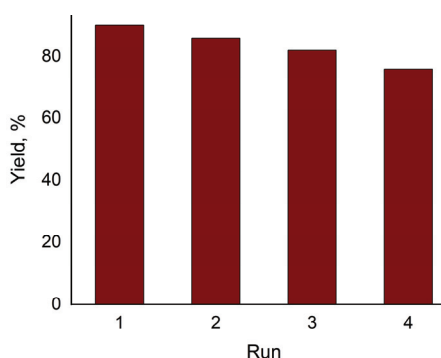


Fig. 1. Reusability of the DES.

CONCLUSIONS

In conclusion, a simple and efficient methodology for the synthesis of β -amido-aryl carbonyl derivatives was successfully developed by the one-pot three-component reaction of dimedone/barbituric acid derivatives, arylglyoxals, and amides in the presence of choline chloride/urea as a green and eco-friendly

catalyst and solvent. Several noticeable advantages such as simplicity of operation, safe method, high yields of products, and biodegradable, non-toxic, inexpensive materials were found. Also, the deep eutectic solvent (DES) could be easily recycled and reused in at least four consecutive runs without significant loss of catalytic activity.

SUPPLEMENTARY MATERIAL

Additional data are available electronically at the pages of journal website: <https://www.shd-pub.org.rs/index.php/JSCS/index>, or from the corresponding author on request.

Acknowledgement. We are thankful to the Islamic Azad University, Karaj branch, for the support of this work.

ИЗВОД

ЗЕЛЕНА И ЕФИКАСНА СИНТЕЗА НОВИХ β -АМИДО-АРОИЛ КАРБОНИЛНИХ ДЕРИВАТА У ЕУТЕКТИЧНОЈ СМЕШИ ХОЛИН-ХЛОРИД/УРЕА

ANITA BERJIS¹, BEHROOZ MIRZA¹ и HOSSEIN ANARAKI-ARDAKANI²

¹Department of Chemistry, Faculty of Science, Islamic Azad University, Karaj Branch, Alborz, Iran

²Department of Chemistry, Mahshahr Branch, Islamic Azad University, Mahshahr, Iran

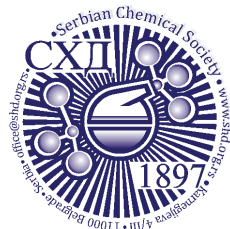
Зелена и веома ефикасна синтеза нових β -амидо-ароил карбонилних деривата постигнута је у једном реакционом кораку у тро-компонентној реакционој смеши која садржи димедон/деривате барбитурне киселине, арил-глиоксале и амиде у смеши холин хлорида/уреа као дубоком еутектичком растварачу (deep eutectic solvent, DES). Због употреба биодеградабилних материјала, кратког реакционог времена и високог приноса производа овај поступак припада ефикасним и еколошки прихватљивим методама синтезе. Еутектички растварач се лако може рециклирати и поново користити четири пута без губитка каталитичке активности.

(Примљено 6. маја 2020, ревидирано 9 марта, прихваћено 11. марта 2021)

REFERENCES

1. B. M. Trost, *Science* **254** (1991) 1471 (<https://doi.org/10.1126/science.1962206>)
2. S. Pal, M. Nasim Khan, S. Karamthulla, L. H. Choudhury, *Tetrahedron Lett.* **56** (2015) 359 (<https://doi.org/10.1016/j.tetlet.2014.11.095>)
3. A. J. Von Wangelin, H. Neumann, D. Gördes, S. Klaus, D. Strübing, M. Beller, *Chem. Eur. J.* **9** (2003) 4286 (<https://doi.org/10.1002/chem.200305048>)
4. P. T. Anastas, *Crit. Rev. Anal. Chem.* **29** (1999) 167 (<https://doi.org/10.1080/10408349891199356>)
5. P. Liu, J. W. Hao, L. P. Mo, Z. H. Zhang, *RSC Adv.* **5** (2015) 48675 (<https://doi.org/10.1039/c5ra05746a>)
6. Y. Cui, C. Li, J. Yin, S. Li, Y. Jia, M. Bao, *J. Mol. Liq.* **236** (2017) 338 (<https://doi.org/10.1016/j.j.molliq.2019.03.002>)
7. Q. Zhang, K. De.Oliveira Vigier, S. Royer, F. Jerome, *Chem. Soc. Rev.* **41** (2012) 7108 (<https://doi.org/10.1039/c2cs35178a>)
8. N. Azizi, T. Soleymani Ahoori, M. Mahmoudi Hashemi, *J. Mol. Liq.* **246** (2017) 221 (<https://doi.org/10.1016/j.molliq.2017.09.049>)
9. P. Liu, J.-W. Hao, L.-P. Mo, Z.-H. Zhang, *RSC Adv.* **5** (2015) 48675 (<https://doi.org/10.1039/c5ra05746a>)

10. E. Habibi, K. Ghanemi, M. Fallah-Mehrjardi, A. Dadolahi-Sohrab, *Anal. Chim. Acta* **762** (2013) 61 (<https://doi.org/10.1016/j.aca.2012.11.054>)
11. A. Shaabani, S. E. Hooshmand, A. Tavousi Tabatabaei, *Tetrahedron Lett.* **57** (2016) 351 (<https://doi.org/10.1016/j.tetlet.2015.12.017>)
12. A. K. Sanap, G. S. Shankarling, *RSC Adv.* **4** (2014) 34938 (<https://doi.org/10.1039/C4RA05858E>)
13. A. P. Abbott, R. C. Harris, K. S. Ryder, C. D'Agostino, L. F. Gladden, M. D. Mantle, *Green Chem.* **13** (2011) 82 (<https://doi.org/10.1039/C0GC00395F>)
14. S. Khandelwal, Y. K. Tailor, M. Kumar, *J. Mol. Liq.* **215** (2016) 345 (<https://doi.org/10.1016/j.molliq.2015.12.015>)
15. E. L. Smith, A. P. Abbott, K. S. Ryder, *Chem. Rev.* **114** (2014) 11060 (<https://doi.org/10.1021/cr.300162p>)
16. J. Barluenga, B. Olano, S. Fustero, *J. Org. Chem.* **50** (1985) 4052 (<https://doi.org/10.1021/jo00221a018>)
17. I. Nageshwar Rao, E. N. Prabhakaran, S. Kumar Das, J. Iqbal, *J. Org. Chem.* **68** (2003) 4079 (<https://doi.org/10.1021/jo020559c>)
18. R. P. Cheng, S. H. Gellman, W. F. De. Grado, *Chem. Rev.* **101** (2001) 3219. (<https://doi.org/10.1021/cr000045i>)
19. U. Dahn, H. Hagenmaier, H. Hohne, W. A. König, G. Wolf, H. Zahner. *Arch. Microbiol.* **107** (1997) 143 (<https://doi.org/10.1007/bf00446834>)
20. R. M. Kumbhare, M. Sridhar, *J. Chem. Sci.* **124** (2012) 495 (<https://doi.org/10.1007/s12039-011-0183-3>)
21. G. L. Buchanan, *Chem. Soc. Rev.* **17** (1988) 91 (<https://doi.org/10.1039/CS9881700091>)
22. D. Bahulayan, S. K. Das, J. Iqbal, *J. Org. Chem.* **68** (2003) 5735 (<https://doi.org/10.1021/jo02734p>)
23. A. Javid, M. M. Heravi, F. F. Bamoharram, *Monatsh. Chem.* **143** (2012) 831 (<https://doi.org/10.1007/s00706-011-0669-1>)
24. R. Khoeiniha, A. Olyaei, M. Saraei, *J. Heterocyclic Chem.* **54** (2017) 1746 (<https://doi.org/10.1002/jhet.2752>)
25. O. N. Petrova, L. L. Zamigajlo, K. S. Ostras, S. V. Shishkina, O. V. Shishkin, A. V. Borisov, V. I. Musatov, M. G. Shirobokova, V. V. Lipson, *Chem. Heterocycl. Comp.* **51** (2015) 310 (<https://doi.org/10.1007/s10593-015-1700-y>)
26. F. Jafari, S. Kodabakhshi, S. Gharehzadeh Shirazi, *RSC Adv.* **4** (2014) 48095 (<https://doi.org/10.1039/C4RA90049A>)
27. S. Khodabakhshi, B. Karami, *Tetrahedron Lett.* **55** (2014) 7136 (<https://doi.org/10.1016/j.tetlet.2014.11.016>)
28. S. Khodabakhshi, M. Khaleghi Abbasabadi, M. Baghrnejad, F. Marahel, *J. Chin. Chem. Soc.* **62** (2015) 9 (<https://doi.org/10.1002/jccs.201400266>)
29. B. Khalili, P. Jajarmi, B. Eftekhari-Sis, M. M. Hashemi, *J. Org. Chem.* **73** (2008) 2090 (<https://doi.org/10.1021/jo702385n>)
30. J. Khalafy, M. Ezzati, M. Rimaz, A. d Poursattar Marjani, H. Yaghoobnejad Asl, *J. Iran. Chem. Soc.* **11** (2014) 1067 (<https://doi.org/10.1007/s13738-013-0378-2>)
31. J. Khalafy, M. Rimaz, M. Ezzati, R. H. Prager, *Bull. Korean Chem. Soc.* **33** (2012) 9 (<http://dx.doi.org/10.5012/bkcs.2012.33.9.2890>)



SUPPLEMENTARY MATERIAL TO
Green and efficient synthesis of new β -amido-aroyl carbonyl derivatives catalyzed by choline chloride/urea as a deep eutectic solvent

ANITA BERJIS¹, BEHROOZ MIRZA^{1*} and HOSSEIN ANARAKI-ARDAKANI²

¹Department of Chemistry, Faculty of Science, Islamic Azad University, Karaj Branch, Alborz, Iran and ²Department of Chemistry, Mahshahr Branch, Islamic Azad University, Mahshahr, Iran

J. Serb. Chem. Soc. 86 (6) (2021) 547–553

THE SPECTRAL AND ANALYTICAL DATA FOR THE NEW COMPOUNDS

N-[1-(2-Hydroxy-4,4-dimethyl-6-oxocyclohex-1-enyl)-2-(4-nitrophenyl)-2-oxoethyl]-benzamide (**4a**). White powder; m.p.: 200 °C; Anal. calcd. for C₂₃H₂₂N₂O₆: C, 65.39; H, 5.25; N, 6.63 %. Found: C, 65.58; H, 5.41; N, 6.39 %; IR (KBr, ν_{\max} / cm⁻¹): 3417 (OH), 3258 (NH), 1710 & 1610 (C=O); ¹H-NMR (250 MHz, CDCl₃, δ / ppm): 0.63 (3H, s, CH₃), 0.99 (3H, s, CH₃), 1.85–2.25 (2H, m, CH₂), 2.67 (2H, s, CH₂), 5.81 (1H, s, CH), 7.50–8.27 (10H, m, Ar & NH), 12.43 (1H, broad, OH); ¹³C-NMR (62.90 MHz, CDCl₃, δ / ppm): 26.08, 30.03, 31.05, 43.69, 49.44, 51.76, 114.12, 123.56, 127.47, 128.90, 131.50, 132.98, 140.33, 150.88, 163.15, 169.48, 177.85, 192.88, 196.34.

N-[2-(4-Chlorophenyl)-1-(2-hydroxy-4,4-dimethyl-6-oxocyclohex-1-enyl)-2-oxoethyl]-benzamide (**4b**). White powder; m.p.: 205 °C; Anal. calcd. for C₂₃H₂₂ClNO₄: C, 67.07; H, 5.38; N, 3.40 %. Found: C, 67.31; H, 5.55; N, 3.25 %; IR (KBr, ν_{\max} / cm⁻¹): 3444 (OH), 3308 (NH), 1686 & 1636 (C=O); ¹H-NMR (250 MHz, DMSO-*d*₆, δ / ppm): 1.11 (3H, s, CH₃), 1.25 (3H, s, CH₃), 2.47 (2H, s, CH₂), 2.76–2.80 (2H, m, CH₂), 6.55 (1 H, s, CH), 7.38–8.38 (10 H, m, Ar & NH), 12.23 (1H, broad, OH); ¹³C-NMR (62.90 MHz, CDCl₃, δ / ppm): 26.08, 30.03, 31.87, 42.19, 50.66, 52.39, 107.81, 122.43, 126.64, 127.30, 128.70, 130.08, 131.85, 131.98, 150.36, 166.33, 170.43, 193.75, 196.25.

N-[2-(4-Bromophenyl)-1-(2-hydroxy-4,4-dimethyl-6-oxocyclohex-1-enyl)-2-oxoethyl]-benzamide (**4c**). White powder; m.p.: 225 °C, Anal. calcd. for C₂₃H₂₂BrNO₄: C, 60.54; H, 4.86; N, 3.07 %. Found: C, 60.41; H, 4.66; N, 3.41 %; IR (KBr, ν_{\max} / cm⁻¹): 3416 (OH), 3311 (NH), 1701, 1636 (C=O); ¹H-NMR (250 MHz, DMSO-*d*₆, δ / ppm): 1.15 (3H, s, CH₃), 1.24 (3H, s, CH₃), 2.45 (2H,

* Corresponding author. E-mail: b_mirza@azad.ac.ir

s, CH₂), 2.79 (2H, *s*, CH₂), 6.53 (1H, *s*, CH), 7.40–8.33 (10H, *m*, Ar & NH), 12.23 (1H, broad, OH); ¹³C-NMR (62.90 MHz, CDCl₃, δ / ppm): 27.59, 28.46, 29.44, 43.25, 52.53, 60.25, 106.59, 126.51, 127.99, 128.84, 129.34, 130.41, 132.33, 133.56, 138.75, 165.45, 166.54, 192.13, 193.00.

N-[2-(4-Bromophenyl)-1-(2-hydroxy-4,4-dimethyl-6-oxocyclohex-1-enyl)-2-oxoethyl]-acetamide (**4d**). White powder; m.p.: 210 °C; Anal. calcd. for C₁₈H₂₀BrNO₄: C, 54.84; H, 5.11; N, 3.55 %. Found: C, 54.92; H, 5.35; N, 3.72 %; IR (KBr, ν_{max} / cm⁻¹): 3412 (OH), 3322 (NH), 1698, 1621 (C=O); ¹H-NMR (250 MHz, CDCl₃, δ / ppm): 0.66 (3H, *s*, CH₃), 0.99 (3H, *s*, CH₃), 2.11 (3H, *s*, CH₃), 2.29–2.44 (2H, *m*, CH₂), 2.79 (2H, *s*, CH₂), 5.53 (1H, *s*, CH), 6.59–7.65 (5H, *m*, Ar & NH), 12.09 (1H, broad, OH); ¹³C-NMR (62.90 MHz, CDCl₃, δ / ppm): 22.48, 26.10, 30.06, 30.93, 43.61, 49.55, 51.16, 114.59, 126.64, 129.40, 131.69, 131.82, 172.92, 177.07, 193.75, 196.32.

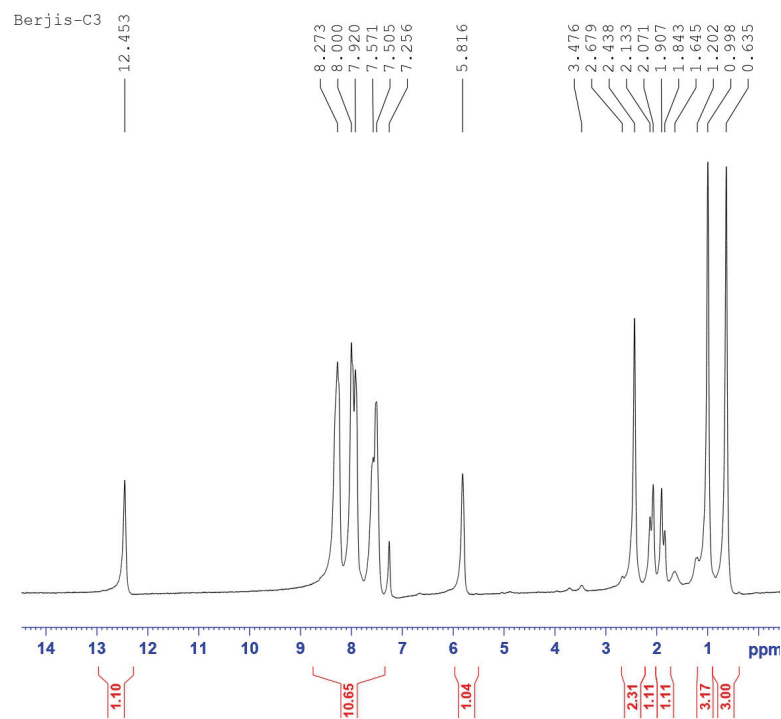
N-[1-(2-Hydroxy-4,4-dimethyl-6-oxo cyclohex-1-enyl)-2-(4-nitrophenyl)-2-oxoethyl]-acetamide (**4e**). White powder; m.p.: 215 °C; Anal. calcd. for C₁₈H₂₀N₂O₆: C, 59.99; H, 5.59; N, 7.77 %. Found: C, 59.76; H, 5.68; N, 7.51 %; IR (KBr, ν_{max} / cm⁻¹): 3447 (OH), 3324 (NH), 1702, 1673 (2 C=O); ¹H-NMR (250 MHz, CDCl₃, δ / ppm): 0.60 (3H, *s*, CH₃), 0.99 (3H, *s*, CH₃), 2.15 (3H, *s*, CH₃), 2.40–2.48 (2H, *m*, CH₂), 2.85 (2H, *s*, CH₂), 5.58 (1H, *s*, CH), 7.90–8.25 (5H, *m*, Ar & NH), 12.18 (1H, broad, OH); ¹³C-NMR (62.90 MHz, CDCl₃, δ / ppm): 22.49, 26.04, 30.01, 31.00, 42.69, 49.41, 51.52, 114.32, 123.52, 124.05, 125.39, 128.87, 173.11, 177.78, 193.75, 196.36.

N-[2-(4-Bromophenyl)-1-(2-hydroxy-4,4-dimethyl-6-oxocyclohex-1-enyl)-2-oxoethyl]-propionamide (**4f**). White powder; m.p.: 210 °C; Anal. calcd. for C₁₉H₂₂BrNO₄: C, 55.89; H, 5.43; N, 3.43 %. Found: C, 55.75; H, 5.64; N, 3.57 %; IR (KBr, ν_{max} / cm⁻¹): 3433 (OH), 3307 (NH), 1695 & 1623 (2 C=O); ¹H-NMR (250 MHz, CDCl₃, δ / ppm): 0.66 (3H, *s*, CH₃), 0.98 (3H, *s*, CH₃), 1.18–2.24 (3H, *m*, CH₃), 1.83–2.04 (2H, *m*, CH₂), 2.36–2.45 (4H, *m*, CH₂), 5.53 (1H, *s*, CH), 7.42–7.73 (5H, *m*, Ar & NH), 12.24 (1H, broad, OH); ¹³C-NMR (62.90 MHz, CDCl₃ δ / ppm): 9.39, 22.48, 26.10, 30.06, 30.93, 43.61, 49.55, 51.16, 114.59, 126.64, 129.40, 131.69, 131.82, 172.92, 177.07, 193.75, 196.32.

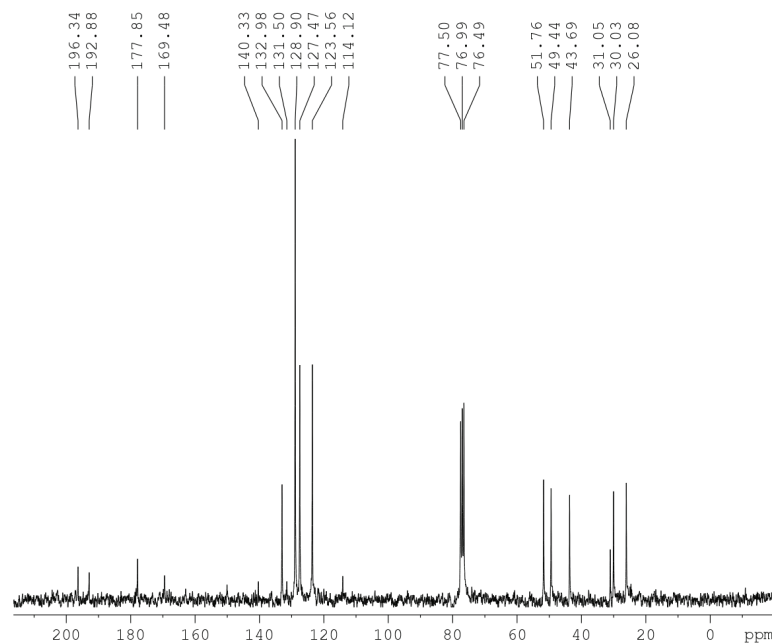
N-[1-(6-Hydroxy-1,3-dimethyl-2,4-dioxo-1,2,3,4-tetrahydro-pyrimidin-5-yl)-2-oxo-2-p-tolyl-ethyl]-acetamide (**4g**). White powder; m.p.: 200–203 °C, Anal. calcd. for C₁₇H₁₉N₃O₅: C, 59.12; H, 5.55; N, 12.17 %. Found: C, 59.32; H, 5.81; N, 12.34 %; IR (KBr, ν_{max} / cm⁻¹): 3418 (OH, NH), 1677, 1639 (2 C=O). ¹H-NMR (250 MHz, CDCl₃): δ = 2.02 (3H, *s*, CH₃), 3.13 (1H, *s*, CH₃), 3.30 (6H, *s*, 2N-CH₃), 3.33 (3H, *s*, CH₃), 5.62 (1H, *s*, CH), 7.32–8.19 (5H, *m*, Ar & NH), 12.24 (1H, broad, OH); ¹³C-NMR (62.90 MHz, CDCl₃, δ / ppm): 22.48, 23.78, 28.05, 28.82, 49.05, 81.55, 128.05, 129.25, 135.42, 138.82, 160.24, 171.45, 177.32, 182.75, 187.32.

N-[2-(4-Chlorophenyl)-1-(6-hydroxy-4-oxo-2-thioxo-1,2,3,4-tetrahydro-pyrimidin-5-yl)-2-oxoethyl]-propionamide (**4h**). White powder, m.p.: 215–217 °C, Anal. calcd. for C₁₅H₁₄ClN₃O₄S: C, 48.98; H, 3.84 N, 11.42 %. Found: C, 48.76; H, 3.63 N, 11.61 %; IR (KBr, ν_{\max} / cm⁻¹): 3386 (OH), 3203(NH), 1657 & 1630 (2 C=O); ¹H-NMR (250 MHz, CDCl₃, δ / ppm): 0.91 (3H, *m*, CH₃), 2.18–2.42 (2H, *m*, CH₂), 6.15 (1H, *s*, CH), 7.36–8.04 (5H, *m*, Ar & NH), 11.15 (1H, *s*, NH), 12.26 (1H, *s*, NH), 12.58 (1H, broad, OH); ¹³C-NMR (62.90 MHz, CDCl₃, δ / ppm): 11.61, 31.09, 51.05, 76.79, 129.08, 129.59, 131.44, 135.09, 164.27, 165.55, 172.55, 176.09, 186.09.

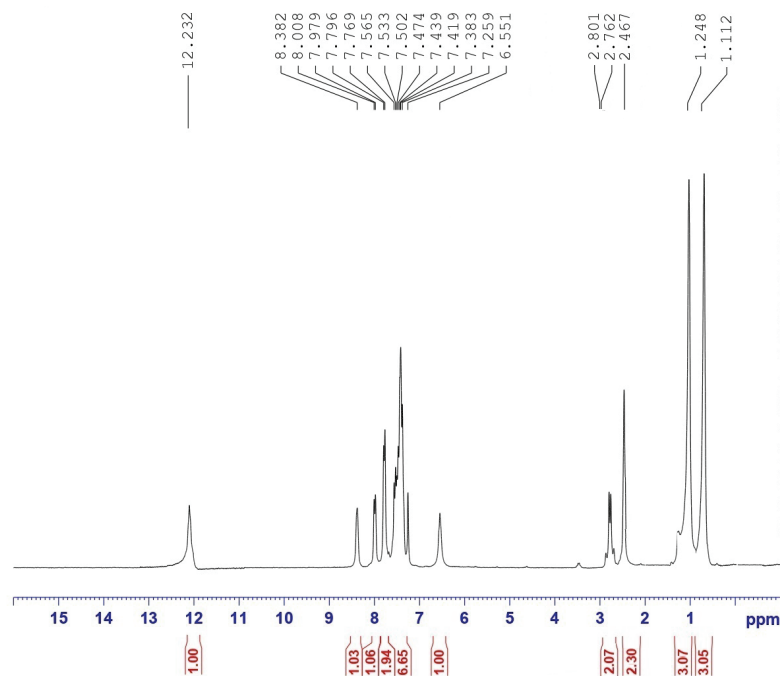
SELECTED ORIGINAL SPECTRA OF THE SYNTHESIZED B-AMIDO-AROYL
CARBONYL DERIVATIVES



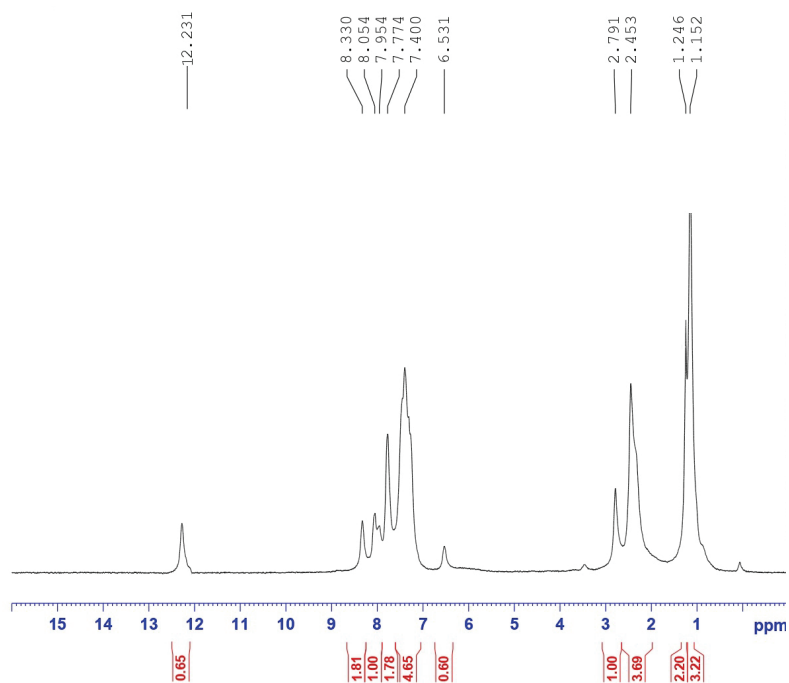
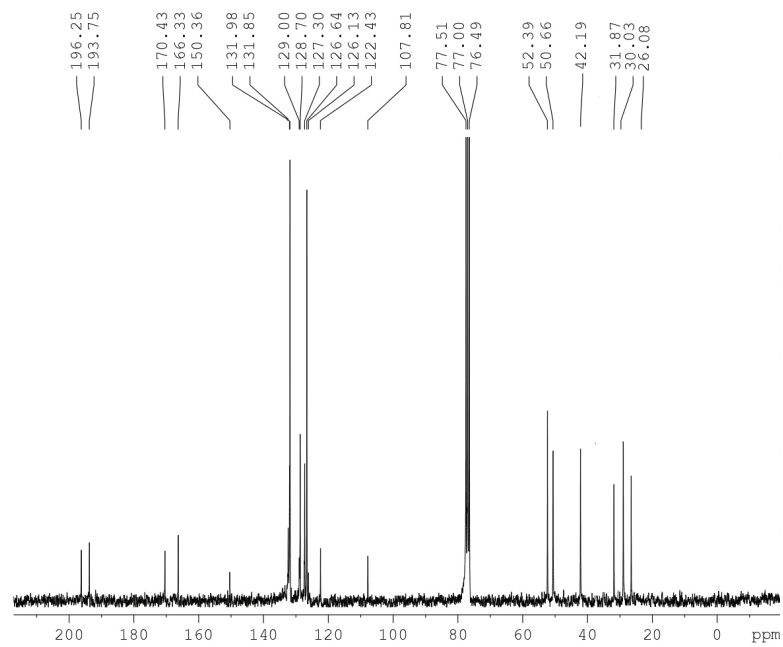
¹H-NMR-4a.

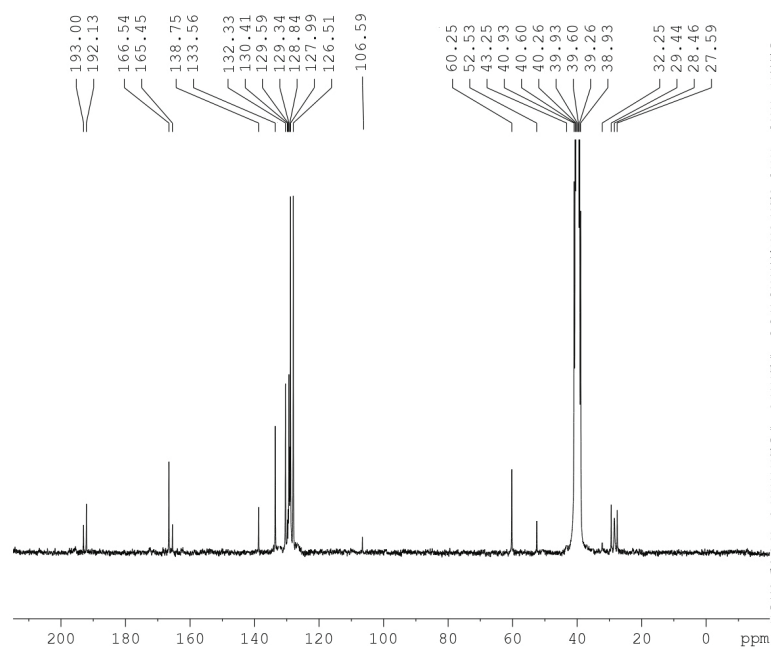


¹³C-NMR-4a.

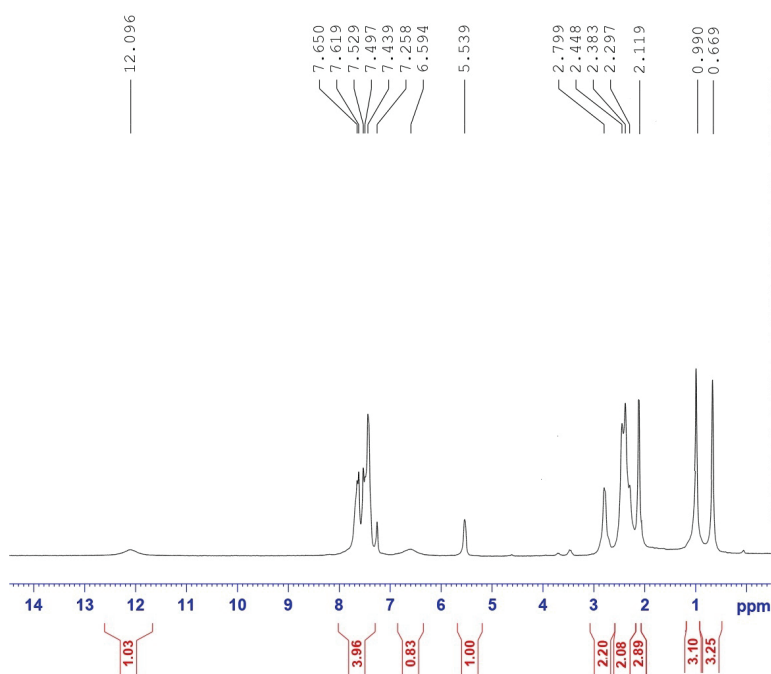


¹H-NMR-4b.

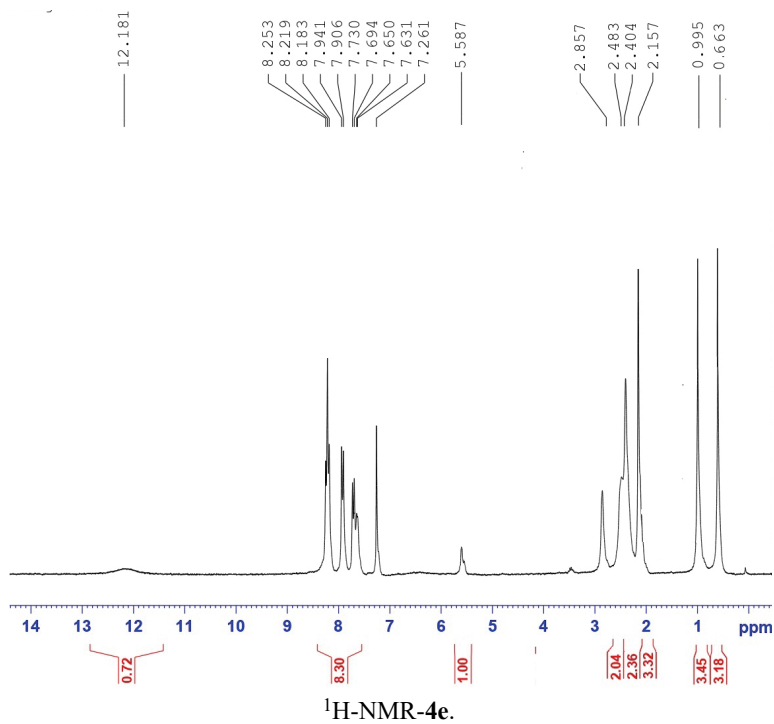
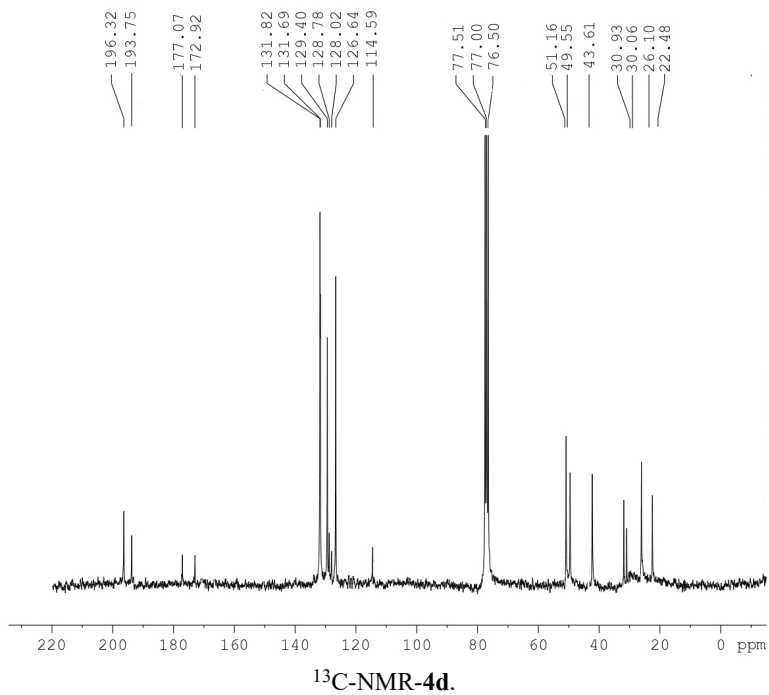


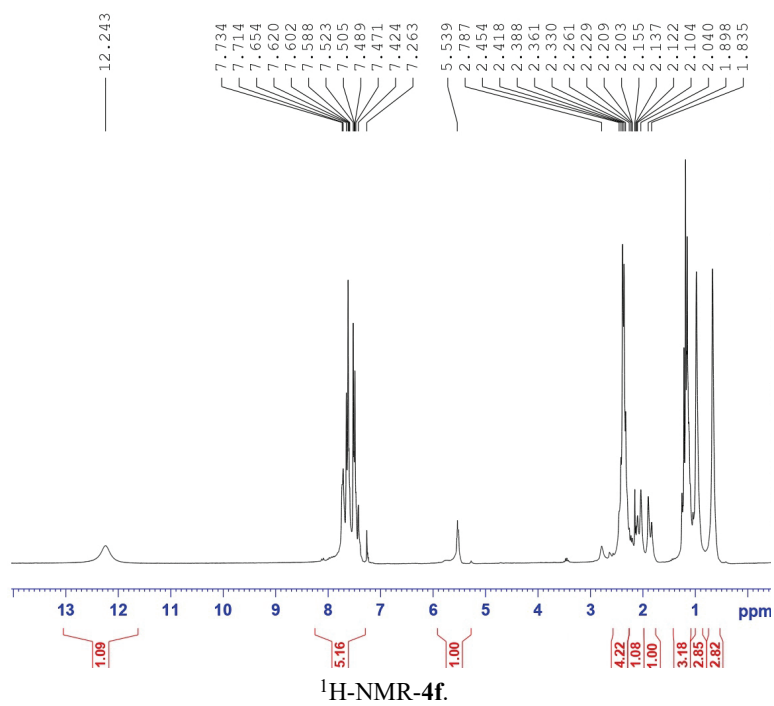
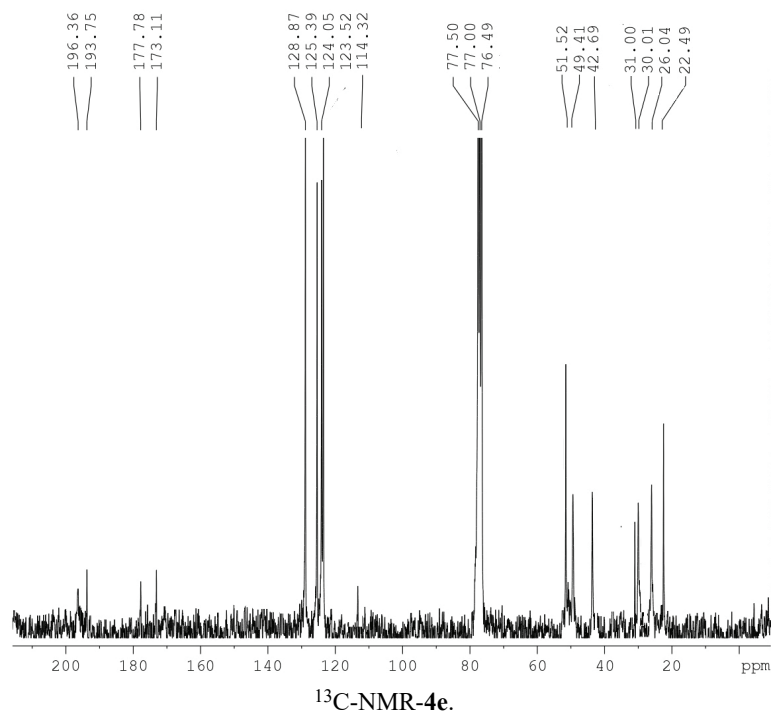


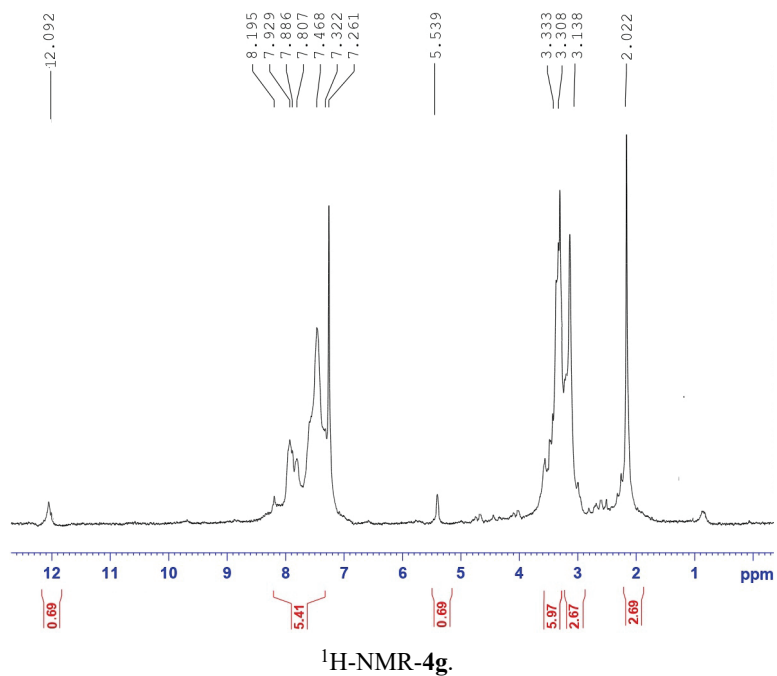
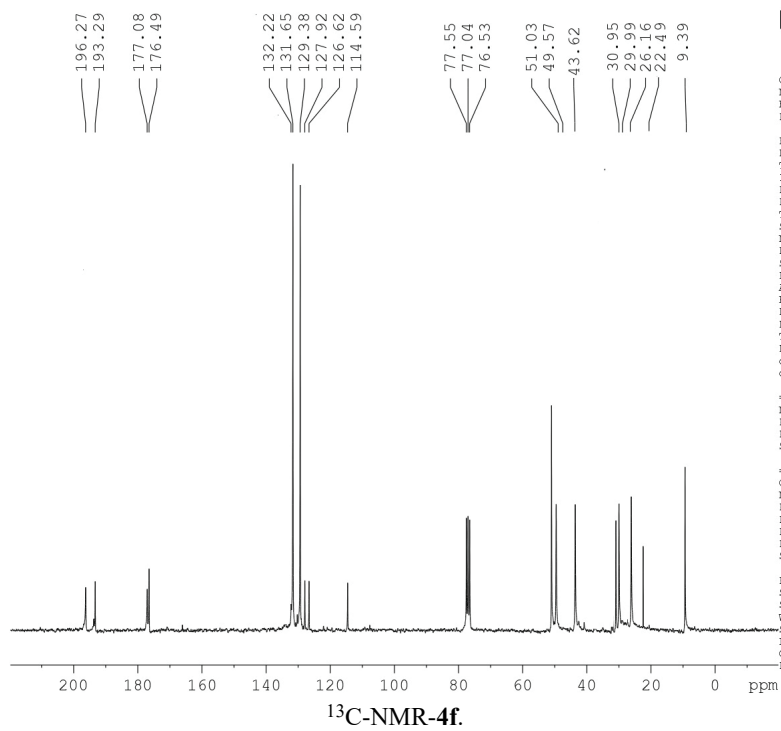
¹³C-NMR-4c.

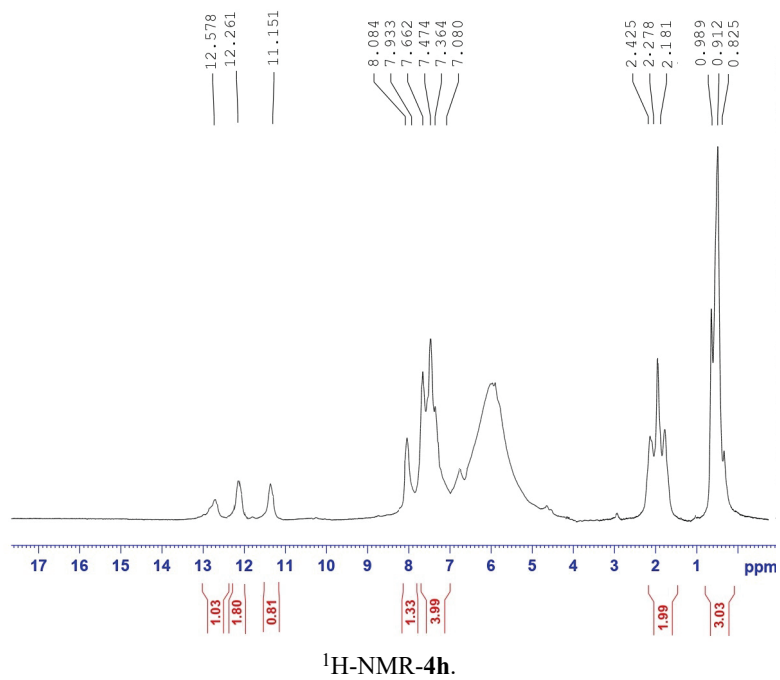
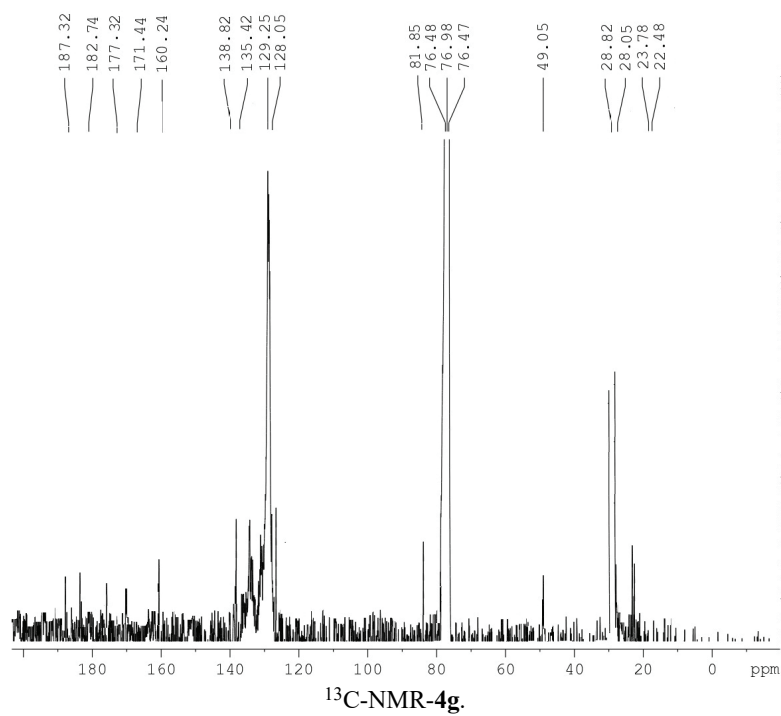


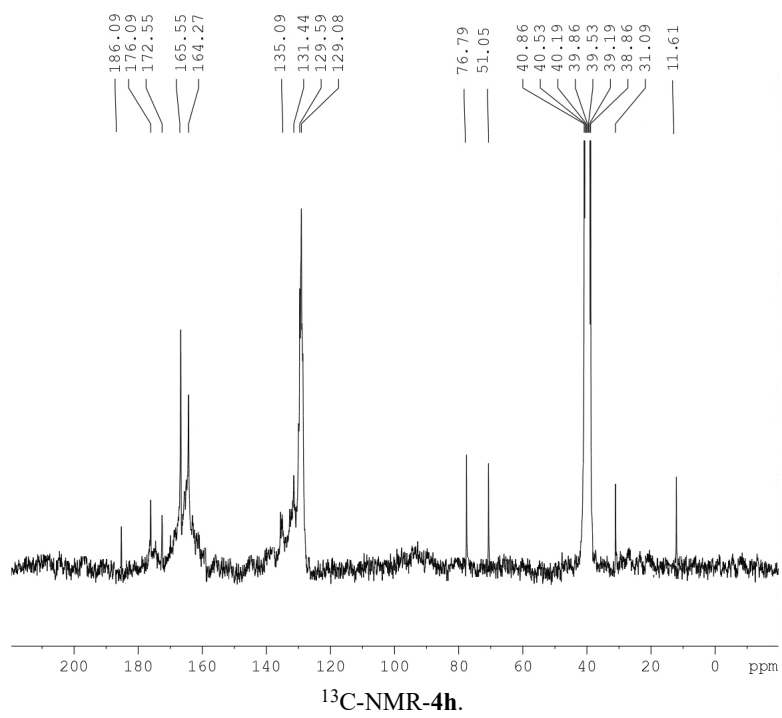
¹H-NMR-4d.













NOTE

Cytotoxicity of amorphous calcium phosphate multifunctional composite coatings on titanium obtained by *in situ* anodization/anaphoretic deposition

MARIJANA R. PANTOVIĆ PAVLOVIĆ^{1,2#}, MIROSLAV M. PAVLOVIĆ^{1*#}, JOVANKA N. KOVAČINA^{1#}, BORIS P. STANOJEVIĆ³, JASMINA S. STEVANOVIĆ^{1,2}, VLADIMIR V. PANIĆ^{1,2,4#} and NENAD L. IGNJATOVIĆ⁵

¹University of Belgrade, Institute of Chemistry, Technology and Metallurgy, National Institute of the Republic of Serbia, Department of Electrochemistry, Belgrade, Serbia, ²Center of Excellence for Environmental Chemistry and Engineering, Institute of Chemistry, Technology and Metallurgy, Belgrade, Serbia, ³Faculty of International Engineering Management, Belgrade, Serbia, ⁴State University of Novi Pazar, Department of Chemical-Technological Science, Novi Pazar, Serbia and ⁵Institute of Technical Science of the SASA, Belgrade, Serbia

(Received 11 February, accepted 23 March 2021)

Abstract: The cytotoxicity of amorphous calcium phosphate (ACP) and chitosan lactate (ChOL) multifunctional and hybrid composite coatings on MRC-5 human lung fibroblast cell line was elucidated. ACP/TiO₂ and ACP/TiO₂/ChOL were deposited onto Ti by a novel *in situ* anodization/anaphoretic process at constant voltage. Cytotoxicity tests showed that there was no significant decrease in the survival of healthy MRC-5 cells exposed to composite samples without chitosan lactate, while there was an increase in the number of viable cells in the sample containing ChOL. These findings show that there was improved cell proliferation, differentiation and cell viability in the ChOL-containing sample, which makes ACP/TiO₂/ChOL coating a good candidate for applications in medicine and stomatology.

Keywords: cytotoxicity; dye exclusion test; colorimetric test with tetrazolium salts; amorphous calcium phosphate; chitosan oligolactate.

INTRODUCTION

Calcium phosphates (CP), amongst which amorphous calcium phosphate (ACP) and hydroxyapatite (HAp), along with TiO₂ layers on Ti, have found vast applications in preventive and regenerative medicine due to their excellent biocompatibility, nontoxic properties and ability to participate in the normal meta-

* Corresponding author. E-mail: mpavlovic@tmf.bg.ac.rs

Serbian Chemical Society member.

<https://doi.org/10.2298/JSC210211024P>

bolism of organisms.^{1–7} New research on chitosan oligolactate (ChOL) coated HAp particles for drug delivery indicated the advanced properties of this derivative.⁴ The authors have already published results about the synthesis, physico-chemical and bioactive properties of new ACP and ChOL-based multifunctional hybrid composite materials by novel *in situ* anodization/anaphoretic process.^{1–3} However, in order to complete the research, there was a need for *in vitro* cytotoxicity tests of the obtained materials, in order to elucidate their biomedical compatibility. This note aims at reporting the cytotoxicity analysis to round up the research on these novel materials.

EXPERIMENTAL

ACP powder, as well as ACP/TiO₂ and ACP/TiO₂/ChOL composite coatings on Ti substrates, made using *in situ* anodization/anaphoretic deposition, were prepared as explained in a previous work.² Briefly, deposition of these coatings was performed at a constant voltage of 60 V for 180 s at 25 °C, starting from prepared suspensions.² Upon synthesis and prior to cytotoxicity tests, the appearance of the coatings were checked by FE–SEM, Tescan Mira 3 XMU FEG–SEM.

Studies on the cytotoxicity of the materials were performed on a human lung fibroblast cell line (MRC-5). The cells were grown attached to a plate (Costar, 25 cm³) in Dulbecco's-modified Eagle's medium with 4.5 g L⁻¹ glucose, 10 mass % fetal calf serum and antibiotic/antimycotic solution, all from Sigma. The temperature was maintained at 37 °C in a 5 % CO₂ (Heraeus) humidity saturated atmosphere. The cells were passaged twice a week and only viable cells in the logarithmic growth phase between the 3rd and 10th passage were used in the experiments.

For the dye exclusion test (DET), viable cells were trypsinized, resuspended and counted in 0.1 % Trypan Blue, then seeded on tested samples (2×10⁵ mL⁻¹) in Petri dishes (Center well, Falcon) at 37 °C, with 5 % CO₂ for 48 h. Control samples had no tested material. After incubation, the cells were counted by an invert microscope (Reichert) in the counting chambers.

After DET, cytotoxicity was investigated from the aspect of cell recovery using colorimetric test with tetrazolium salts (MTT test). Upon incubation, the cells were sieved from the tested substances into fresh medium and viable cells were seeded (5×10³ per 100 µL) in quadruplicate in a 96-well microtiter plate. Plates with seeded cells were tempered at 37 °C in a 5 % CO₂ humidity saturated atmosphere for the next 48 h. Then 10 µL of freshly prepared MTT solution was added to each well and incubation was continued for the next 3 h (at 37 °C, 5 % CO₂). Post incubation, 100 µL of 0.04 mol L⁻¹ HCl in 2-propanol was added to each well. The absorbance was determined immediately after incubation on a microtiter plate reader (Multiscan, MCC/340) at 540 and 690 nm. Medium with MTT served as a control.

RESULTS AND DISCUSSION

The FE-SEM images are shown in Fig. 1 indicating that the synthesized coatings cover the Ti surface evenly, as expected from previous research.^{1,2}

The coatings consist of agglomerated nanoparticles smaller than 100 nm in size. ACP/TiO₂ agglomerates are larger in size, having a rougher surface in comparison to the ACP/TiO₂/ChOL coating. This morphology enabled high level adhesions of the coatings to the substrate.²

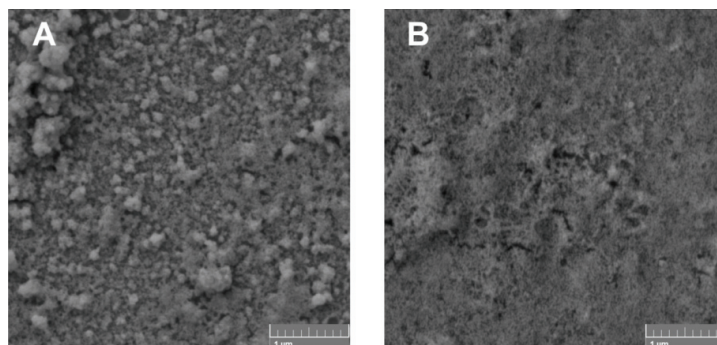


Fig. 1. FE-SEM images of: a) ACP/TiO₂ and b) ACP/TiO₂/ChOL hybrid multifunctional composite coatings on Ti.

The results of cytotoxicity test of DET and MTT assays for MRC-5 cells on Ti, ACP/TiO₂ and ACP/TiO₂/ChOL composite samples are shown in Fig. 2. Cytotoxicity, CI , in the DET assay was calculated as $CI = 100(1 - N_s/N_k)$, and for MTT assay as $CI = 100(1 - A_s/A_k)$, where N_k is the number of cells in the control, N_s is the number of cells in the test samples, A_k is the absorbance of the control and A_s is the absorbance of the test samples.

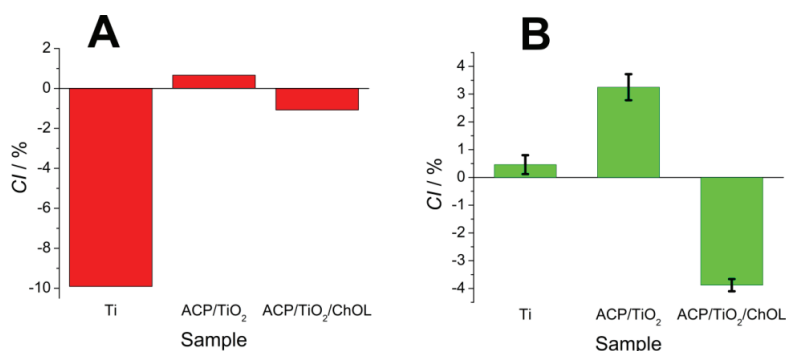


Fig. 2. a) DET cytotoxicity after 48 h and b) MTT cytotoxicity after 48 h + 48 h of recovery for MRC-5 cell line challenged by Ti, ACP/TiO₂ and ACP/TiO₂/ChOL samples.

The results of comparative DET testing of Ti, ACP/TiO₂ and ACP/TiO₂/ChOL composite samples for cytotoxicity towards MRC-5 cells are shown in Fig. 2a. Pure Ti and ACP/TiO₂/ChOL samples showed negative cytotoxicity, *i.e.*, there was an increase in the number of viable cells compared to the control. The survival rate of healthy MRC-5 cells on the composite containing ChOL in relation to the control is 101.1 % in the DET test. ACP/TiO₂ did not exhibit a significant cytotoxic effect (<5 %) toward the examined cell line after 48 h. In general, the ACP/TiO₂ samples showed negligible inhibitory effects on healthy MRC-5 cells.

Comparing the obtained results of the DET (Fig. 2a) and MTT assay (Fig. 2b), it could be noticed that the findings are consistent and do not collide with each other. Both the DET and MTT tests showed that there was no significant reduction in the survival of healthy MRC-5 cells in the ACP/TiO₂ composite sample, whereas Ti showed increased cytotoxicity in the MTT assay. Hence, both ACP/TiO₂ and Ti can still be classified as non-cytotoxic to the MRC-5 cell line.^{4,8,9}

Besides DET, samples having an ACP/TiO₂/ChOL coating also showed negative cytotoxicity in the MTT test. A more pronounced recovery of MRC-5 human lung fibroblasts cells was observed in comparison to control sample after 48 h of recovery. From these results, it could be concluded that not only the ACP/TiO₂/ChOL multifunctional composite coating is non-cytotoxic, but the presence of ChOL in the coating improves cell proliferation, differentiation and cell viability.

Based on the obtained results, it could be concluded that both composite materials used in the studies are non-cytotoxic to the cell lines used, and that 5 mass % of ChOL has a positive effect on the non-toxicity of the material.

CONCLUSIONS

The cytotoxicity of Ti substrate, ACP/TiO₂ and ACP/TiO₂/ChOL biomaterials-coated Ti for possible application in medicine and stomatology was tested in the reported research. Cytotoxicity tests showed that there was no significant decrease in the survival of healthy MRC-5 cells exposed to the Ti substrate and ACP/TiO₂ composite coatings, whereas an increase in the number of viable cells for the ACP/TiO₂/ChOL coating was noticed. Improved cell proliferation, differentiation and cell viability in the presence of ACP/TiO₂/ChOL was found. Based on the presented results and previously published findings on the physico-chemical and bioactive properties of ACP/TiO₂/ChOL composites, it could be concluded that further development of this material and potential preclinical studies would be largely justified.

Acknowledgement. This work was supported by the Ministry of Education, Science and Technological Development of the Republic of Serbia (Grants No. 451-03-9/2021-14/200026 and No. 451-03-9/2021-14/200175).

ИЗВОД
ЦИТОТОКСИЧНОСТ МУЛТИФУНКЦИОНАЛНИХ КОМПОЗИТНИХ ПРЕВЛАКА ОД
АМОРФНОГ КАЛЦИЈУМ-ФОСФАТА НА ТИТАНУ ДОБИЈЕНИХ *IN SITU*
АНОДИЗАЦИЈОМ/АНАФОРЕТСКИМ ТАЛОЖЕЊЕМ

МАРИЈАНА Р. ПАНТОВИЋ ПАВЛОВИЋ^{1,2}, МИРОСЛАВ М. ПАВЛОВИЋ¹, ЈОВАНКА Н. КОВАЧИНА¹, БОРИС П.
СТАНОЈЕВИЋ³, ЈАСМИНА С. СТЕВАНОВИЋ^{1,2}, ВЛАДИМИР В. ПАНИЋ^{1,2,4} и НЕНАД Л. ИГЊАТОВИЋ⁵

¹Институт за хемију, технологију и металургију, Институт од националног значаја за Републику Србију, Универзитет у Београду, Београд, ²Центар изузетних вредности за хемију и инжењеринг животне средине, Институт за хемију, технологију и металургију, Београд, ³Факултет за инжењерски менаџмент, Београд, ⁴Државни Универзитет у Новом Пазару, Дејаршман за хемијско-технолошке науке, Нови Пазар и ⁵Институт техничких наука САНУ, Београд

Приказани су резултати испитивања цитотоксичности мултифункционалних и хибридних композитних превлака на бази аморфног калцијум-фосфата (ACP) и хитозан-олиголактата (ChOL) на титану према MRC-5 ћелијској линији хуманих фибробласта плућа. ACP/TiO₂ и ACP/TiO₂/ChOL су исталожени новим *in situ* поступком анодизације/анафоретског таложења под константним напоном од 60 V током 180 s на 25 °C. Тести цитотоксичности су показали да није дошло до значајног смањења преживљавања здравих MRC-5 ћелија код композита који не садржи ChOL, док је код оних са додатим ChOL дошло до повећања броја одрживих ћелија. Резултати показују да је побољшана пролиферација, диференцијација и одрживост ћелија у узорку са ChOL, што овај узорак чини добрим кандидатом за примену у медицини и стоматологији.

(Примљено 11. фебруара, прихваћено 23. марта 2021)

REFERENCES

1. M. Pantovic-Pavlovic, M. Pavlovic, S. Erakovic, T. Barudzija, J. Stevanovic, N. Ignjatovic, V. Panic, *J. Serb. Chem. Soc.* **84** (2019) 1305 (<https://doi.org/10.2298/jsc190730105p>)
2. M. R. Pantović Pavlović, M. M. Pavlović, S. Eraković, J. S. Stevanović, V. V. Panić, N. Ignjatović, *Mater. Lett.* **261** (2020) 127121 (<https://doi.org/10.1016/j.matlet.2019.127121>)
3. M. R. Pantović Pavlović, S. G. Eraković, M. M. Pavlović, J. S. Stevanović, V. V. Panić, N. L. Ignjatović, *Surf. Coat. Technol.* **358** (2019) 688 (<https://doi.org/10.1016/j.surfcoat.2018.12.003>)
4. N. L. Ignjatović, M. Sakač, I. Kuzminac, V. Kojić, S. Marković, D. Vasiljević-Radović, V. M. Wu, V. Uskoković, D. P. Uskoković, *J. Mater. Chem., B* **6** (2018) 6957 (<https://doi.org/10.1039/c8tb01995a>)
5. N. L. Ignjatovic, Z. R. Ajdukovic, V. P. Savic, D. P. Uskokovic, *J. Biomed. Mater. Res., B* **94** (2010) 108 (<https://doi.org/10.1002/jbm.b.31630>)
6. C. Qi, J. Lin, L. H. Fu, P. Huang, *Chem. Soc. Rev.* **47** (2018) 357 (<https://doi.org/10.1039/c6cs00746e>)
7. W. Habraken, P. Habibovic, M. Epple, M. Bohner, *Mater. Today* **19** (2016) 69 (<https://doi.org/10.1016/j.mattod.2015.10.008>)
8. T. Puškar, B. Trifković, D. D. Koprivica, V. Kojić, A. Jevremović, S. Mirković, D. Eggbeer, *Vojnosanitetski Pregled* **76** (2019) 502 (<https://doi.org/10.2298/VSP170721127P>)
9. G. Sjögren, G. Sletten, J. E. Dahl, *J. Prosthet. Dent.* **84** (2000) 229 (<https://doi.org/10.1067/mpr.2000.107227>).



J. Serb. Chem. Soc. 86 (6) 561–570 (2021)
JSCS–5443

3D-QSAR study of adenosine 5'-phosphosulfate (APS) analogues as ligands for APS reductase

SLAVICA ERIC^{1*}, ILIJA CVIJETIĆ² and MIRE ZLOH^{3,4}

¹University of Belgrade – Faculty of Pharmacy, Vojvode Stepe 450, 11221 Belgrade, Serbia,

²University of Belgrade – Innovation Center of the Faculty of Chemistry, Studentski trg 12–16, 11000 Belgrade, Serbia, ³Nanopuzzle Medicines Design, Stevenage, United Kingdom and

⁴Faculty of Pharmacy, University Business Academy, Novi Sad, Serbia

(Received 28 November 2020, revised 21 January, accepted 26 February 2021)

Abstract: Metabolism of sulfur (sulfur assimilation pathway, SAP) is one of the key pathways for the pathogenesis and survival of persistent bacteria, such as *Mycobacterium tuberculosis* (Mtb), in the latent period. Adenosine 5'-phosphosulfate reductase (APSR) is an important enzyme involved in the SAP, absent from the human body, so it might represent a valid target for development of new antituberculosis drugs. This work aimed to develop 3D-QSAR model based on the crystal structure of APSR from *Pseudomonas aeruginosa*, which shows high degree of homology with APSR from Mtb, in complex with its substrate, adenosine 5'-phosphosulfate (APS). 3D-QSAR model was built from a set of 16 nucleotide analogues of APS using alignment-independent descriptors derived from molecular interaction fields (MIF). The model improves the understanding of the key characteristics of molecules necessary for the interaction with target, and enables the rational design of novel small molecule inhibitors of Mtb APSR.

Keywords: sulfur assimilation pathway; interactions; MIF; pentacle; PLS.

INTRODUCTION

Various studies showed that the metabolic pathway of sulfur (sulfur assimilation pathway, SAP) is crucial for the survival of persistent bacteria, such as *Mycobacterium tuberculosis* (Mtb) in the latent period, after adaptation on primary cell response from the host.^{1–3} This pathway provides reduced form of sulfur which serves for biosynthesis of a number of metabolites, including cysteine, methionine, various coenzymes, as well as mycothiol.⁴ The metabolic pathway of sulfur starts with the active transport of sulfates catalyzed by sulfate-permease. Adenylation catalyzed by ATP sulfurylase (CysD) yields adenosine-5'-phosphosulfate (APS). This product is then converted to sulfite and adenosine by APS-

* Corresponding author. E-mail: seric@pharmacy.bg.ac.rs
<https://doi.org/10.2298/JSC201128015E>

reductase (APSR), with cofactor thioredoxin.⁵ APSR is not synthesized in human organism, therefore could be one of the selective targets for blocking sulfur metabolic pathway. Upregulation of CysH, that codes APSR, was observed during the resting state of bacteria, as well as during exposition to hydrogen peroxide and starving, which suggests that APSR is activated immediately after the initial infection and allows survival of bacteria.⁶

Recently, small-molecule inhibitors of APS reductase were discovered through virtual ligand screening.⁷ However, it was stated that the development of more specific and potent inhibitors would be greatly aided through knowledge of the functional importance of interactions between the substrate and enzyme at the active site. For that purpose, several analogues of APS were synthesized and their affinities for APSR were experimentally determined. These studies define chemical groups that are essential for molecular recognition and reveal a network of electrostatic interactions, which play an important role in substrate discrimination. To gain further insight into substrate recognition of Mtb APS reductase, energetic contribution of individual portions of APS to the enzyme-binding interaction was analyzed.

For further contribution in design of APSR inhibitors, we used 16 synthesized analogues with determined K_d values for generation of pharmacophoric model based on interactions of ligands with the active site of homologous APSR. Since three-dimensional structure of Mtb APSR is not known, we used the structure of APS in complex with APSR of *Pseudomonas aeruginosa*, that shows high degree of homology (27.2 % identical sequences and 41.4 % similar). As expected for phylogenetically related proteins, the highest degree of similarity was observed for the APSR active site residues.⁶ Using a known structure of natural substrate for APSR and its 16 structural analogues, alignment-independent 3D-QSAR model was developed from the MIF-based descriptors. The model was interpreted in order to elucidate interactions between APS analogues and APSR. The obtained pharmacophoric hot-spots could serve as the basis for rational design of novel APSR inhibitors.

EXPERIMENTAL

The structure of APS ligand was retrieved from the complex with APSR from *P. aeruginosa* (PDB code 2GOY). Since three-dimensional (3D) crystal structure of APSR of Mtb is not defined, structural data from the complex of APS with *P. aeruginosa*, showing high degree of homology,⁸ were utilized for QSAR studies.

The set of 16 APS analogues, along with their K_d values are collected from literature⁵ and in house laboratory data that are not published yet. The conformer ensemble for each molecule was generated by Omega – e,^{9,10} and conformers most similar to the conformation of natural APS ligand were selected by vROCS.^{11,12} These conformers were used for generation of 3D-QSAR models, computing GRIND descriptors from the encoded molecular interaction fields (MIF) in Pentacle program.¹³ MIFs characterize the interaction features of a molecule with the environment which could be mapped using chemical probes. Four mole-

cular probes mapping different chemical/pharmacophoric features of ligands were applied in this study: DRY probe that simulates hydrophobic interactions of molecules with active center of the target; N1 probe (amide nitrogen) mapping hydrogen-bonding acceptors (HBA) of a ligand; O probe (carbonyl oxygen) mapping hydrogen-bonding donors (HBD), and TIP probe showing what shape of the molecules fits within the active center of the enzyme. The MIFs are computed by placing the molecule in a grid having certain, predefined resolution. The chemical probes are then positioned at each nodal point and the corresponding interaction energy is computed. Obtained interaction energies represent the molecular descriptors of hydrophobic, hydrogen bonding interactions, and shape complementarity with the protein target.

RESULTS AND DISCUSSION

Chartron *et al.* published 3D crystal structure of APSR of bacterium *P. aeruginosa* in complex with the substrate (APS).¹⁴ APSR of *P. aeruginosa* and *M. tuberculosis* show high degree of homology (27.2 % of identical sequences and 41.4 % of similar), especially within the active site. This structure was the base for investigation of significant interactions between enzyme and substrate, which could give an idea for rational design of potential APSR inhibitors.

Hong *et al.*⁵ performed structure–activity study of various substrates and product analogues in order to analyse molecular determinants important for binding and specificity on APSR. Study showed that binding of dianions is more favorable compared to monoanions. Analysis of adenosine, D-ribose and adenine fragments showed that they exhibit weak binding affinity comparing to the whole molecule. Detailed study of substrates and products showed: loss of sulphate reduces binding affinity, β -sulphate groups play a modest role in recognition of substrate, sulphur substitution is considered to be a good mimic of the phosphate moiety because it is isosteric, pseudoisoelectronic, and similar charge distribution and net charge at physiological pH. Contribution of α - β bridging oxygen was analysed in respect to geometry, charge density and distribution, as well as ionization state of the molecules. The substitution of α -nonbridging oxygen by sulphur, indicated possible disruption of contacts with residues, which could be important for stabilizing charge development in transition state. The similarity of K_d for different analogues, however, could possibly indicate the different modes of nucleotide binding, so further studies should be performed for detailed mechanisms of action.

This study provides additional insights into ligand binding to APSR. The hydrophobic, shape and hydrogen bonding properties of 16 nucleotide analogues of APS (Table S-I of the Supplementary material to this paper) are quantified by computing GRID molecular interaction fields (MIFs). This ligand-based approach utilized the bioactive conformation of APS in complex with *P. aeruginosa* APSR. The most similar conformation was extracted from the conformer ensemble of ligands and used for model generation. The interaction profiles are encoded into alignment-independent GRIND independent descriptors (GRid) descriptors and correlated with inhibitory activities to develop 3D-QSAR models.^{5,7} GRIND

descriptors describe the most important network interactions as a function of distance instead of describing precise position of every point in the net.

Compounds from the data set were classified, on the basis of structural similarity, into three main groups: 1) adenosine 5'-monophosphate (AMP) and analogues: 3'-AMP, 5'-AMP, AMPS, AMPCF2P, AMPCP, AMPNP and AMPPN; 2) adenosine 5'-diphosphate (ADP) and analogues: 3',5'-ADP, ADP α S, ADP β S and ADP β F; 3) APS and analogues: APS α S and APS β M. Structural modifications in analogues are explained in the text.⁵

The large differences in APSR inhibitory activity were observed between three classes of compounds, indicating that slight differences in structure lead to significant changes in protein-ligand binding. For example, the K_d values for APS, ADP and AMP are 0.2, 4.3 and 5.4 μ M, respectively. Following classification of compounds, the groups of ligands were further investigated. APS is a natural ligand of APS reductases with K_d value of 0.2 μ M. Replacing sulfate group of APS with phosphate, as it is in the case of ADP, or by elimination of that group in AMP, the affinity for APS reductase decreases, which proves the importance of this group. Phosphate and sulfate groups are of similar size and shape, and they differ in the net charge. Sulfate group is mono-anion (charge -1) whilst phosphate group is di-anion (charge -2). Additional insights into the important structural and pharmacophoric features were obtained from the 3D-QSAR model.

The preliminary SAR complemented by the analysis of GRIND descriptors

Fig. 1 shows all interactions that natural ligand APS might form with the active site of APSR, including possibility of hydrophobic interactions, H-bond donors, H-bond acceptors, as well as favorable shape of the molecule.

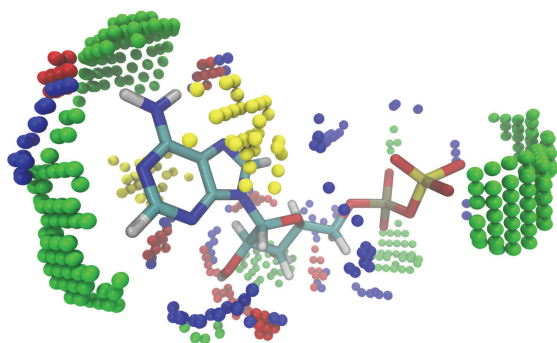


Fig. 1. Interactions of APS and active place of APSR: hydrophobic interactions (yellow), H-bond donors (blue), H-bond acceptors (red), MIFs describing the favorable shape of the molecule (green).

Concerning shape analysis, the significant differences were observed between APS, ADP and AMP. The most significant differences are observed between 6.8 and 10.4 \AA , where APS shows significant shape complementarity

while ADP do not exert such interactions and do not completely fit within the active site.

The net charge for AMP and APS is the same, -2 , which is a prerequisite for excellent binding to APSR.⁵ Similar binding of two ligands is visible in TIP–TIP correlograms, where AMP shows favorable regions. The difference is that the charge of AMP is localized in α -position, and the implications of such charge arrangement on binding affinity will be further discussed.

The analysis of hydrophobic interactions indicated that purine part of the ligand is responsible for the hydrophobic interactions with the active site of enzyme. The heatmaps of DRY–DRY interactions show that APS forms the weakest hydrophobic interactions on short distance (between 3.8 and 5.6 Å), whilst interactions with ADP are the strongest. This could be the consequence of the particular conformation of ADP that enables intramolecular hydrogen bonding between the oxygen on β -phosphate and $-\text{NH}$ at position 2 of purine ring. We suppose that additional intramolecular bonding decreases the overall binding affinity for APSR. As the position 2 of purine ring does not establish energetically favorable interactions within the APS reductase active site,⁵ its modification to $=\text{CH}-$ will probably lead to more potent analogues.

To study whether the decreased binding affinity of ADP is connected with additional charge of phosphate group in β -position, we further evaluated how the replacement of negatively charged oxygen (ADP) with sulfur (ADP β S) or fluorine (ADP β F) atoms influence the binding affinity. Two analogues show higher degree of binding for APS reductase, whilst significant improvement is observed for compound ADP β S. Higher affinity of ADP β S compared to ADP β F might be explained by larger size and polarizability of S atom. This substitution might enable the additional interactions that improve fitting of ligand in the active site. Additional hydrophobic interactions could be observed at the distances from 4.0 to 5.6 Å and 8.0–9.6 Å.

The replacement of negatively charged oxygen in α -position of ADP with sulfur also increases the binding affinity. Better shape complementarity of ADP α S with the active site is observed in the range between 7.2 and 12.0 Å.

The introduction of phosphate at 3'-OH of ribose yields 3'5'-ADP with significantly decreased binding energy. The changes in the skeleton of the molecule imposed by the introduction of additional ribose moiety reflect in the restricted conformational freedom and possibly lower fit with the APS reductase. Weaker DRY–DRY interactions of 3'5'-ADP compared to ADP and ADP β S are observed at the distance range from 4.4 to 9.6, suggesting that certain portion of important hydrophobic interactions are missing.

Concerning APS analogues, modification of APS in α and β -positions decreases the binding energy. In general, APS α S can be a substrate for APSR, but in the case of saturation of enzyme with the substrate there is no evidence that inter-

medier, *S*-sulfocysteine, could be formed.⁵ It is not clear why APSR does effectively reduce APS α S. By analogy with α -S substitution in ADP, one of the explanations would be that the added S is an obstacle for contact with amino acid residues of active center of enzyme, while at the same time allowing the formation of some unfavorable hydrophobic interactions at the distance range from 3.6 to 5.6 and 7.6–9.2 Å.

In APS β M, oxygen bridge was replaced with methylene with an idea to explain the importance of this bridge during binding with enzyme. The binding energy decreased significantly, and the reason could be that methylene bridge increases the length of S–X–P bond and decreases the angle of rotation. It is also reflected as an increase in hydrophobic interactions with APSR between 4.4 and 5.6 Å and 7.6 and 8.4 Å. In further text, the importance of oxygen bridge will be explained through the analysis of AMP and its analogues.

The AMP is an important part of APS and plays role in enzyme recognition. However, the binding affinity of AMP for APSR is smaller comparing to ADP and ASP. It indicates that P α –O–S β bridge is essential for the activity. To determine the importance of oxygen in the bridge we compared the following AMP analogues: AMPCP, AMPCF2P and AMPNP. Each derivative has smaller binding affinity comparing to ADP and ASP. Among those analogues, the highest affinity is observed for AMPCF2P and lowest for AMPNP. However, concerning the size of AMPNP, it fits better within active site of enzyme than AMPCF2P, as observed on heatmaps of TIP–TIP interactions at the distance between 4.4 and 8.6 Å. It could be the consequence of voluminous –CF₂– bridge that hinders fitting of compound into active site.

The neutralization of negatively charged oxygen in β -position decreases the activity. Consequently, the activity of AMPPN is significantly lower than the activity of AMPNP. On DRY–DRY correlograms, it can be seen that AMPPN forms weak hydrophobic interactions at the distance between 4.0 and 5.6 Å, and 8.4 and 9.6 Å, opposite to AMPNP. This trend might be explained by the protonation of β -NH₂ group at physiological pH and subsequent formation of intramolecular electrostatic interactions that prevent ligand binding to enzyme.⁵

The influence of α -substituents was further investigated by comparing the biological activities of AMP and α -substituted derivatives with sulfur (5'-AMPS) or amino group (5'-AMPN). Better shape complementarity of 5'-AMPS compared to AMP is indicated through stronger TIP–TIP interactions between 12.0 and 14.4 Å, allowing better fit into the APS reductase active site and lower K_d values (3.3 vs. 5.4 μ M).

A significant decrease in binding affinity of 5'-AMPN analogue might also be explained through the formation of additional hydrogen bonds that prevent optimal fitting of substrate in the active site. This is visible from the differences in O–N1 interactions at the larger distances (from 15.2 to 17.2 Å), where 5'-

-AMPN forms hydrogen bonds while AMP cannot establish these interactions with the environment.

Table with structures and K_d values used in the study is presented in Table S-I, as well as in figures connected with the preliminary QSAR studies: TIP-TIP interactions for ADP and APS, and TIP-TIP probe heatmap for ADP, AMP and APS (Fig. S-1 of the Supplementary material), the location of favorable hydrophobic interactions of ADP mapped using DRY probe (Fig. S-2 of the Supplementary material), differences in DRY-DRY interactions that ADP β F and ADP β S form with target and differences in TIP-TIP interactions ADP α S and ADP (Fig. S-3 of the Supplementary material), DRY-DRY interactions that ADP β S and ADP β F form with enzyme (Fig. S-4 of the Supplementary material), differences in DRY-DRY interactions between APS and APS α S, and APS and APS β M (Fig. S-5 of the Supplementary material), TIP-TIP interactions for AMPCF2P and AMPNP (Fig. S-6 of the Supplementary material), TIP-TIP interaction 5'-AMPS and AMP and O-N1 interaction 5'-AMPN and AMP (Fig. S-7 of the Supplementary material) and the structural features associated with the additional variables positively and negatively correlated with the APS reductase inhibitory activity (Fig. S-8 of the Supplementary material).

Partial least square regression model

To establish the quantitative relation between the biological activity and computed GRIND descriptors, partial least square (PLS) regression was applied. The optimum model, by means of r^2 and q^2 , was generated using 3 latent variables (LV). Further increase in the number of LV didn't improve the statistical quality of the model. Statistically acceptable models are those with $r^2 > 0.5$ and $q^2 > 0.9$.

The statistical parameters of the developed model are shown in Table I.

TABLE I. The statistics of PLS model developed for the APS reductase inhibitory activity of APS analogues; SSX – X variable explanation; $SSXacc$ – X accumulation (cumulative value); $SDEC$ – standard deviation of error of calculation; $SDEP$ – standard deviation of error of prediction; r^2acc – r^2 accumulation; q^2acc – q^2 accumulation

LV	SSX	$SSXacc$	$SDEC$	$SDEP$	$r^{2\#a}$	$r^{2acc\#b}$	$q^{2acc\#c}$
1	30.75	30.75	0.89	1.15	0.52	0.52	0.19
2	21.05	51.8	0.57	0.95	0.28	0.8	0.44
3	7.7	59.51	0.37	0.94	0.12	0.92	0.46
4	9.92	69.42	0.27	0.94	0.04	0.96	0.46
5	4.23	73.66	0.18	0.98	0.03	0.98	0.41

From the PLS scores plot (Fig. 2) several variables positively and negatively correlated with the biological activity are observed.

The most significant variables obtained in PLS analysis are presented in Table II. Each variable represents the product of interaction energies of two

chemical probes at certain distance. PLS correlates these variables with biological activity where positive variable values indicate positive influence on biological activity and vice versa.

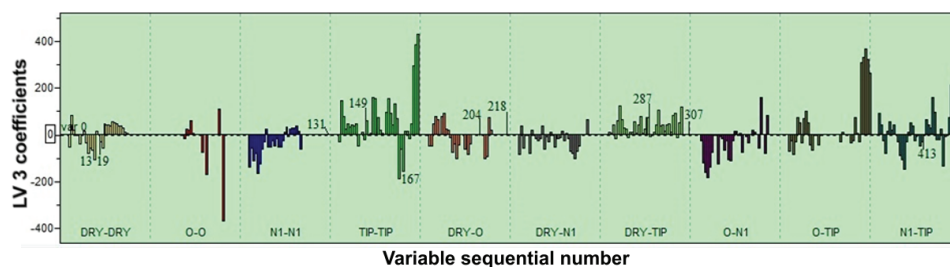


Fig. 2. PLS scores plot for 3LV model where the most significant variables are labeled.

TABLE II. The most significant variables obtained by PLS analysis

Variable	Distance, Å	Correlogram	The influence on activity
13	5.2-5.6	DRY-DRY	Negative
19	7.6-8.0	DRY-DRY	Negative
149	3.2-3.6	TIP-TIP	Positive
167	10.4-10.8	TIP-TIP	Negative
287	2.0-2.4	DRY-TIP	Positive
393	16.4-16.8	O-TIP	Positive
413	14.8-15.2	N1-TIP	Negative

CONCLUSION

Concerning that APSR is essential for the survival of mycobacteria in latent phase of infection, discovery of small molecules that would inhibit its action is of interest for the development of new potential antitubercotics. In this study, the set of synthesized ligands for APSR was studied using 3D QSAR methodology with the descriptors derived from MIFs. Compounds from the data set, 16 analogues of natural substrate, were classified on the base of structural similarity, into three main groups: 1) AMP and analogues, 2) ADP and analogues and 3) APS and analogues.

Significant differences in APSR inhibitory activity, probed on DRY, O, N1 and TIP interactions, were observed between three classes of compounds, indicating that slight differences in structure leads to significant changes in protein-ligand binding. Studies showed the differences of analogues in shape complementarity. Interactions with active site were also influenced by modifications in α and β positions, charge, size and polarizability of groups and atoms, conformational freedom, as well as protonation at physiological pH. Quantitative relation between biological activity and computed GRIND descriptors was established by partial least square (PLS) regression. The optimum model ($r^2_{acc} = 0.92$ and

$q^2_{acc} = 0.46$) was generated using 3 latent variables (LV). The most significant variables obtained in PLS analysis were further interpreted.

SUPPLEMENTARY MATERIAL

Additional data are available electronically at the pages of journal website: <https://www.shd-pub.org.rs/index.php/JSCS/index>, or from the corresponding author on request.

Acknowledgement. This work was supported by Ministry of Science, Education and Technological Development of Republic of Serbia under contract with University of Belgrade – Faculty of Pharmacy (No 451-03-9/2021-14/200161) and Innovation Center of the Faculty of Chemistry, University of Belgrade (No 451-03-68/2020-14/200168).

ИЗВОД

3D-QSAR СТУДИЈА АНАЛОГА АДЕНОЗИН 5'-ФОСФОСУЛФАТА (APS) КАО ЛИГАНДА ЗА APS РЕДУКТАЗУ

СЛАВИЦА ЕРИЋ¹, ИЛИЈА ЦВИЈЕТИЋ² И МИРЕ ЗЛОХ^{3,4}

¹Универзитет у Београду, Фармацеутички факултет, Војводе Степе 450, 11 221 Београд, Србија;

²Универзитет у Београду, Иновациони центар Хемијског факултета, Студентски пут 12-16, 11 000 Београд, Србија; ³Nanopuzzle Medicines Design, Stevenage, United Kingdom; ⁴Фармацеутички факултет, Универзитет Привредна Академија, Нови Сад, Србија

Метаболизам сумпора (пут асимилације сумпора, SAP) један је од кључних путева за патогенезу и преживљавање *Mycobacterium tuberculosis* (Mtb) у латентном периоду. Аденозин 5'-фосфосулфат редуктаза (APSR) је значајан ензим који је укључен у SAP, не налази се у људском организму и може бити валидно циљно место за развој нових анти-туберкулотика. Циљ овог рада је развој 3D-QSAR модела који се заснива на кристалној структури APSR из *Pseudomonas aeruginosa*, који има висок степен хомологије са APSR из Mtb, у комплексу са супстратом, аденозин 5'-фосфосулфатом (APS). 3D-QSAR модел је постављен коришћењем сета 16 нуклеотидних аналога APS применом дескриптора независних од поларних тачака, изведених из поља молекуларних интеракција (MIF). Модел служи за боље разумевање кључних карактеристика молекула неопходних за интеракцију са циљним местом, у сврху рационалног дизајнирања малих молекула, инхибитора APSR из Mtb.

(Примљено 28. новембра 2020, ревидирано 21. јануара, прихваћено 26. фебруара 2021)

REFERENCES

1. R. Schnell, G. Schneider, *Biochem. Biophys. Res. Comm.* **396** (2010) 33 (<https://doi.org/10.1016/j.bbrc.2010.02.118>)
2. O. Poyraz, K. Brunner, B. Lohkamp, H. Axelsson, L. G. J. Hammarström, R. Schnell, G. Schneider, *PLOS ONE* **10** (2015) e0121494 (<https://doi.org/10.1371/journal.pone.0127016>)
3. R. Iwanicka-Nowicka, A. Zielak, A. M. Cook, M. S. Thomas, M. M. Hryniewicz, *J. Bacteriol.* **189** (2007) 1675 (<https://doi.org/10.1128/JB.00592-06>)
4. P. B. Palde, A. Bhaskar, L. E. Pedro Rosa, F. Madoux, P. Chase, V. Gupta, T. Spicer, L. Scampavia, A. Singh, K. S. Carroll, *ACS Chem. Biol.* **11** (2015) 172 (<https://doi.org/10.1021/acscchembio.5b00517>)
5. J. A. Hong, D. P. Bhave, K. S. Carroll, *J. Med. Chem.* **52** (2009) 5485 (<https://doi.org/10.1021/jm900728u>)

6. S. K. Hatzios, C. R. Bertozzi, *PLOS Pathog* **7** (2011) e1002036 (<https://doi.org/10.1371/journal.ppat.1002036>)
7. S. Cosconati, J. A. Hong, E. Novellino, K. S. Carroll, D. S. Goodsell, A. J. Olson, *J. Med. Chem.* **51** (2008) 6627 (<https://doi.org/10.1016/j.biotechadv.2011.08.021>)
8. H. Wieman, K. Tøndel, E. Anderssen, F. Drabløs, *Mini Rev. Med. Chem.* **4** (2004) 79 (<https://doi.org/10.2174/1389557043403639>)
9. *OMEGA 2.5.1.4: OpenEye Scientific Software*, Santa Fe, NM (<http://www.eyesopen.com>)
10. P. C. D. Hawkins, A. G. Skillman, G. L. Warren, B. A. Ellingson, M. T. Stahl, *J. Chem. Inf. Model.* **50** (2010) 572 (<https://doi.org/10.1021/ci100031x>)
11. ROCS 3.2.1.4: OpenEye Scientific Software, Santa Fe, NM (<http://www.eyesopen.com>)
12. P. C. D. Hawkins, A. G. Skillman, A. Nicholls, *J. Med. Chem.* **50** (2007) 74 (<https://doi.org/10.1021/jm0603365>)
13. M. Pastor, G. Cruciani, I. McLay, S. Pickett, S. Clementi, *J. Med. Chem.* **43** (2000) 3233 (<https://doi.org/10.1021/jm000941m>)
14. J. Chartron, K. S. Carroll, C. Shiau, H. Gao, J. A. Leary, C. R. Bertozzi, C. David Stout C. *J. Mol. Biol.* **364** (2006) 152 (<https://doi.org/10.1016/j.biotechadv.2011.08.021>).

SUPPLEMENTARY MATERIAL TO
3D-QSAR study of adenosine 5'-phosphosulfate (APS) analogues as ligands for APS reductase

SLAVICA ERIĆ^{1*}, ILIJA CVIJETIĆ² and MIRE ZLOH^{3,4}

¹University of Belgrade – Faculty of Pharmacy, Vojvode Stepe 450, 11221 Belgrade, Serbia,

²University of Belgrade – Innovation Center of the Faculty of Chemistry, Studentski trg 12–16, 11000 Belgrade, Serbia, ³Nanopuzzle Medicines Design, Stevenage, United Kingdom and

⁴Faculty of Pharmacy, University Business Academy, Novi Sad, Serbia

J. Serb. Chem. Soc. 86 (6) (2021) 561–570

TABLE S-I. The structures of nucleoside analogues of APS and inhibition constants toward APSR

Compound	Structure	$K_d / \mu\text{M}$	Compound	Structure	$K_d / \mu\text{M}$
ADPβS		0.15	AMPPN		410
ADPαS		0.80	APSβM		700
ADPβF		2.5	5'-AMPS		3.3

* Corresponding author. E-mail: seric@pharmacy.bg.ac.rs

Compound	Structure	$K_d / \mu\text{M}$	Compound	Structure	$K_d / \mu\text{M}$
ADP		4.3	5'-AMPN		100
AMPCF ₂ P		13	3'5'-ADP		700
AMPCP		27	3'-AMP		3200
APSA		43	AMP		5.4
AMPNP		260	APS		0.2

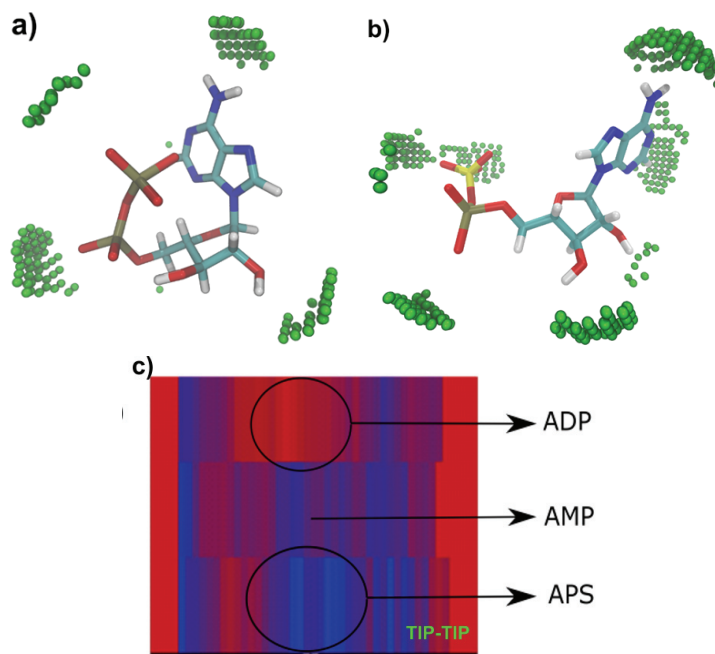


Fig. S-1. a) TIP – TIP interactions for ADP and b) APS, and c) TIP – TIP probe heatmap for ADP, AMP, and APS.

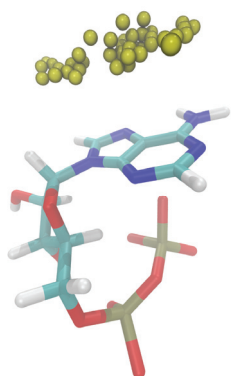


Fig. S-2. The location of favorable hydrophobic interactions of ADP mapped using DRY probe.

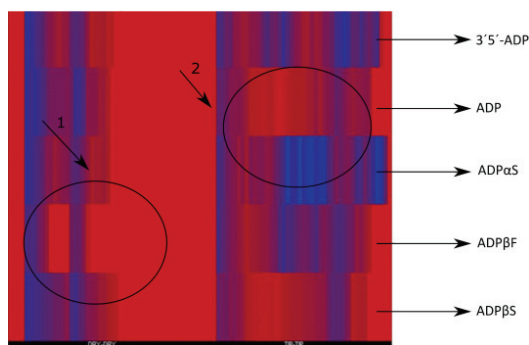


Fig. S-3. Differences in DRY – DRY interactions that ADP β F and ADP β S form with target (1) and differences in TIP – TIP interactions ADP α S and ADP (2).

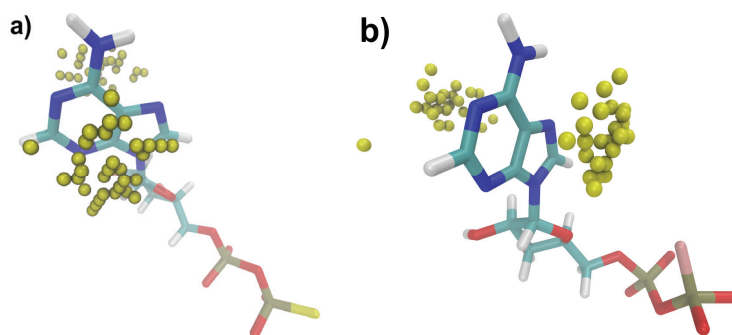


Fig. S-4. a) DRY – DRY interactions that ADP β S and b) ADP β F forms with enzyme.

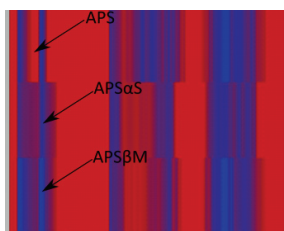


Fig. S-5. Differences in DRY – DRY interactions between APS, APS α S, and APS β M.

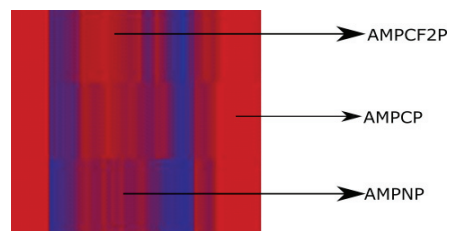


Fig. S-6. TIP – TIP interactions for AMPCF2P, AMPCP and AMPNP.

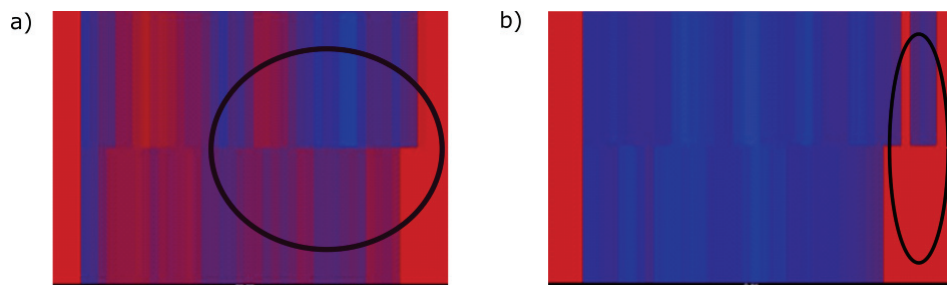


Fig. S-7. a) TIP – TIP interaction 5' AMPS and AMP and b) O – N1 interaction 5' AMPN and AMP.

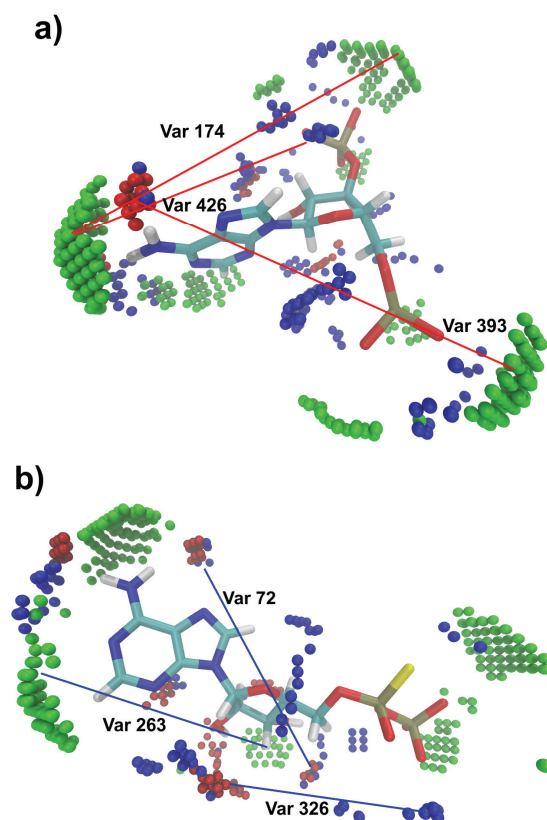
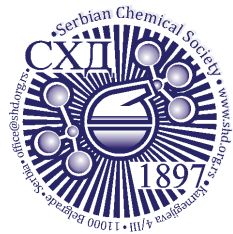


Fig. S-8. The structural features associated with the additional variables a) positively (red lines) and b) negatively (blue lines) correlated with the APS reductase inhibitory activity.



J. Serb. Chem. Soc. 86 (6) 571–584 (2021)
JSCS–5444

Improved dissolution of ibuprofen after crystallization from polymeric solution: Correlation with crystal parameter

RUDRA NARAYAN SAHOO^{1,2}, BHABANI SANKAR SATAPATHY¹
and SUBRATA MALLICK^{1*}

¹School of Pharmaceutical Sciences, Siksha 'O' Anusandhan (Deemed to be University),
Bhubaneswar-751003, Odisha, India and ²Centurion University of Technology and
Management, Odisha, India

(Received 9 December 2020, revised 10 March, Accepted 16 March 2021)

Abstract: The objective of the present work was to investigate the effect of various hydrophilic polymers, such as hydroxypropylmethyl cellulose, methyl cellulose, carboxymethyl cellulose and poly vinyl alcohol, on the *in vitro* dissolution property of ibuprofen (IBU) crystallized from aqueous polymeric solutions. By using the solvent-change technique, IBU crystal products were produced in the presence of the selected polymers. The results showed that in the presence of polymers, the crystallization yield of IBU was higher than that of pure drug crystals (absence of polymer). SEM photographs revealed visible changes in the crystal morphology in the presence of polymers. The FTIR spectra of the crystallized IBU (polymer-treated) showed a shift of the acid-dimer peak from 1718 to 1721 cm⁻¹ but the absence of specific peaks for polymers. An XRD study further confirmed the absence of polymers in the crystallized IBU as no specific peaks were observed for the polymers. A higher percentage of cumulative drug release was reported for the polymeric-treated IBU crystals than that of plain IBU. Further *in vivo* studies are warranted to establish the *in vitro*–*in vivo* correlation for future technology transfer of the formulation.

Keywords: steroidal anti inflammatory drug; *in vitro* solubility; lattice strain; dislocation density.

INTRODUCTION

Enhancement of the dissolution rate for poorly water soluble drugs is the need of the time in formulation design of orally administered dosage forms to obtain improved bioavailability and rapid onset of action. Controlled crystallization of poorly soluble drug from an aqueous polymeric solution is an emerging strategy to increase their solubility and dissolution rate.¹ The crystallization method was evolved as a simple, effective and industrially viable technique,

* Corresponding author. E-mail: subratamallick@soa.ac.in
<https://doi.org/10.2298/JSC201209021N>

although several drug delivery techniques, such as solid dispersion, salt forms, multiple emulsion, complexation *etc.*, have been reported to improve the solubility and dissolution rate of poorly soluble drugs.² Manipulation of the crystallization process from an aqueous polymeric solution is comparatively less explored and could be a promising area of research in drug delivery. Crystalline products could be produced by using several conventional techniques, including solvent evaporation, pH change, thermal treatment, vapor diffusion, growth in the presence of additives (surfactants/polymers), *etc.*³ The crystallization approach of poorly soluble drug from an aqueous polymeric solution to improve the aqueous solubility and dissolution rate of the drug has not been explored properly. The presence of a soluble polymer at a low concentration may assist in maintaining super saturation level of the drug after dispersion into the vehicle.^{4,5} Side by side, polymers have the ability to alter the viscosity of the medium *via* manipulation of the nucleation phase during crystal development, which ultimately leads to alteration in crystal habits or generation of crystal defects. Changes in nanostructural parameters of the crystallized products from a polymeric solution can be estimated quantitatively. Modification of crystal forms by defect crystallization may in turn lead to increase in solubility and oral bioavailability.⁵

Ibuprofen (IBU) is a non-steroidal anti inflammatory drug that has been commonly recommended in the treatment of arthritis (rheumatoid/osteoarthritis/gout), spondylitis, inflammation, fever, *etc.*⁶ Chemically, IBU is a propanoic acid derivative (*i.e.*, 2-(4-isobutylphenyl)propanoic acid) with an *n*-octanol/water partition coefficient of 11.7. Its profound analgesic effect is mostly related to the inhibition of the enzyme cyclooxygenase-2. However, being a class II type drug (under the Biopharmaceutical Classification System), the main problem associated with oral administration is its extremely low solubility in aqueous media.^{7,8} Thus, its dissolution rate is the major limiting step for the successful absorption of the drug to achieve the desired onset of action. Several advanced formulation techniques have been reported over the past years to improve the solubility and bioavailability of IBU.⁹⁻¹³ In a recent study, Yuliandra *et al.* reported the co-crystal formulation of IBU with nicotinamide (as conformer) for improved solubility and *in vivo* analgesic activity. The co-crystal form of IBU showed significant increase in solubility as compared to a physical mixture of drug/coformer and pure IBU.¹⁴ Similarly, in another study, dissolution of IBU was found to be increased by co-milling with different polymeric excipients.¹⁵ As per a report, co-milling of IBU with hydroxymethylpropyl cellulose polymer improved the solubility and dissolution rate of IBU up to 4-fold compared to pure IBU. Crystallization of ibuprofen from aqueous polymeric solution for improved dissolution has rarely been reported to date. Further, establishing the correlation of dissolution with crystal grain size and crystal lattice strain is really novel.

In the present study, IBU crystals were produced by the simple controlled crystallization method using the anti-solvent technique in presence of an aqueous polymeric solution. Ethanol was used as the main solvent to solubilize IBU; whereas aqueous solution of polymer was used as the anti-solvent. Polymers, as discussed previously, tend to prolong the super saturation process, offer steric hindrance with simultaneous increase in the viscosity of the dispersed system to induce controlled crystallization. Four different hydrophilic polymers, *i.e.*, hydroxypropyl methylcellulose (HPMC), methyl cellulose (MC), carboxymethyl cellulose (CMC) and poly(vinyl alcohol) (PVA) were used for crystallization of IBU and the correlation of dissolution with crystal imperfection parameters such as grain size, full width at half maximum (FWHM), lattices strain and dislocation density were investigated.

EXPERIMENTAL

Materials

IBU was a free sample from Tejani Life Care, Cuttack, India. HPMC, CMC, MC and PVA were purchased from Merck Private Ltd. Mumbai, India. All other chemicals/solvents used during the experiments were of analytical grade.

Method of preparation

An ethanolic solution of IBU (2 g in 50 ml) was prepared in a 1 L crystallization vessel and maintained at 50 °C under continuous agitation at a speed of 100 rpm. Then, in another container, a polymer solution (0.5 mass %) was prepared in 600 ml of water and added slowly to the above drug solution (3.0 ml min⁻¹).¹⁶ Simultaneous cooling was also applied to the above crystallization vessel (50 down to 10 °C) at a rate of 0.22 °C min⁻¹ using an external probe. Four such batches were prepared separately with each of the above four polymers (*viz.* HPMC, MC, CMC and PVA) at a constant drug-polymer concentration. The crystals were separated by filtration (Whatman[®], Grade 40 circle) and dried in an incubator at 40 °C until constant weight was attained.

Yield percentage

The crystallized yield was evaluated from the weight expressed as the % of IBU dissolved initially in 50 ml of ethanol during first step of the preparation to the weight of final amount of crystal products recovered and the mean value was recorded (mean \pm SD; $n = 4$).

Scanning electron microscopy (SEM)

Scanning electron microscopy (Carl ZEISS Sigma 300, India) was used for visualizing the surface morphology of the experimental crystal products by introducing a high beam of electrons through 0.5–1.5 kV acceleration voltage.¹⁷

FTIR spectroscopy study

FTIR spectroscopy is the commonly used technique to analyze the presence of the types of functional groups in drugs, drug crystals as well as to detect any interaction between them. For the study, the experimental samples were placed over zinc selenide crystal and pressed on to the attenuated total reflectance crystal by using an integrated pressure application device.¹⁵ The experimental samples were observed using a FTIR spectrometer (FT/IR-4600, JASCO)

over the wave number range 4000 to 400 cm^{-1} and the data were interpreted by Spectra Manager Software (version 2.0).

Powder X-ray diffraction (PXRD)

For the study, about 1 mg of dry powdered sample was taken on the glass slide and analyzed using an X-ray diffractometer (RIGAKU ultimate PXDL software, Japan). Anode Material Cu, K-Alpha (1.5406 Å) was used as the source of X-rays.¹⁸ The voltage and current were set at 40 kV and 15 mA, respectively. Measurements were undertaken at a scan speed of 1°min^{-1} over the scanning angle 2θ range from 5 to 50° .

In vitro dissolution study

The *in vitro* dissolution study was performed using a USP paddle type II dissolution apparatus (dissolution tester (USP) TDT06L, Electrolab). For the study, double distilled water (900 ml maintained at 37°C) was used as the dissolution medium in each vessel and the test was conducted for 2 h. Briefly, 10 mg of IBU and experimental crystal products (equivalent to IBU 10 mg) were placed in the dissolution vessel.¹⁹ The powder sample was allowed to settle at the bottom of the vessel before starting rotation of the paddle (50 rpm). About 10 ml of samples were withdrawn from the dissolution vessel at regular time intervals (10, 20, 30, 45, 60, 75, 90 and 120 min) through a syringe fitted with a membrane filter (0.45 μm) with simultaneous replenishment of fresh release medium. The collected samples were analyzed at 222 nm using a UV-Vis spectrophotometer (JASCO V-630, Japan) against water as the blank.¹⁹ The studies were performed in triplicate ($n=3$), and the mean values of cumulative drug release (%) were obtained.

RESULTS AND DISCUSSION

The study was undertaken to understand the crystallization behavior of poorly soluble drug IBU from selected aqueous polymeric solutions of CMC, PVA, MC and HPMC and the correlation of the drug dissolution profile with the critical nanostructural parameters of the crystallized IBU. Super saturation was maintained after employing low concentration of polymeric additive that interfered with the regular crystal growth. The crystal arrangement pattern or packing of molecules of IBU crystal structure viewing randomly is depicted in Fig. 1. Centro-symmetric hydrogen bonded dimers are exhibited in the crystal packing of IBU. Four sets of product crystallized from aqueous polymeric solution and one in absence of polymer (as the control) are reported in Table I. The amount of polymer and drug were kept constant for each batch to compare the effect of selected polymers on the crystal property and the dissolution behavior of IBU.

Yield

The results showed that the crystallization yield of IBU was influenced by the presence of polymer (Table I). Among various polymers, HPMC resulted in the highest crystal yield (95.51 %) in contrast to IBU crystallized without polymer with the yield of 80.52 %. The presence of polymer clearly induced the crystallization process and the yield increased in presence of polymer in the order as: None < PVA < MC < CMC < HPMC.

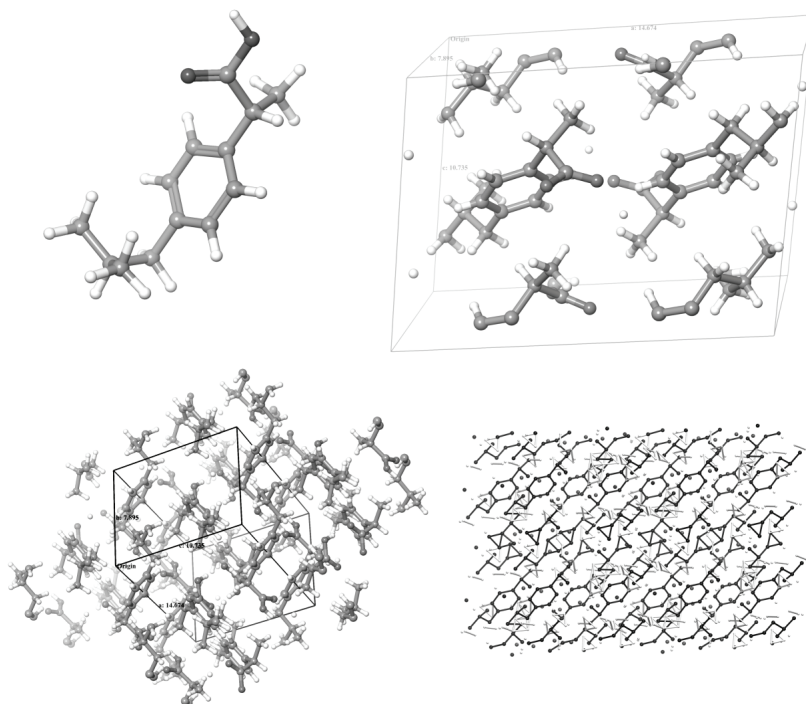


Fig. 1. Molecular packing arrangement of ibuprofen crystals viewed randomly (source: *Pubchem*).

TABLE I. Formulation of experimental ibuprofen crystallized from aqueous polymeric solutions

Formulation code	Polymer	Polymer concentration, wt. %	Yield \pm SD, % ($n = 4$)
IBU ⁰	None	—	80.52 \pm 0.64
IBU ¹	CMC	0.5	91.95 \pm 0.82
IBU ²	PVA	0.5	86.45 \pm 0.71
IBU ³	MC	0.5	88.38 \pm 1.31
IBU ⁴	HPMC	0.5	95.51 \pm 2.05

SEM study

The surface morphology of the pure drug and the crystallized products are depicted in Fig. 2. For pure IBU drug powder, polyhedral type of crystals were seen in the SEM image (Fig. 2A), very similar to pure crystallized IBU from aqueous medium (Fig. 2B). The size of the crystals was smaller when crystallized in presence of polymer as seen clearly in the photomicrograph. However, such a definite crystal geometry started to disappear in subsequent SEM images of crystal products; those were produced in presence of polymer. The rod shaped morphology of pure IBU gradually changed to a distorted plate and needle type (Fig. 2C–F) in case of polymer treated IBU crystals. Although, certain geometrical

forms still existed in IBU¹, IBU², IBU³ and IBU⁴ crystals, the overall morphology was somehow distorted. Clearly, some irregularities in the crystal geometry were noticed due to the influence of polymer presence relative to its absence. Irregularities in the crystal geometry could be the reflection of surface dislocation and defects in the crystal sample.

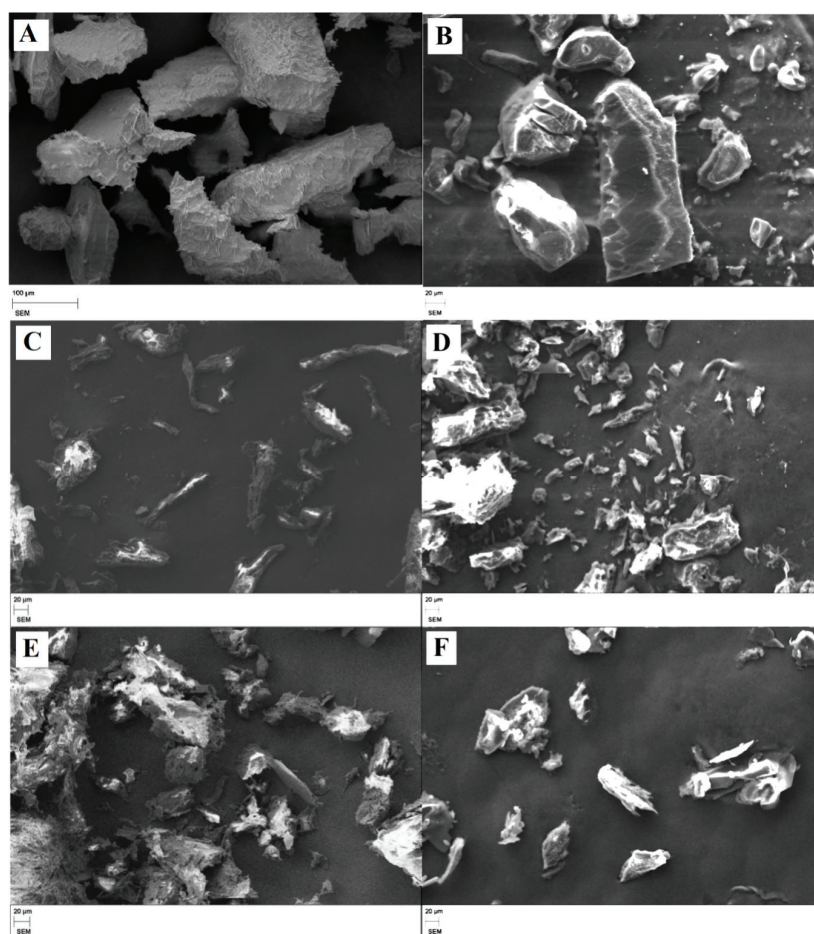


Fig. 2. Examination of photomicrograph of pure drug and the crystallized products: A) pure IBU, B) IBU⁰, C) IBU¹, D) IBU², E) IBU³ and F) IBU⁴.

FTIR study

The FTIR spectra of the pure IBU, IBU pure crystal as well as the polymeric treated IBU crystal products were recorded to obtain information about the possible interaction between IBU and the selected polymers during controlled crystallization (Fig. 3). The FTIR spectrum of IBU showed medium to very strong bands at 3094, 2958 and 2901 cm^{-1} , which could be assigned to CH_2 asymmetric

stretching, CH₃ asymmetric stretching and C–H symmetric stretching, respectively. Strong bands in the region of 2800 to 3000 cm⁻¹ of IBU were due to symmetric and asymmetric stretching vibrations of alkyl chains. The high intensity carbonyl peak of IBU at 1722 cm⁻¹ became slightly weaker in the polymeric-treated crystal products, which indicates the effect of polymers in modulating crystal habits. However, there was absence of specific peaks for polymers in the polymer treated crystal products. In the case of polymers such HPMC, a common peak appears in the FTIR spectrum at 2825–2845 cm⁻¹ (assigned to OCH₃ stretching), which was clearly absent in the HPMC treated IBU crystal (IBU⁴). Similarly, in the FTIR spectrum of PVA, the main peaks appearing at 3280, 1324 and 839 cm⁻¹, *etc.* (assigned to O–H stretching, CH₂ symmetric stretching, CH₂ bending respectively), were clearly absent in the PVA treated IBU crystal product. The peak around 2800 to 3000 cm⁻¹ that often appears as a shoulder type peak (H–C=O stretching) was present in the IBU and polymer treated IBU crystal products, which overall indicate the absence of polymers in the final crystal products. Polymers in low concentration (0.5 mass %) were used to induce supersaturation (anti-solvent system) and slight modification in crystal habits; however, these were not present in the final recovered IBU crystals as evidenced by the FTIR study. The results further confirmed the absence of any incompatibility or interaction between the drug and the selected polymer during the crystallization process. Neither new peaks of polymer nor major shifting of any characteristics peaks of the drug were observed.

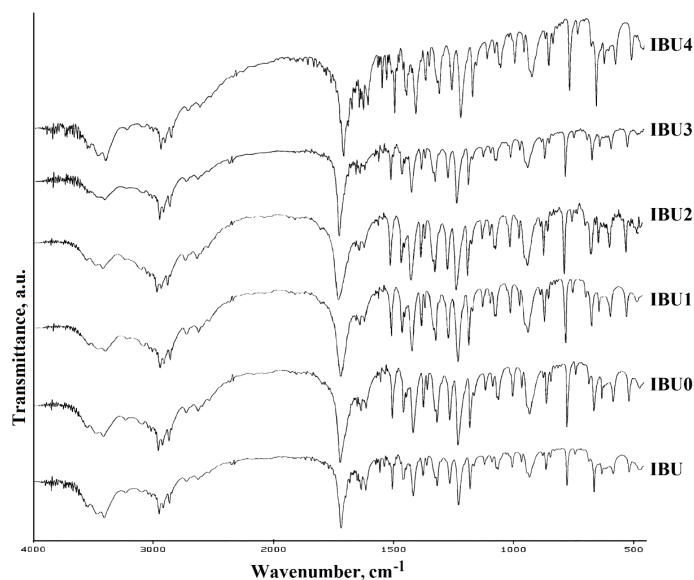


Fig. 3. FTIR spectra of pure ibuprofen, ibuprofen crystals and polymer treated ibuprofen crystal products.

PXRD study

PXRD has proved itself to be an essential tool in the study crystalline structures at the supramolecular level. In XRD, the interaction of the incident X-ray with the experimental sample leads to the generation of constructive interference along with a diffracted ray, according to Bragg's Law ($n\lambda = 2d \sin \theta$).²⁰ The wave length of the incident X-ray is related to the angle of diffraction in a crystal lattice. In the present study, XRD measurements were performed to determine the possible changes in the crystallinity of the components during the crystallization process. Diffractograms of the pure IBU, IBU crystal and polymeric treated IBU crystals (IBU¹, IBU², IBU³ and IBU⁴) are depicted in Fig. 4. The XRD pattern of pure IBU exhibited characteristic diffraction peaks at various diffraction angles, viz. 6, 12.3, 16, 20.4 and 22.3° indicating the presence of crystallinity. These peaks although detected in the diffractogram of the polymer treated IBU crystal products were of much lower intensity compared to those of those of the pure drug and IBU⁰ (without polymer treatment). The decrease in peak intensity in the polymer treated crystal products indicated a loss of crystallinity and generation of amorphization of the crystal samples. The X-ray diffraction peaks of the crystallized samples were slightly broader suggesting more nanosized particles compared to pure IBU. However, it should be further noted that no new peaks were identified for the polymers in the XRD data, which again indicated the absence of polymers in the final recovered IBU crystal products. However, the presence of polymer-induced slight amorphization in the crystal property could not fully alter the molecular arrangement of the crystals. Such limited amorphization would thus help to increase in solubility and dissolution profile of the drug compared to that of its pure form.

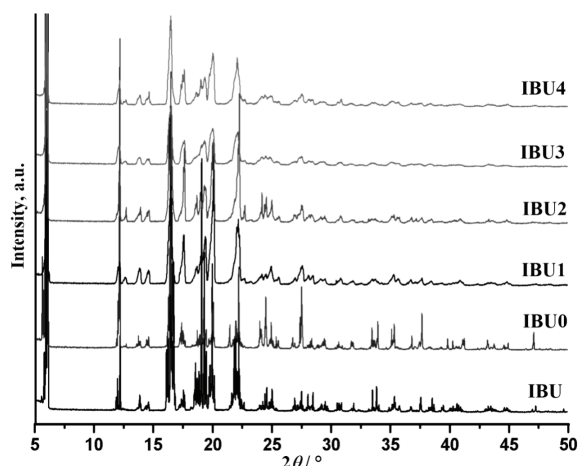


Fig. 4. PXRD data of pure drug, pure crystal (without polymer) and polymer treated crystal products.

TABLE II. Crystal grain size and lattice strain arising from crystal imperfection and their correlation with dissolution

Drug sample	Grain size \pm SD, nm	FWHM	(Strain \pm SD) $\times 10^{-3}$	(Dislocation density \pm SD) $\times 10^{-4}$, nm ⁻²
IBU	26.96 \pm 1.42	0.314	7.53 \pm 1.32	13.83 \pm 1.41
IBU ⁰	23.35 \pm 0.47	0.365	9.27 \pm 1.53	18.35 \pm 0.73
IBU ¹	22.19 \pm 0.94	0.380	9.73 \pm 1.11	20.38 \pm 1.70
IBU ²	20.26 \pm 0.27	0.416	10.63 \pm 1.57	24.36 \pm 0.65
IBU ³	19.99 \pm 1.73	0.424	10.80 \pm 2.45	25.40 \pm 4.38
IBU ⁴	18.87 \pm 0.88	0.447	12.07 \pm 1.70	28.20 \pm 2.55
Correlation Equation	T_{60} vs. grain size $y = -8.1877x + 237.94$	T_{60} vs. FWHM $y = 510.19x - 141.15$	T_{60} vs. strain $y = 15.574x - 97.488$	T_{60} vs. dislocation $y = 4.7402x - 44.782$
R^2	0.908	0.947	0.912	0.969

Using the XRD data, the Debye–Scherrer formula was employed to determine other characteristic properties, such as particle size, strain, dislocation density, *etc.*, of the formed crystal products (Table II).

Thus, the Debye–Scherrer Equation was used to estimate the strain in the lattice, Eq. (1):

$$\varepsilon = \beta/4\tan\theta \quad (1)$$

The crystallite size was determined using Eq. (2):

$$D = 0.9\lambda/\beta\cos\theta \quad (2)$$

where ε = strain, β = FWHM (full width half maxima), D = crystallite size, λ = wavelength.

The dislocation density (δ) describes the extent of defects in the crystal sample. It is a measure as the length of dislocation lines per unit volume of the crystal and calculated by Eq. (3):

$$\delta = 1/D^2 \quad (3)$$

The particle size, strain, dislocation density showed small variations between pure drug, drug crystal and polymer treated drug crystal products. These variations could be due to the effect of polymers during the crystallization process, which generated to some extent amorphous properties of the experimental crystal products.

Dissolution of drug

Drug dissolution is the most important evaluation parameter of crystallized products. Dissolution data is inevitable to establish the *in vitro*–*in vivo* correlation, which is again essential for clinical translation of formulations from the laboratory to the bed side. A higher dissolution rate signifies higher rate of absorption, faster onset of action along with increased bioavailability.^{21,22} In the

present work, *in vitro* dissolution studies of the pure drug, and drug crystallized from aqueous polymeric were performed in double distilled water at 37 ± 0.5 °C in a USP type II dissolution apparatus (Fig. 5). In view of the very low solubility of IBU in aqueous medium, double distilled water was used as the release medium during the study. Similar reports for the use of water as release medium for poorly soluble drugs have already been reported previously including ibuprofen.^{17,23–33} Hu *et al.* reported *in vitro* drug release of IBU from an experimental micro emulsion in distilled water.²⁶ It was found that the *in vitro* release profiles of IBU did not show much change in different drug release media, *i.e.*, the amount of drug release from the micronized formulation was very similar both in the case of double distilled water and simulated gastric fluid (pH 1.2). In addition, it has been reported that many non-steroidal anti-inflammatory drugs having low solubility (including IBU) tend to self-assemble themselves in aqueous medium by forming micelle-like structures, for which their solubility–pH profiles cannot be properly explained using the Henderson–Hasselbalch Equation.³⁴ Thus, in the present study, double distilled water was used as the drug release medium to obtain the overall idea about the possible improvement of dissolution of ibuprofen.

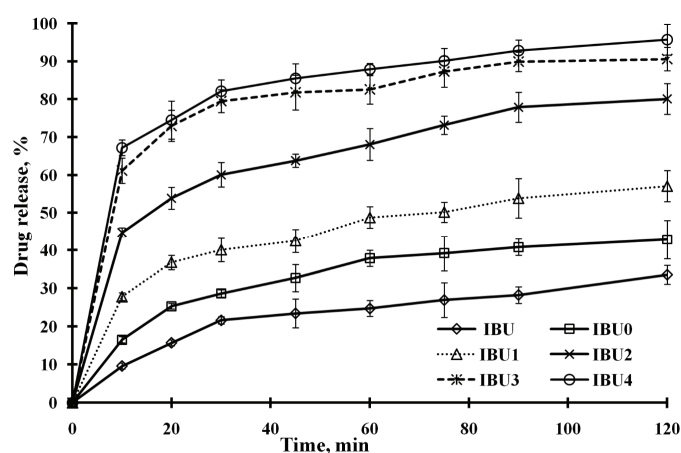


Fig. 5. Dissolution data of pure drug (IBU), pure drug crystal (IBU⁰) and crystallized IBU from aqueous polymeric solution (IBU¹, IBU², IBU³ and IBU⁴) in double distilled water for 120 min. All sets of experiments were performed in triplicate. The data show mean \pm SD ($n = 3$). Error bars indicate the standard deviation values.

From the data, it was observed that the dissolution rate of all experimental polymer treated crystal products was higher than that of plain IBU and IBU pure crystals during the period of the 120 min experimental study. Clearly, the presence of polymers during crystallization influenced the dissolution profile of IBU. Furthermore, among the four selected polymers, HPMC improved the drug

dissolution to an extent of 95 % as compared to the other polymers. The order of dissolution was observed as $IBU < IBU^0 < IBU^1 < IBU^2 < IBU^3 < IBU^4$. The reduced crystalline intensity of IBU to the maximum extent in the presence of HPMC could result in maximum dissolution of drug, which was supported by the XRD and SEM data. A significant improvement in dissolution of IBU^4 would be helpful for further *in vivo* studies to gather data for its future clinical translation. The dislocations due to linear defects on the atomic scale preferentially have been brought about improved dissolution. The highest dislocation density of IBU^4 exhibited a higher dissolution rate as compared to that of the other recrystallized product.

Correlation of *in vitro* dissolution with crystal imperfection parameters, such as grain size, dislocation density, lattice strain and FWHM, was attempted and the results are presented in Fig. 6. Dissolution at 60 min (T_{60}) is linearly correl-

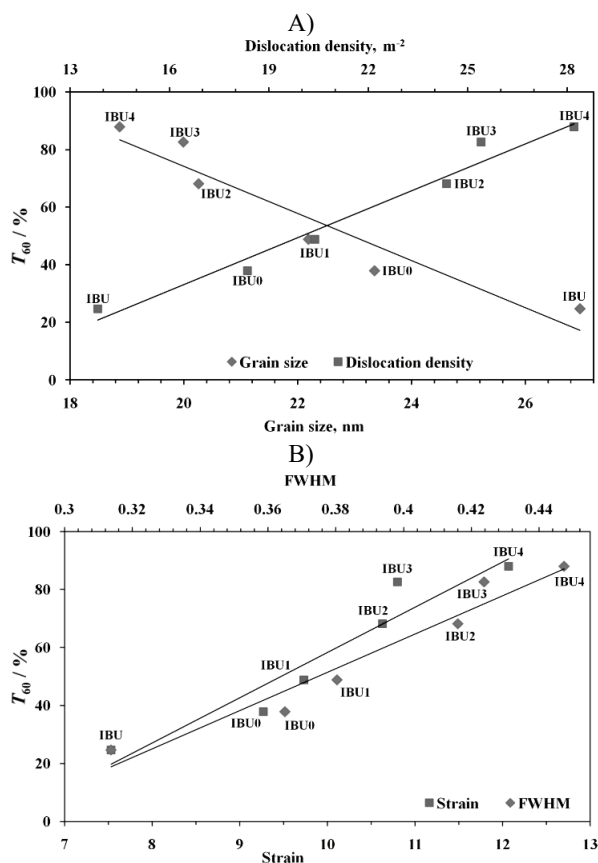


Fig. 6. Establishing linear correlation of: A) *in vitro* dissolution (T_{60} , %) vs. grain size and dislocation density and B) *in vitro* dissolution vs. strain and FWHM of the crystal data.

ated with grain size, dislocation density, lattice strain and FWHM. The respective regression equation and R^2 values (0.908 to 0.969) are presented in Table II. From the dissolution data, any of the crystal imperfection parameters could be predicted using the regression equation.

CONCLUSIONS

Ibuprofen was successfully crystallized from aqueous polymeric solutions in good yields, 86.45 to 95.51 %. The highest crystal yield was obtained from HPMC solution where crystallized IBU without polymer showed 80.52 %. Polymer presence in the supersaturation process induced the crystallization process and increased the crystal yield. Absence of any specific peaks in the FTIR spectra of the respective polymer in the experimental crystal product clearly indicated that the resultant IBU crystals were free from polymer in their crystal lattice. In XRD diffractogram, diminishing in intensity/broadening of certain peaks of IBU in polymer-treated crystal products indicated the extent of defects in the crystal sample, which might be responsible for their improved solubility and drug release property. Crystal grain size and lattice strain parameters arising from crystal imperfection were evaluated and their correlation with dissolution was established. The dissolution data any of the crystal imperfection parameters can be estimated using regression equation. Further *in vitro* and *in vivo* studies were hereby warranted to establish the optimized drug crystal for its future technology transfer to the industrial scale.

Acknowledgements. The authors acknowledge gratefulness to the Department of Science & Technology, Ministry of Science & Technology, New Delhi, India, for providing an INSPIRE fellowship to Rudra Narayan Sahoo (IF 150987). We also acknowledge Prof. Manojranjan Nayak, President, Siksha O Anusandhan (Deemed to be University) for providing the necessary research facilities in the School of Pharmaceutical Sciences.

ИЗВОД

ПОБОЉШАНА РАСТВОРЉИВОСТ ИБУПРОФЕНА НАКОН КРИСТАЛИЗАЦИЈЕ ИЗ РАСТВОРА ПОЛИМЕРА: КОРЕЛАЦИЈА СА ПАРАМЕТРИМА КРИСТАЛА

RUDRA NARAYAN SAHOO,^{1,2} BHABANI SANKAR SATAPATHY¹ и SUBRATA MALLICK¹

¹School of Pharmaceutical Sciences, Siksha 'O' Anusandhan (Deemed to be University), Bhubaneswar-751003, Odisha, India и ²Centurion University of Technology and Management, Odisha, India

Предмет рада је било испитивање утицаја различитих хидрофилних полимера као што су хидроксипропилметил целулоза, метил целулоза, карбоксиметил целулоза и поли винил алкохол на *in vitro* карактеристике растварања ибупрофена (IBU) кристалисаног из водених раствора полимера. Применом технике замене растварача, кристални производи IBU су добијени у присуству одабраних полимера. Резултати су показали да је у присуству полимера кристалizacionи принос IBU већи него у случају чистих кристала лека (без полимера). SEM фотографије су показале видљиве промене у морфологији кристала у присуству полимера. FTIR спектри кристалисаног IBU (третираног полимером) показују померај траке која потиче од димера киселине са 1718 на 1721 cm^{-1} и одсуство трака карактеристичних за полимере. XRD испитивања су потврдила одсуство полимера у случају кристалисаног IBU јер нису детектоване карактеристичне реф-

лексије полимера. Већи проценat кумулативног ослобађања лека је детектован у случају IBU кристала третираних полимерима у односу на чист IBU. Даље студије *in vivo* ће успоставити корелацију *in vitro*–*in vivo* за будући технолошки трансфер формулације.

(Примљено 9. децембра 2020, ревидирано 10 марта, прихваћено 16. марта 2021)

REFERENCES

1. D. B. Warren, H. Benameur, C. J. H. Porter, C. W. Pouton, *J. Drug Target.* **18** (2010) 704 (<https://doi.org/10.3109/1061186X.2010.525652>)
2. R. Thakuria, A. Delori, W. Jones, M. P. Lipert, L. Roy, N. Rodriguez-Hornedo, *Int. J. Pharm.* **453** (2013) 101 (<https://doi.org/10.1016/j.ijpharm.2012.10.043>)
3. A. M. Pherson, B. Cudney, *Acta Cryst., F* **70** (2014) 1445. (<https://doi.org/10.1107/S2053230X14019670>)
4. N. R. Hornedo, D. Murphy, *J. Pharm. Sci.* **88** (1999) 651 (<https://doi.org/10.1021/js980490h>)
5. K. Kachrimanis, S. Malamataris, *J. Pharm. Pharmacol.* **51** (1999) 1219 (<https://doi.org/10.1211/0022357991776949>)
6. R. Bushra, N. Aslam, *Oman Med. J.* **25** (2010) 155 (<https://doi.org/10.5001/omj.2010.49>)
7. O. C. Larbi, H. Merine, Y. Ramli, F. B. Toumi, K. Guemra, A. Dehbi, *J. Serb. Chem. Soc.* **83** (2018) 1243 (<https://doi.org/10.2298/JSC171112065LA>)
8. B. J. Orlando, M. J. Lucido, M. G. Malkowski, *J. Struct. Biol.* **189** (2015) 62 (<https://doi.org/10.1016/j.jsb.2014.11.005>)
9. S. Mallick, S. Pattnaik, K. Swain, P. K. De, A. Saha, G. Ghoshal, A. Mondal, *Eur. J. Pharm. Biopharm.* **68** (2008) 346 (<https://doi.org/10.1016/j.ejpb.2007.06.003>)
10. S. Mallick, S. Pattnaik, K. Swain, P. K. De, A. Saha, P. Mazumdar, G. Ghoshal., *Drug Dev. Ind. Pharm.* **34** (2008) 726 (<https://doi.org/10.1080/03639040801901868>)
11. H. H. Baek, D. H. Kim, S. Y. Kwon, S. J. Rho, D. W. Kim, H. G. Choi, Y. R. Kim, C. S. Yong, *Arch. Pharm. Res.* **35** (2012) 683 (<https://doi.org/10.1007/s12272-012-0412-4>)
12. M. Newa, K. H. Bhandari, D. X. Li, T. H. Kwon, J. A. Kim, B. K. Yoo, J. S. Woo, W. S. Lyoo, C. S. Yong, H. G. Choi. *Int. J. Pharm.* **343** (2007) 228 (<https://doi.org/10.1016/j.ijpharm.2007.05.031>)
13. Z. Emire, E. Yabalak, O. Görmez, A. Gizir, *J. Serb. Chem. Soc.* **82** (2017) 99 (<https://doi.org/10.2298/JSC160520079E>)
14. Y. Yuliandra, E. Zaini, S. Syofyan, W. Pratiwi, L. N. Putri, Y. S. Pratiwi, H. Arifin, *Sci. Pharm.* **86** (2018) 1 (<https://doi.org/10.3390/scipharm86020023>)
15. A. Hussain, G. Smith, K. A. Khan, N. I. Bukhari, N. I. Pedge, I. Ermolina, *Eur J. Pharm.Sci.* **123** (2018) 395 (<https://doi.org/10.1016/j.ejps.2018.08.001>)
16. S. Mallick, P. K Dey, S. Sannigrahi, A. Mitra, *Acta Pol. Pharm.* **61** (2004) 447
17. R. N. Sahoo, A. Nanda, A. Pramanik, S. Nandi, R. Swain, S. K. Pradhan, S. Mallick, *Acta Chim. Slov.* **66** (2019) 1 (<https://doi.org/10.17344/acsi.2019.5139>)
18. T. S. Latha, M. C. Reddy, V.D. Prasad, S. V. Muthukonda, D. Lomada, *Ind. J. Pharmacol.* **49** (2017) 458 (https://doi.org/10.4103/ijp.IJP_536_16)
19. M. Acharya, S. Mishra, R. N. Sahoo, S. Mallick, *Acta Chim. Slov.* **64** (2017) 45 (<https://doi.org/10.17344/acsi.2016.2772>)
20. J. Pi, S. Wang, W. Li, D. Kebebe, Y. Zhang, B. Zhang, *Asian J. Pharm. Sci.* **14** (2019) 154 (<https://doi.org/10.1016/j.ajps.2018.04.009>)
21. Y. Lu, S. Kim, K. Park, *Int. J. Pharm.* **418** (2011) 142 (<https://doi.org/10.1016/j.ijpharm.2011.01.010>)

22. F. Kesisoglou, A. Hermans, C. Neu, K. L. Yee, J. Palcza, J. Miller, *J. Pharm. Sci.* **104** (2015) 2913 (<https://doi.org/10.1002/jps.24362>)
23. P. Arya, K. Pathak. *Int. J. Pharm.* **460** (2014) 1 (<https://doi.org/10.1016/j.ijpharm.2013.10.045>)
24. F. L. Mota, A. P. Carneiro, A. J. Queimada, S. P. Pinho, E. A. Macedo. *Eur. J. Pharm. Sci.* **37** (2009) 499 (<https://doi.org/10.1016/j.ejps.2009.04.009>)
25. F. A. Maulvi, S. J. Dalwadi, V. T. Thakkar, T. G. Soni, M. C. Gohel, T. R. Gandhi. *Powder Technol.* **207** (2011) 47 (<https://doi.org/10.1016/j.powtec.2010.10.009>)
26. L. Hu, J. Yang, W. Liu, L. Li, *Drug Deliv.* **18** (2011) 90 (<https://doi.org/10.3109/10717544.2010.522613>)
27. B. S. Satapathy, A. Patel, R. N. Sahoo, S. Mallick, *J. Serb. Chem. Soc.* **86** (2021) 5 (<https://doi.org/10.2298/JSC200705049S>)
28. L. Xu, S. M. Li, H. Sunada, Q. F. Wang, *J. Drug Deliv. Sci. Technol.* **17** (2007) 145 ([https://doi.org/10.1016/S1773-2247\(07\)50022-5](https://doi.org/10.1016/S1773-2247(07)50022-5))
29. L. Xu, S. M. Li, Y. Wang, M. Wei, H. M. Yao, H. Sunada, *J. Drug Deliv. Sci. Technol.* **19** (2009) 113 ([https://doi.org/10.1016/S1773-2247\(09\)50018-4](https://doi.org/10.1016/S1773-2247(09)50018-4))
30. M. Aroso, J. C. Silva, F. Mano, A. S. Ferreira, M. Dionísio, I. Sá-Nogueira, S. Barreiros, R. L. Reis, A. Paiva, A. R. Duarte, *Eur. J. Pharm. Biopharm.* **98** (2016) 57 (<https://doi.org/10.1016/j.ejpb.2015.11.002>)
31. M. M. Santos, L. R. Raposo, G. V. Carrera, A. Costa, M. Dionísio, P. V. Baptista, A. R. Fernandes, L. C. Branco, *Chem. Med. Chem.* **14** (2019) 907 (<https://doi.org/10.1002/cmdc.201900040>)
32. H. Stevens, M. Voelker, L. Gow, F. MacDougall, G. Bieri, *J. Drug Deliv. Sci. Technol.* **51** (2019) 535 (<https://doi.org/10.1016/j.jddst.2019.02.027>)
33. M. Alemanni, S. C. Gatoulis, M. Voelker, *Minerva Med.* **107** (2016) 125 (<https://www.minervamedica.it/en/journals/minerva-medica/article.php?cod=R10Y2016N03A0125>)
34. A. Avdeef, *ADMET DMPK* **2** (2014) 33. (<https://doi.org/10.5599/admet.2.1.30>).



J. Serb. Chem. Soc. 86 (6) 585–590 (2021)
JSCS–5445

SHORT COMMUNICATION

Influence of electrochemical conditions on the regio- and stereoselectivity of selenocyclization of alkenyl hydantoin

BILJANA M. ŠMIT^{1*}, PETAR B. STANIĆ¹, LJUBINKA G. JOKSOVIĆ²,
DARKO P. AŠANIN¹ and ZORAN SIMIĆ²

¹*Institute for Information Technologies, University of Kragujevac, Jovana Cvijića bb, Kragujevac, Serbia* and ²*Faculty of Science, University of Kragujevac, Radoja Domanovića 12, Kragujevac, Serbia*

(Received 22 October 2020, revised 21 February, accepted 23 March 2021)

Abstract: 5-Alkenyl hydantoin and alkenyl spirohydantoin are converted into bicyclic and tricyclic hydantoin, under indirect electrochemical conditions, generating the phenylselenyl cation *in situ*. The reactions proceeded in good to excellent yields. The influence of electrochemical conditions on regio- and diastereoselectivity of the selenocyclization reactions is investigated.

Keywords: electrosynthesis; constant-current electrolysis; selenylation; ring closure.

INTRODUCTION

The use of electrochemical methods in organic synthesis has become increasingly more popular due to simple procedures and laboratory techniques and the use of cleaner and greener solvents. It is worth noting that the outcomes of the reactions can be vastly different, while some reactions can only be carried out under electrochemical conditions.¹ The hydantoin core represents an important pharmacophore occurring in many biologically active compounds mostly known due to their antimicrobial, anticancer and anticonvulsant activity.^{2,3} Spirohydantoin⁴ and fused⁵ polycyclic hydantoin are the leading compounds in drug discovery, due to their various biological activities. Selenocyclization is a convenient and useful tool for the construction of heterocycles.^{6,7} We described a methodology for the synthesis of bicyclic and tricyclic fused hydantoin scaffold, using selenocyclization for the construction of sterically constrained structures that have potential in peptidomimetic drug design.^{8,9} In this work we decided to use the electrochemically generated phenylselenyl cation in the cyclization of 5-alkenyl hydantoin and alkenyl spirohydantoin and explore whether these condi-

* Corresponding author. E-mail: biljana.smit@uni.kg.ac.rs
<https://doi.org/10.2298/JSC201022023S>



ions have an effect on the course of the reaction, especially on regio- and stereo-selectivity.

EXPERIMENTAL

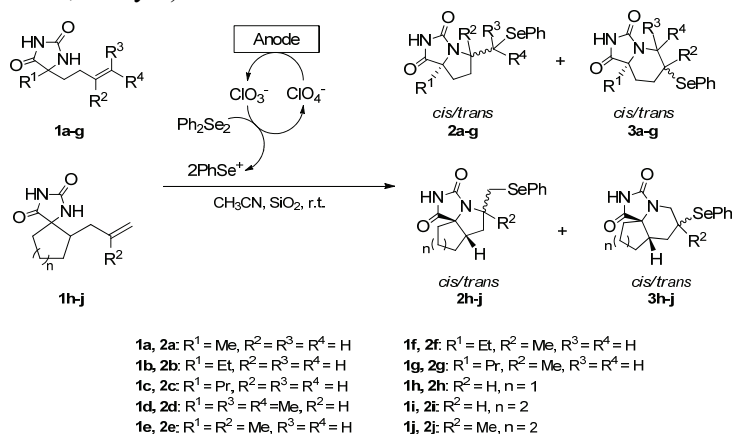
General. All alkenyl hydantoin s used as substrates were synthesized according to the procedures described previously.⁸ Reagent Ph_2Se_2 was used as supplied by Aldrich. Gas-liquid chromatography (GLC) was performed by Varian instrument model 3400. $^1\text{H-NMR}$ spectra were run in CDCl_3 on a Varian Gemini 2000 spectrometer at 200 MHz.

General procedure for the electrochemical selenocyclization of hydantoin s (1a–j). A solution of **1a–j** (1 mmol), Ph_2Se_2 (156 mg, 0.5 mmol), silica gel (150 mg, 5 mmol) and NaClO_4 (123.5 mg, 1 mmol) in MeCN (10 ml) was placed in an undivided electrolysis cell and electrolyzed under a constant current (10 mA) at room temperature. After completion, the reaction mixture was stirred overnight. The solvent was distilled off, residue dissolved in CH_2Cl_2 , washed with sat. NaHCO_3 solution and brine, and dried over anh. Na_2SO_4 . The solvent was evaporated and the reaction mixture was analyzed by GLC and $^1\text{H-NMR}$ spectroscopy.

RESULTS AND DISCUSSION

The alkenyl hydantoin s contain a double bond and an internal nitrogen nucleophile, and they are suitable substrates for the intramolecular electrophilic cyclization. Over several decades, electrophilic selenium reagents have been proven to be quite useful for this purpose. In some cases, electrochemical selenylations have advantages over other related methods.^{10,11}

The cyclization of the previously synthesized 5-alkenyl hydantoin s **1a–g** and alkenyl spirohydantoin s **1h–j** was performed by the means of electrochemically generated phenylselenenyl cation, which originates from diphenyldiselenide in a MeCN solution of NaClO_4 (Scheme 1). Perchlorate in this process serves as a mediator. Before that, we tried to perform the reaction of the commercially available product **1d**, with other supporting electrolytes (LiCl , KCl , NaBr , KI), solvents and electrodes, but NaClO_4 in MeCN and C–Pt electrodes gave the best results (Table I, Entry 6).



Scheme 1. Selenocyclization of alkenyl hydantoin s **1a–g** and alkenyl spirohydantoin s **1h–j**.

TABLE I. Optimization of electrochemical conditions for the cyclization reaction of **1d**

Entry	Anode–cathode	Supporting electrolyte	Solvent	Overall yield ^a (6/5), %	Diastereomeric ratio ^a <i>cis/trans</i> , %
1	Pt–Pt	KCl	CH ₃ CN	10	78:21
2	Pt–Pt	NaBr	CH ₃ CN	6	–
3	Pt–Pt	KI	CH ₃ CN	5	75:25
4	Pt–Pt	NaClO ₄	CH ₃ CN	31	62:38
5	Pt–Pt	NaClO ₄	CH ₃ CN	4	–
6	C–Pt	NaClO ₄	CH ₃ CN	63 (46:54)	6(59:41); 5(69:31)
7	C–Cu	Et ₄ NBr	CH ₃ CN	1	–
8	C–Cu	NaClO ₄	CH ₃ CN	47 (68:32)	6(51:49); 5(7:93)
9	C–Cu	LiCl	CH ₃ CN	traces	–
10	C–Cu	KI	CH ₃ CN	34 (42:58)	6(52:48); 5(72:28)
11	C–Pt	NaClO ₄	CH ₂ Cl ₂ :CH ₃ CN=2:1	Traces	–
12	C–Pt	NaClO ₄	Py:CH ₃ CN=1:1	Traces	–
13	C–Pt	NaClO ₄	Toluene:CH ₃ CN=2:1	57 (83:17)	6(48:52); 5(84:16)
14	C–Pt	NaClO ₄	THF	Undetectable	–
15	C–Pt	NaClO ₄	Ethanol	Undetectable	–
16	C–Pt	NaClO ₄	DMF	Traces	–

^aRatio of regio and diastereoisomers are obtained from GLC and ¹H-NMR spectra

The easy oxidation of perchlorate at the anode provides *in situ* generation of PhSe⁺ able to react with the π -electron system of the substrate. The reaction yields products resulting from the nucleophilic attack of the nitrogen atom to the cyclic seleniranium ion intermediate during the cyclization step.

Under the chosen reaction conditions, a series of alkenyl hydantoin **1a–j** was subjected to electrochemical selenocyclization (Table II). In the previously reported results,^{8,9} the reaction was regiospecific and 5-membered regioisomers were formed *via* favorable 5-*exo-trig* ring closure process which is both kinetically and thermodynamically favoured.¹² Products where the bridgehead substituent and CH₂SePh group are in *cis* positions one to another were formed predominantly. In contrast, when the phenylselenyl cation is electrochemically generated *in situ*, it was noticed that the regio- and diastereoselectivity both depend on the steric hindrance at C-5 of the hydantoin ring and the C-C double bond. 5-*Exo-trig* cyclization products are also obtained regiospecifically in most cases, but with poorer stereoselectivity. The amount of *trans*-diastereoisomers is increased in comparison to the previous results, implying higher thermodynamic control of the cyclization process. Exceptions are the cyclizations of **1c** and **1j** where the steric hindrance is most pronounced and the kinetic control is favoured, increasing the *cis*-selectivity. Only in the absence of steric hindrance in the starting alkenyl hydantoin, 6-membered regioisomers are formed *via* 6-*endo-trig* ring closure process. In the case of **1a**, where a methyl group is attached on C-5 and the double bond is unsubstituted, the six-membered regioisomer is obtained almost exclusively and as a *trans*-isomer stereospecifically. Six-mem-

bered product is also obtained in the cyclization of **1d**, where a methyl group is attached on C5 and the double bond is terminally disubstituted, but without regio- and stereoselectivity. When the double bond is non-terminally substituted, like in **1e**, despite having a methyl group attached on C-5, the six-membered regioisomer is not formed at all. It is assumed that the methyl group on the double bond directly hinders the approach of seleniranium cation to the nitrogen atom during cyclization. Regardless of the substitution of the double bond, the cyclization of alkenyl spirohydantoin **1h–j** depends on the size of the cycloalkyl group. The product of *6-endo-trig* ring closure occurs predominantly only in the case of **1h** without any stereocontrol, while the minor product of *5-exo-trig* ring closure occurs with the reversed stereoselectivity compared to results reported previously.⁹ The bulkier six-membered ring in **1i** and **1j** presumably prevents the formation of another six-membered ring.

TABLE II. Selenocyclization of alkenyl hydantoin **1a–g** and alkenyl spirohydantoin **1h–j**

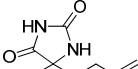
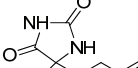
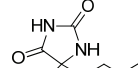
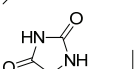
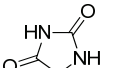
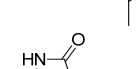
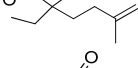
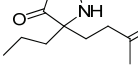
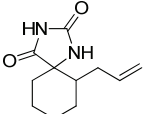
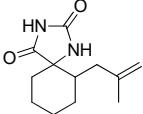
Substrate	Yield, %	Regioisomer ratio ^a 2 : 3	dr (<i>cis/trans</i>) ^a 2	dr (<i>cis/trans</i>) ^a 3
	72	1:99	–	0:100
	88	100:0	70:30	–
	96	100:0	71:29	–
	63	54:46	69:31	59:41
	73	100:0	56:44	–
	63	100:0	44:56	–
	75	100:0	48:52	–
	86	35:65	24:76	50:50

TABLE II. Continued

Substrate	Yield, %	Regioisomer ratio ^a 2:3	dr (cis/trans) ^a 2	dr (cis/trans) ^a 3
	97	100:0	68:32	–
	82	100:0	100:0	–

^aRatio of regio- and diastereoisomers are obtained from GLC and ¹H NMR spectra

CONCLUSION

The influence of electrochemical conditions on selenocyclization reactions of alkenyl hydantoin and spirohydantoin has been explored. Various different solvent/mediator systems have been taken into consideration and MeCN/NaClO₄ showed the best results. Steric hindrances in the starting alkenyl hydantoin influence the regio- and the stereochemical outcome of the reactions and in these conditions thermodynamic control is more present.

Acknowledgement. This work was supported by the Ministry of Education, Science and Technological Development of the Republic of Serbia (Cont. No: 451-03-9/2021-14).

ИЗВОД

УТИЦАЈ ЕЛЕКТРОХЕМИЈСКИХ УСЛОВА НА РЕГИО- И СТЕРЕОСЕЛЕКТИВНОСТ СЕЛЕНОЦИКЛИЗАЦИЈЕ АЛКЕНИЛХИДАНТОИНА

БИЉАНА М. ШМИТ¹, ПЕТАР Б. СТАНИЋ¹, ЉУБИНКА Г. ЈОКСОВИЋ², ДАРКО П. АШАНИН¹ и ЗОРАН СИМИЋ²

Институт за информационе технологије, Универзитет у Крагујевцу, Јована Цвијића бб, Крагујевац и ¹Природно-математички факултет, Универзитет у Крагујевцу, Радоја Домановића 12, Крагујевац

5-Алкенилхидантоини и алкенилспирохидантоини су преведени у бицикличне и трицикличне хидантоине под индиректним електрохемијским условима при којима се фенилселенил-катјони стварају *in situ*. Реакције су се одигравале у добрим до одличним приносима. Испитиван је утицај електрохемијских услова на регио- и дијастереоселективност реакција селеноциклизације.

(Примљено 22. октобра 2020, ревидирано 21 фебруара, прихваћено 23. марта 2021)

REFERENCES

1. Y. Jiang, K. Xu, C. Zeng, *Chem. Rev.* **118** (2018) 4485 (<https://doi.org/10.1021/acs.chemrev.7b00271>)
2. J. C. Thenmozhiyal, P. T. Wong, W. Chui, *J. Med. Chem.* **47** (2004) 1527 (<https://dx.doi.org/10.1021/jm030450c>)
3. A. Volonterio, C. R. de Arellano, M. Zanda, *J. Org. Chem.* **70** (2005) 2161 (<https://dx.doi.org/10.1021/jo0480848>)
4. Y. Fujiwara, G. C. Fu, *J. Am. Chem. Soc.* **133** (2011) 12293 (<https://dx.doi.org/10.1021/ja2049012>)

5. F. Brockmeyer, D. Kröger, T. Stalling, P. Ullrich, J. Martens, *Helv. Chim. Acta* **95** (2012) 1857 (<https://dx.doi.org/10.1002/hlca.201200441>)
6. D. W. Knight, *Prog. Heterocyc. Chem.* **14** (2002) 19 ([https://dx.doi.org/10.1016/S0959-6380\(02\)80004-6](https://dx.doi.org/10.1016/S0959-6380(02)80004-6))
7. N. Petraghani, H. A. Stefani, C. J. Valduga, *Tetrahedron* **57** (2001) 1411 ([https://dx.doi.org/10.1016/S0040-4020\(00\)01033-4](https://dx.doi.org/10.1016/S0040-4020(00)01033-4))
8. B. M. Šmit, R. Z. Pavlović, *Tetrahedron* **71** (2015) 1101 (<https://dx.doi.org/10.1016/j.tet.2014.12.088>)
9. B. M. Šmit, M. Rodić, R. Z. Pavlović, *Synthesis-Stuttgart* **48** (2016) 387 (<https://dx.doi.org/10.1055/s-0035-1561285>)
10. P. Röse, S. Emge, J. Yoshida, G. Hilt, *Beilstein J. Org. Chem.* **11** (2015) 174 (<https://dx.doi.org/10.3762/bjoc.11.18>)
11. D. Stevanović, A. Pejović, M. D. Vukićević, G. Dobrikov, V. Dimitrov, M. S. Denić, N. S. Radulović, R. D. Vukićević, *Helv. Chim. Acta* **96** (2013) 1103 (<https://dx.doi.org/10.1002/hlca.201200610>)
12. B. M. Šmit, R. Z. Pavlović, D. A. Milenković, Z. S. Marković, *Beilstein J. Org. Chem.* **11** (2015) 1865 (<https://dx.doi.org/10.3762/bjoc.11.200>).



J. Serb. Chem. Soc. 86 (6) 591–602 (2021)
JSCS–5446

Investigation of the thermal, mechanical and biological properties of PVC/ABS blends loaded with cobalt chloride for biomedical and electronics applications

MUHAMMAD SHABBIR SHAKIR¹, MUHAMMAD KALEEM KHOSA^{1*},
KHALID MAHMOOD ZIA¹, MUHAMMAD JAWWAD SAIF²
and TANVEER HUSSAIN BOKHARI¹

¹Department of Chemistry Government College University Faisalabad 38000, Pakistan
and ²Department of Applied Chemistry Government College University Faisalabad,
38000, Pakistan

(Received 23 November 2020, revised 2 March, accepted 4 March 2021)

Abstract: New PVC/ABS and CoCl₂ composites with various concentrations of cobalt chloride (≤10 wt. %) were synthesized by solution casting techniques and investigated by spectro-chemical, morphological and thermal mode of characterization. The FT-IR, XRD and SEM analyses proved the smooth distribution and uniformity of the constituents of the composite materials. Thermal behavior showed that the addition of CoCl₂ to the PVC/ABS blends enhanced the thermal stability and improved mechanical properties of composites due to crosslinking between PVC/ABS blend and CoCl₂. Thus based on their remarkable morphology, thermomechanical stability and promising bio-activities, the synthesized composites could be applied for high performance polymeric materials in the field of biomedics and electronics.

Key words: poly(vinyl chloride); acrylonitrile; composites; metal salt.

INTRODUCTION

A composite substance comprises two phases named as matrix and reinforcing phases, which are continuous and discontinuous, respectively. Both these phases collectively work together and enhance different properties of the resulting material. During the manufacture of composite materials two or more different substances having different properties, including morphology and macroscopic composition, are mixed together.¹ Composite materials exhibit better properties than those of the constituents from which they are synthesized. Due to their extraordinary properties, including corrosion resistance, high tensile strength, light weight, high loadbearing capacity, and better surface finishing and

* Corresponding author. E-mail: mkhosapk@yahoo.com
<https://doi.org/10.2298/JSC201123018S>

higher fatigue strength, composite materials are superior to the pristine components in various fields.² During the past few decades, composite material have attracted intense attraction as compared to neat and pure organic materials because of their great and novel properties, including mechanical, thermal stability, flame retardancy, recyclability, aging resistance, dimension stability, *etc.*^{3–9} Polymeric composite substances containing either a bio or synthetic polymer matrix and reinforcing natural fibers, having excellent biocompatibility, are especially employed in different biomedical fields, mainly dental, regenerative medicine, tissue engineering, and for the manufacture of artificial body parts.¹⁰ Poly(vinyl chloride) is a globally used thermoplastic material, over about 23 million ton per year in various fields.¹¹ Poly(vinyl chloride) (PVC) polymer (40 % of dedicated polymeric materials) is suitably employed in the fields of biomedicine and food. Medical and food grade poly(vinyl chloride) are considered as the major polymer for the matrix of antimicrobial composite materials. In spite of being an outstanding building material, PVC has some disadvantages especially concerning human health and environmental hazards. Acrylonitrile–butadiene styrene (ABS) has very interesting features in the polymeric class of compounds with respect to its structures, composition and manufacturing quality. ABS has been applied in a variety of fields because of phase system, mechanical properties, recyclability and cost effective.¹² Acrylonitrile–butadiene styrene comprises two composite systems one of which is the polybutadiene rubber phase and the second is the styrene–acrylonitrile copolymer rigid phase. Polybutadiene–styrene is dispersed and imprinted in the styrene–acrylonitrile co-polymer rigid phase that behaves as a matrix.¹³ Inorganic additives, such as CNTs,^{14–18} graphene,¹⁹ carbon black,²⁰ clay,²¹ MMTs,²² Cal. carbonate,²³ Al₂O₃,²⁴ and SiO₂,²⁵ were selected to dope into different polymer matrices for the manufacture of novel composites. The hydrophilic nature of the inorganic additives and their weak interaction with the organic matrix result in inhomogeneous dispersions. To minimize such difficulties a series of research projects consisting of chemical modification and physical coating were performed.¹²

Keeping in mind previous results, the present research work was based on the synthesis of ternary composites of PVC/ABS and CoCl₂, which was used as a filler attached onto the polymeric chains and disperses through the disordered regions (amorphous regions) forming aggregates between the polymeric chains. Different concentration of CoCl₂ (≤10 weight) were used to enhance the thermo mechanical properties of the composite materials. Structural and morphological studies were performed using FT-IR, SEM and XRD. Thermogravimetric analysis (TGA) was used to investigate the thermal stability and degradation behavior of the ternary composites. Furthermore, such composite materials were subjected to antibacterial and antioxidant investigations.

MATERIALS AND METHOD

Materials

Poly(vinyl chloride) (PVC, M_w 48000 D), acrylonitrile–butadiene styrene (ABS) and cobalt chloride of analytical grade were purchased from Sigma Aldrich and employed as such without further purification. Tetrahydrofuran (THF) as the solvent was purchased from Sigma Aldrich and dried before use.

Instrumental techniques

Various techniques were used to confirm the formation of composite material. An FT-IR spectrophotometer (Bruker) was used for the confirmation of functional groups in the composites. The IR spectra were recorded at room temperature in the range 400 to 4000 cm^{-1} at a resolution of 2 cm^{-1} . For the thermogravimetric analyses, a DSC 404C Netzsch and a Perkin Elmer TGA-7 under nitrogen atmosphere were used. Crystallites of the composites were examined by single-crystal XRD from wide-angle (WA) diffractograms obtained using a 3040/60 X'Pert PRO diffractometer. The thermal stabilities, investigated by heating the composites at a rate of 10 $^{\circ}\text{C min}^{-1}$, were characterized by the initial decomposition temperature (T_0), temperature for 50 % gravimetric loss (T_{50}), maximum degradation temperature (T_{max}) and residual weight at 800 $^{\circ}\text{C}$.

Preparation of PVC/ABS/CoCl₂ composite

The films of PVC/ABS/CoCl₂ composite were prepared by the solution casting technique.²⁶ Typically, different weight ratios of PVC/ABS (80:20), were homogenized in dried THF by constant stirring for about 8 h. At 40 $^{\circ}\text{C}$, a solution of CoCl₂ was dropped into the resulting viscous solution at different weight percents (2.5, 5.0, 7.5 and 10 %) and then the resulting mixtures were stirred overnight at ambient temperature. The films of PVC/ABS/CoCl₂ were casted onto glass Petri dishes and air dried.

RESULTS AND DISCUSSION

Structural elucidation by FT-IR analysis

The FT-IR absorption spectra of PVC/ABS blends loaded with various concentrations of CoCl₂ are shown in Fig. 1. The characteristic absorption band at 2919 cm^{-1} ($-\text{CH}$), 2915 and 2820 cm^{-1} ($-\text{CH}_2$)_{asym} and 1423, 1329, 1256, 968, 615 cm^{-1} were attributed to ($-\text{CH}$) bending of pure PVC.²⁴ The absorption band at 698 cm^{-1} was attributed the $-\text{CH}_2$ rocking vibration and the band at 2235 cm^{-1} was attributed with the CN^- functional group, characteristic of acrylonitrile in ABS and absent in this region for PVC. Mixing of constituents (PVC/ABS) of polymer showed characteristic absorption bands, the small band at 1465 cm^{-1} vanished and sharp bands at 1680, 1140 and 759 cm^{-1} become smaller, while the sharp band at 610 cm^{-1} increased in intensity, which may be due to interaction among the functionality of the polymers back bone with the cation of the inorganic additive cobalt.²⁷

X-Ray diffraction analysis

The degree of crystallinity of synthesized ternary composite of PVC/ABS blended with different contents of cobalt chloride (2.5, 5, 7.5 and 10 %) was

studied by wide angle X-ray diffraction analysis. The X-ray spectra depicted a semi-crystallinity pattern and indicated two halos functional are present at 2θ 18° and 26° under the two peaks having broad areas while ABS have a shoulder at 13° and broad peak at 23.9° because of the amorphous structure of the copolymer, as shown in Fig. 2. The X-ray spectra showed the merging of ABS shoulder and the broad peak of ABS in two halo peaks of PVC, which indicated the uniform dispersion of ABS in PVC. Furthermore, as the content of CoCl_2 increased, intensity of the two halos decreased without any change in the halo position. Such results indicate that different weight ratios of CoCl_2 resulted in changes in the polymeric matrices.²⁸ However, a significant difference between blend doped with CoCl_2 and PVC/ABS blend was observed, which may be due to the good dispersion of CoCl_2 in the polymeric matrices, except the decrease in area under the peaks. It is clear that there are decreases in the area under the two peaks as the contents of CoCl_2 increased (Fig. 2d, e and f) that indicated that CoCl_2 may affect the degree of crystallinity and increased the amorphous regions.²⁹

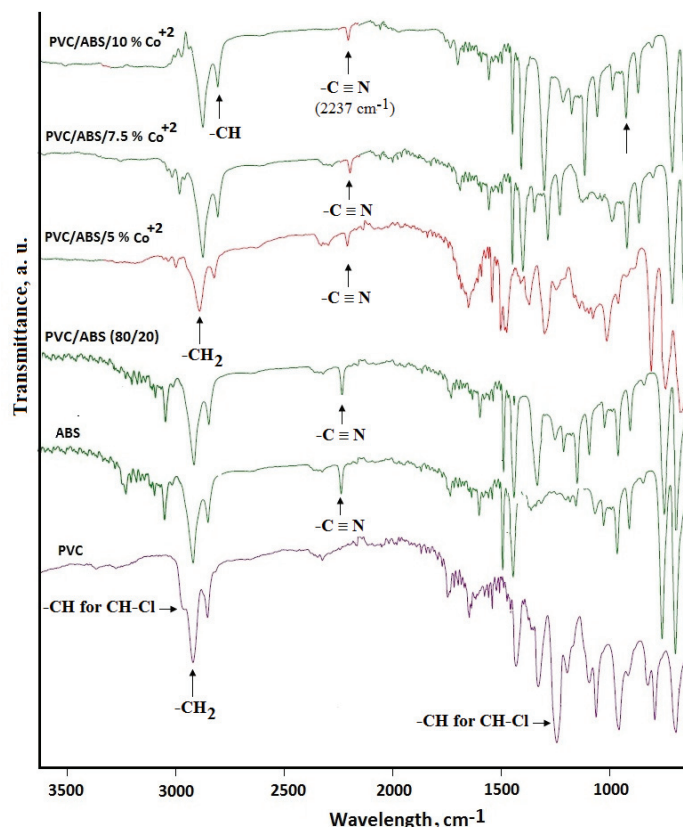


Fig. 1. The FT-IR spectra of PVC/ABS/ Co^{2+} ternary composites.

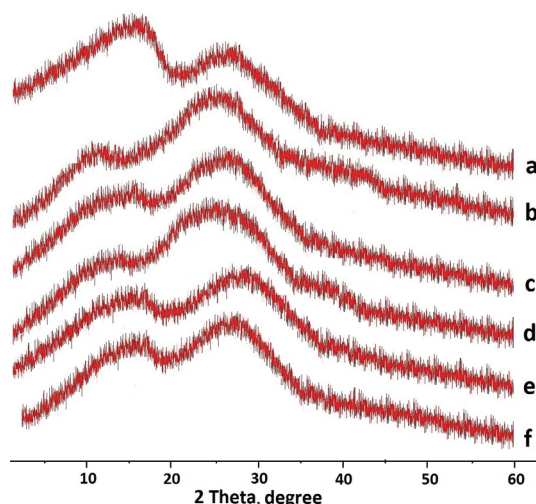


Fig. 2. XRD pattern of PVC/ABS/Co²⁺ composite a: PVC, b: ABS, c: PVC/ABS, d–f: ternary composite with 5, 7.5 and 10 % of Co²⁺.

Thermogravimetric analysis (TGA)

The thermal stabilities of the PVC/ABS blend as well as the blends with various contents of cobalt chloride were evaluated up to 800 °C at a heating rate of 10 °C min⁻¹ in terms of initial decomposition temperature (T_0), the temperature for 50 % mass loss (T_{50}), maximum degradation temperature (T_{max}) and residual weight at 800 °C, as calculated from the respective degradation curves (Fig. 3) and the results are presented in Table I. The thermogram curves showed that ABS decomposed in a single stage that was initiated at about 250 °C with sharp weight loss which was complete at 400 °C; almost 100 % decomposition occurred within an interval of 56 °C. The degradation process of PVC was a two-step process in agreement with literature.³⁰ The first step of the decomposition occurred between about 260–400 °C due dehydrochlorination resulting in the production of unsaturated HCs corresponding to 63 % of weight loss. Then, a stable temperature zone of around 60 °C was found. The next second stage of degradation was initiated at about 470–540 °C. During second stage of decomposition there was 28 % weight loss resulting in breakage of backbone of the polymer. While for the PVC/ABS blend and the blends doped with different contents of CoCl₂, three regions of weight loss were visible. Initially, a total of 8 % of water molecules physically bound with composite. Secondly, a substantial weight loss of about 7–93 %, attributed the main degradation of blend, occurred within the temperature range from 280 up to 485 °C. After 510 °C, a sharp weight loss of the blend occurred due to the breakage of the skeleton of organic matrix by the introduction of CoCl₂ to the cross-linked polymers. The data showed that thermal stability of PVC/ABS blend increased as the concentration

of CoCl_2 increased.³¹ Furthermore, the activation energy was calculated using the Coats and Redfern Equation.³² The values of activation energy decreased on increasing cobalt chloride used as filler in the PVC/ABS blend.

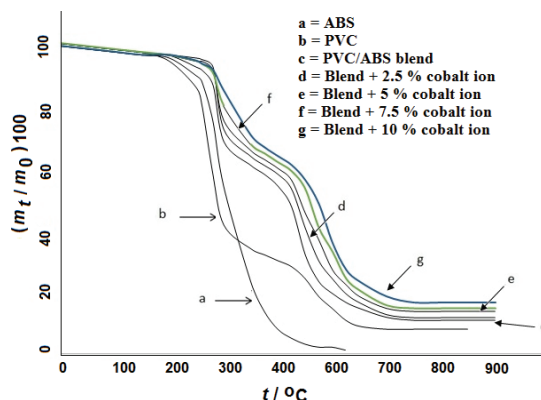


Fig. 3. TGA curves of the prepared ternary (PVC/ABS/CoCl₂) composites.

TABLE I. Results of TGA of PVC/ABS (80:20 weight ratio) with different contents of CoCl₂

CoCl ₂ content, wt. %	$T_0 / ^\circ\text{C}$	$T_{50} / ^\circ\text{C}$	$T_{\text{max.}} / ^\circ\text{C}$	$E_a / \text{J mol}^{-1}$
0	250	425	610	128.75
1.0	255	432	625	105.31
2.5	260	445	640	95.74
5.0	268	450	652	84.63
7.5	272	460	663	76.25
10.0	280	475	680	65.46

Hygroscopic analysis

The moisture absorption capability of composite materials depends on their chemical structure. The water absorption abilities of PVC/ABS blend as well as salt containing composites was determined by weighing the changes of the dried composites before and after immersion in ionized water for 24 h at 25 °C. The water uptake was determined by applying Eq. (1):

$$W_A = 100(W - W_0 / W) \quad (1)$$

where W_0 and W are the weights of dried specimens just after removal from oven and tissue-dried samples after immersion in water, respectively, and found in the range 0.35–0.66 %. Water absorption is due to presence of Co^{2+} . Composites having a lower water uptake value have great importance in the microelectronic industry.³³

Mechanical properties

The effect of the different contents of cobalt chloride on mechanical properties, such tensile strength, elongation at break and Young's modulus, was

investigated and the results are presented in Table II. For all types of the studied synthesized materials, the typical behavior of hard and brittle material was observed. The result showed that the mechanical properties of PVC/ABS/CoCl₂ composites increased many folds as compared to the pure PVC/ABS blend.³³

TABLE II. Mechanical properties of the PVC/ABS (80:20 weight ratio) blend with different contents of CoCl₂

CoCl ₂ content wt. %	Impact strength $\pm SD$, J mol ⁻¹	Tensile strength $\pm SD$, MPa	Young's modulus $\pm SD$, GPa	Elongation at break $\pm SD$, %
0	25 \pm 0.15	43 \pm 0.15	0.95	15 \pm 0.25
1.0	28 \pm 1.34	41 \pm 0.15	0.84 \pm 0.06	18 \pm 0.13
2.5	30 \pm 2.41	38 \pm 0.15	0.81 \pm 0.02	20 \pm 0.24
5.0	35 \pm 1.05	35 \pm 0.15	0.77 \pm 0.04	22 \pm 0.43
7.5	39 \pm 1.16	31 \pm 0.15	0.70 \pm 0.07	26 \pm 0.38
10.0	44 \pm 1.42	30 \pm 0.15	0.69 \pm 0.03	31 \pm 0.22

Scanning electron microscopy

Scanning electron microscopy is an outstanding tool to estimate the smooth distribution and uniformity of the constituents of composite materials. The micrographs of composite investigated under different magnification are shown in Fig. 4. In the absence of fillers, cracks were observed but the application fillers resulted in good distribution and homogeneity. As the contents of cobalt chloride increases, no agglomeration was indicated, which means maximum compatibility of the inorganic fillers with the organic matrix. When the contents of the components of the organic matrix (PVC/ABS) were up to 80:20 weight ratio, the maximum dispersion of phases was observed.³⁴ As the concentration of cobalt chloride was increased, a large number of large particles appeared equally distributed on the fractured surface.

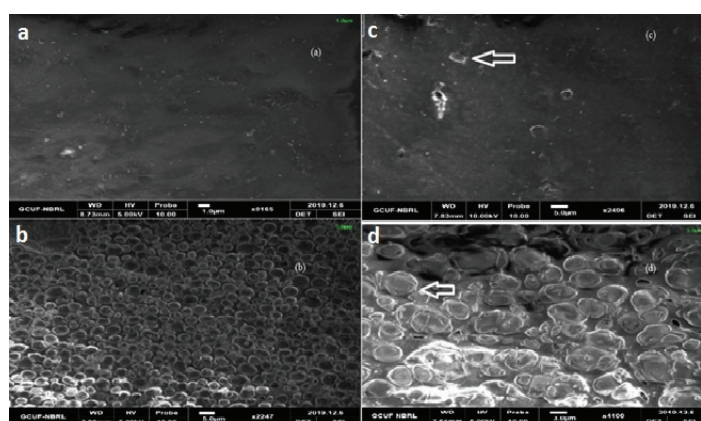


Fig. 4. SEM images of: a) pure PVC; b) PVC/ABS; c) 10 % CoCl₂; d) 5 % CoCl₂ at low and high magnification of 300 and 2000 \times .

BIOLOGICAL INVESTIGATIONS

Antibacterial activity

In order to check the structural–activity relationship, synthesized ternary composites (PVC/ABS/CoCl₂) were screened against six bacterial strains (three Gram-positive strains, *Staphylococcus aureus*, *Bacillus subtilis* and *Streptococcus pyogenes*, and three Gram-negative strains, *Pseudomonas aeruginosa*, *Escherichia coli* and *Salmonella typhi*) by the disc-diffusion method.^{35–37} The strains were cultured at 37 °C in agar–agar nutrient broth for 24 h. The broth culture of the test organisms of approximately 10⁴–10⁶ colony forming units (CFU mL⁻¹) were added to agar medium into sterile Petri dishes at 45 °C and left to solidify. Five µL solution of PVC/ABS/CoCl₂ in DMSO was poured onto sterile paper disks and placed on the nutrient agar plates. Triplicate plates of each organism were prepared and incubated at 37 °C for 24 h and then the zone of inhibition (mm) was measured and compared with standard antibiotic drug (cefixime). In each plate cefixime (1 mg mL⁻¹) served as the reference antibacterial drug. The results are presented in Table III. The PVC/ABS blend and PVC/ABS/CoCl₂ composites showed varying degrees of antibacterial activity with a zone of inhibition. The antibacterial activity of CoCl₂-doped PVC/ABS blends were compared with the standard drug cefixime and it was found that increased contents of CoCl₂ showed remarkable effect from moderate to strong against different bacterial strains. This may be due to the chloro group present in the PVC polymers, which is itself bactericidal.

TABLE III. Antibacterial activity of the PVC/ABS blend with different contents of CoCl₂; 5–10 mm zone of inhibition = activity present, 11–25 mm zone of inhibition = moderate activity, 26–40 mm zone of inhibition = strong activity

Test compounds	Zone of inhibition ± SD, mm					
	<i>S. aureus</i>	<i>S. pyogenes</i>	<i>B. subtilis</i>	<i>E. Coli</i>	<i>S. Typhi</i>	<i>P. aeruginosa</i>
PVC/ABS blend	30±1	22±1	28±1	21±1	28±1	24±1
Blend + 2.5 % CoCl ₂	17±1	15±1	16±1	10±1	14±1	16±1
Blend + 5.0 % CoCl ₂	21±1	19±1	19±1	15±1	19±1	17±1
Blend + 7.5 % CoCl ₂	24±1	23±1	22±1	19±1	21±1	18±1
Blend + 10.0 % CoCl ₂	26±1	25±1	24±1	20±1	24±1	21±1
Cefixime (stand. drug)	33±1.5	31±1	35±1	29±0.5	36±1	31±2

Total antioxidant activity

The free radical scavenging activities of the synthesized composites (PVC/ABS/CoCl₂) were evaluated by the standard DPPH (1,1-diphenyl-2-picrylhydrazyl) method.³⁸ 1,1-Diphenyl-2-picrylhydrazyl (DPPH) is a relatively stable azo radical used to investigate the antioxidant properties of compounds by measurement of the molar absorptivity of DPPH at 517 nm after reaction with a test compound. Stock solutions of the composites (5 mg mL⁻¹) were prepared in DMSO

and different concentrations (5, 10, 20, 40, 100, 200 $\mu\text{g mL}^{-1}$) were obtained by serial dilutions. Each concentration of the composites was mixed with freshly prepared DPPH solution in methanol in glass vials. The vials were sealed and incubated at 37 °C in the dark for 30 min. The deep-violet color of DPPH changed to light-yellow and the absorbance at 517 nm on spectrophotometer (Agilent 8453) was noted. The scavenging activity was calculated.

The antioxidant activity was measured as ascorbic acid equivalent which served as a reference (positive control). The determined results for the antioxidant activity of the PVC/ABS blend and PVC/ABS/CoCl₂ composites are presented in Table IV. The results showed that scavenging activity increased as the concentration of the synthesized composites increased. Comparing the IC_{50} values of the blends and their composites doped with CoCl₂, it was found that such ternary composites are more active in the DPPH activity test than their parent PVC/ABS blends.

TABLE IV. Antioxidant activity of the PVC/ABS blend with different contents of CoCl₂ expressed as the content of DPPH free radical scavenging ($\pm SD$, %)

Compounds	$c / \mu\text{g mL}^{-1}$						$IC_{50} / \mu\text{g mL}^{-1}$
	200	100	50	30	15	5	
PVC/ABS blend	69 \pm 1	42 \pm 1	34 \pm 1	20 \pm 2	10 \pm 1	–	>100
Blend + 2.5 % CoCl ₂	41 \pm 1	33 \pm 1	26 \pm 1	21 \pm 1	15 \pm 1	10 \pm 1	>250
Blend + 5.0 % CoCl ₂	53 \pm 1	44 \pm 2	32 \pm 2	29 \pm 2	18 \pm 1	13 \pm 1	>150
Blend + 7.5 % CoCl ₂	57 \pm 1	41 \pm 2	29 \pm 1	22 \pm 1	19 \pm 1	15 \pm 1	>150
Blend + 10.0 % CoCl ₂	61 \pm 2	46 \pm 1	39 \pm 1	31 \pm 1	28 \pm 2	15 \pm 1	>150
Ascorbic acid	87 \pm 1	84 \pm 1	80 \pm 1	70 \pm 1	56 \pm 1	35 \pm 1	8.75 \pm 1

CONCLUSIONS

PVC/ABS blend and ternary composites decorated with various concentration of CoCl₂ were synthesized and characterized by means of FT-IR, XRD, TGA, mechanical and SEM techniques. The FT-IR analysis showed that the blending of PVC and ABS revealed some characteristic absorption bands for both PVC and ABS due to interaction between them. Shifting of absorption spectra show the interaction between the constituents of polymer and inorganic additives (CoCl₂). The crystalline nature of the synthesized composite was observed by XRD and the area under the peaks was measured. It may be inferred from the result that as the concentration of CoCl₂ increases, the crystallinity is affected due to more defects in the polymer matrices, which reduces the area under the peaks. The thermograms of all the composites (PVC/ABS/CoCl₂) show a similar mode of three step degradation. It could be concluded that enhancing the doping concentration of CoCl₂ in the blend (PVC/ABS) results in higher order, reduced thermal motion and enhancement of the thermal stability due to the predomination of random scission initiated degradation of the macromolecule

chains in the polymeric matrices and decreased activation energy of the process. The mechanical properties of PVC/ABS/CoCl₂ composites are greatly influenced by the composition. The incorporation of cobalt chloride in PVC/ABS enhances the thermal stability of the composite due to interfacial interaction and coordination between cobalt ions (Co²⁺) and nitrile groups (–CN) of ABS in solid state, which result in enhancement in mechanical properties. SEM analysis proved the smooth distribution and uniformity of the constituents of composite materials. Concerning bioactivity, the PVC/ABS blend as well as blends with different concentrations of CoCl₂ showed activity against bacterial strains and free radical scavenging activity. Thus, based on their remarkable morphology, thermomechanical stability and promising bioactivity, the synthesized composites could be applied for high performance polymeric materials in the fields of biomedics and electronics.

Acknowledgement. The Authors thank the HEC, Islamabad, Pakistan for financial support (Grant No. 20-1434/R & D/09/9057).

ИЗВОД

ИСПИТИВАЊЕ ТЕРМИЧКИХ, МЕХАНИЧКИХ И БИОЛОШКИХ СВОЈСТАВА
МЕШАВИНЕ PVC/ABS СА ДОДАТКОМ КОБАЛТ-ХЛОРИДА ЗА ПРИМЕНУ У
БИОМЕДИЦИНИ И ЕЛЕКТРОНИЦИ

МУHAMMAD SHABVIR SHAKIR¹, МУHAMMAD KALEEM KHOSA¹, KHALID MAHMOOD ZIA¹,
МУHAMMAD JAWWAD SAIF² и TANVEER HUSSAIN BOKHARI¹

¹Department of Chemistry Government College University Faisalabad 38000, Pakistan и ²Department of Applied Chemistry Government College University Faisalabad 38000, Pakistan

Нови PVC/ABS и CoCl₂ композит са различитим концентрацијама кобалт-хлорида (≤10 мас. %) синтетисани су техникама изливања из раствора и истражени су спектрохемијском, морфолошком и термичком карактеризацијом. FT-IR, XRD и SEM анализа доказале су глатку расподелу и уједначеност састојака композитних материјала. Термичко понашање показало је да додавање CoCl₂ мешавини PVC/ABS побољшава термичку стабилност и побољшава механичка својства композита услед умрежавања мешавине PVC/ABS и CoCl₂. Тако се на основу изузетне морфологије, термомеханичке стабилности и обећавајуће биоактивности, синтетизовани композити могу применити за полимерне материјале високих перформанси у области биомедицине и електронике.

(Примљено 23. новембра 2020, ревидирано 2 марта, прихваћено 4. марта 2021)

REFERENCES

1. W. Daming, G. Xiaolong, S. Jingyao, W. Dan, L. Ying, S. Kormakov Z. Xiuting, W. Lili, H. Yao, G. Zhanhu, *Compos., A* **102** (2017) 88
(<https://doi.org/10.1016/j.compositesa.2017.07.027>)
2. K. R. Dipen, D. P. Durgesh, L. M. Pradeep, L. Emanoil, *Polymer* **11** (2019) 1667
(<https://doi.org/10.3390/polym11101667>)
3. C. Shao, P. Shang, Y. Mao, Q. Li, C. Wu, *Mater. Res. Express* **5** (2018) 015309
(<https://doi.org/10.1088/2053-1591/aaa466>)

4. H. G. Mohamed, A. A. Mohamed, G. Waheedullah, S. Naheed, A. Mohammad, J. Mohammad, Y. A. Othman, *J. Mater. Res. Technol.* **8** (2019) 853 (<https://doi.org/10.1016/j.jmrt.2018.06.013>)
5. H. Y. Salih, *J. Mater. Res. Technol.* **8** (2019) 4725 (<https://doi.org/10.1016/j.jmrt.2019.08.018>)
6. N. Sabaa, Y. A. Othman, A. Zeyad, M. Jawaida, G. Waheedullah, *J. Mater. Res. Technol.* **8** (2019) 3959 (<https://doi.org/10.1016/j.jmrt.2019.07.004>)
7. R. M. Penchal, F. Ubaid, A. S. Rana, M. A. M. Adel, *J. Mater. Res. Technol.* **7** (2018) 165 (<https://doi.org/10.1016/j.jmrt.2017.10.003>)
8. X. Gao, Y. Huang, X. He, X. Fan, Y. Liu, H. Xu, D. Wu, C. Wan, *Polymers* **11** (2019) 56 (<http://doi.org/10.3390/polym11010056>)
9. S. Cho, W. Choi, *J. Photochem. Photobiol., A* **143** (2001) 221 ([https://doi.org/10.1016/S1010-6030\(01\)00499-3](https://doi.org/10.1016/S1010-6030(01)00499-3))
10. F. Hussain, M. Hojjati, M. Okamoto, R. E. Gorga, *J. Compos. Mater.* **40** (2006) 155 (<https://doi.org/10.1177/0021998306067321>)
11. Z. Aimin, Z. Gouqun, H. Yang, G. Yanjin, *Polym-Plast. Technol. Eng.* **56** (2017) 382 (<https://doi.org/10.1080/03602559.2016.1211698>)
12. R. Amit, A.V. Gawade, Lodha, and P. S. Joshi, *J. Macromol. Sci., B* **47** (2008) 201 (<https://doi.org/10.1080/00222340701748701>)
13. Z. Roslaniec, G. Broza, K. Schulte, *Compos. Interfaces* **10** (2008) 95 (<https://doi.org/10.1163/156855403763586819>)
14. A. Nogales, G. Broza, Z. Roslaniec, K. Schulte, I. Šics, B. S. Hsiao, T. A. Ezquerra, *Macromolecules* **37** (2004) 7669 (<https://doi.org/10.1021/ma049440r>)
15. Y. Ma, D. Wu, Y. Liu, X. Li, H. Qiao, Z. Z. Yu, *Compos., B* **56** (2014) 384 (<https://doi.org/10.1016/j.compositesb.2013.08.026>)
16. A. N. Khan, T.T. Nguyen, L. Dobircau, M. Schmutz, P. J. Mesini, J. M. Guenet, *Langmuir* **29** (2013) 16127 (<https://doi.org/10.1021/la404002k>)
17. X. Wang, Q. Jiang, W. Xu, W. Cai, Y. Inoue, Y. Zhu, *Carbon* **53** (2013) 145 (<https://doi.org/10.1016/j.carbon.2012.10.041>)
18. R. J. Young, I. A. Kinloch, L. Gong, K. S. Novoselov, *Compos. Sci. Technol.* **72** (2012) 1459 (<https://doi.org/10.1016/j.compscitech.2012.05.005>)
19. Y. Kameya, T. Hayashi, M. Motosuke, *Appl. Catal., B* **89** (2016) 219 (<https://doi.org/10.1016/j.apcatb.2016.02.049>)
20. A. N. Khan, A. Hayder, W. T. Chaung, P. D. Hong, *Polym. Sci., A* **57** (2015) 874 (<https://doi.org/10.1134/S0965545X15060127>)
21. A. N. Khan, B. A. Ahmed, *Polym. Bull.* **72** (2015) 1207 (<https://doi.org/10.1007/s00289-015-1333-4>)
22. J. Shi, W. Qi, C. Du, J. Shi, S. Cao, *J. Appl. Polym. Sci.* **129** (2013) 577 (<https://doi.org/10.1002/app.38718>)
23. F. L. Guan, C. X. Gui, H. B. Zhang, Z. G. Jiang, Y. Jiang, Z. Z. Yu, *Compos., B* **98** (2016) 134 (<https://doi.org/10.1016/j.compositesb.2016.04.062>)
24. R. Xu, M. Jia, F. Li, H. Wang, B. Zhang, *J. Appl. Phys., A* **106** (2012) 747 (<https://doi.org/10.1007/s00339-011-6697-1>)
25. M. Z. Rong, M. Q. Zhang, W. H. Ruan, *Mater. Sci. Technol.* **22** (2006) 787 (<https://doi.org/10.1179/174328406X101247>)
26. N. S. Alghunaim, *Res. Physics* **5** (2015) 331 (<http://dx.doi.org/10.1016/j.rinp.2015.11.003>)
27. V. V. Soman, D. S. Kelkar, *Macromol. Symp.* **277** (2009) 152 (<https://doi.org/10.1002/masy.200950319>)

28. S. Rajendran, P. Sivakumar, R. S. Babu, *J. Power Sources* **164** (2007) 815 (<https://doi.org/10.1016/j.jpowsour.2006.09.011>)
29. E. M. Abdelrazek, A. M. Abdelghany, A. H. Oraby, G. M. Asnag, *Inter. J. Eng. Tech.* **12** (2012) 98 (<https://doi.org/10.1007/s11664-020-08342-0>)
30. I. S. Elashmawi, N. H. Elsayed, F. A. Altalhi, *J. Alloys Comp.* **617** (2014) 877 (<https://doi.org/10.1016/j.jallcom.2014.08.088>)
31. I. Klaric, U. Roje, M. Bravar, *J. Appl. Polym. Sci.* **61** (1996) 1123 ([https://doi.org/10.1002/\(SICI\)1097-4628\(19960815\)61:7%3c1123::AID-APP8%3e3.0.CO;2-O](https://doi.org/10.1002/(SICI)1097-4628(19960815)61:7%3c1123::AID-APP8%3e3.0.CO;2-O))
32. A. W. Coats, J. P. Redfern, *Nature* **964** (2011) 68 (<https://doi.org/10.1038/201068a0>)
33. W. Qiao, H. Wang, Y. Zhao, Y. Han, *Adv. Mater. Res.* **217** (2011) 1170 (<https://doi.org/10.4028/www.scientific.net/AMR.217-218.1170>)
34. H. Azman, A. Abozar, K. H. Ngoo, T. R. Chantara, *Polym. Plast. Technol. Eng.* **51** (2012) 473 (<https://doi.org/10.1080/03602559.2011.651242>)
35. F. Annie, G. Bernadette, H. L. Philippe, C. Isabelle, *J. Clin. Microbiol.* **40** (2002) 2766 (<https://doi.org/10.1128/JCM.40.8.2766-2771.2002>)
36. M. Jamil, I. U. Haq, B. Mirza, *Ann. Clin. Microbiol. Antimicrob.* **11** (2012) 11 (<https://doi.org/10.1186/1476-0711-11-11>)
37. A. Sevtap, P. Victor, H. R. John, *Antimicrob. Agents Chemother.* **46** (2002) 3084 (<https://doi.org/10.1128/AAC.46.9.3084-3087.2002>)
38. G. Cao, E. Sofic, R. L. Prior, *J. Agric. Food Chem.* **44** (1996) 3426 (<https://doi.org/10.1021/jf9602535>).



Subcritical water extraction of horse chestnut (*Aesculus hippocastanum*) tree parts

TANJA GAGIĆ¹, ŽELJKO KNEZ^{1,2} and MOJCA ŠKERGET^{1*}

¹Laboratory for Separation Processes and Product Design, Faculty of Chemistry and Chemical Engineering, University of Maribor, Smetanova ulica 17, 2000 Maribor, Slovenia and ²Faculty of Medicine, University of Maribor, Taborska ulica 8, 2000 Maribor, Slovenia

(Received 11 November 2020, revised and accepted 18 February 2021)

Abstract: Subcritical water extraction of horse chestnut (*Aesculus hippocastanum*) parts, such as seeds, seed shell, bark and leaves has been performed in a batch reactor at temperatures of 150, 200 and 250 °C and extraction times of 5, 15 and 30 min. The obtained extracts were analyzed by spectrophotometric methods to determine the total phenols, total carbohydrates and antioxidant activity. Furthermore, the compounds detected in the extracts, such as triterpene saponins (escins), coumarin glycosides (esculin and fraxin), phenolic compounds (chlorogenic, neochlorogenic and gallic acids) and furfurals (5-hydroxymethylfurfural, furfural, and 5-methylfurfural) were quantified using HPLC. High amount of escins was obtained in the seed extracts, while the highest amounts of esculin and fraxin were obtained in bark extracts. The total phenol content was the highest in shell and bark extracts, which implies that these extracts gave the highest antioxidant activity.

Keywords: antioxidant activity; extraction; escins; coumarin glycosides; phenolic compounds.

INTRODUCTION

The horse chestnut (*Aesculus hippocastanum*) tree is widely distributed all over the world due to its excellent resistance to environmental conditions.¹ Horse chestnut seeds contain high amounts of starch, minerals, vitamins, flavonoids, carotenoids, fatty acids, but they are not edible due to presence of saponins.² Knowing that horse chestnut seeds are not edible, they are usually treated as biowaste.³ The most important bioactive component found in horse chestnut seeds is aescin, which represents a mixture of triterpene saponins mainly consisting of escin Ia, escin Ib, isoescin Ia and isoescin Ib.⁴ Escin Ia and Ib are β -escins that are dominant in seeds, while isoescin Ia and Ib are α -escins.⁴ In order to use horse chestnut seeds in the food industry and as a safe addition to the

* Corresponding author. E-mail: mojca.skerget@um.si
<https://doi.org/10.2298/JSC201111013G>

food supply, Rafiq *et al.* studied the method for reduction of toxic compounds found in horse chestnut (*Aesculus indica*) seeds.² They showed that pre-treatments, such as soaking and especially microwave heating, drastically reduced the anti-nutritional components.²

Although these escins are toxic compounds and are the reason why seeds are not edible, they have other positive properties, such as anti-oedematous, anti-inflammatory and venotonic properties.¹ Thus, the extracts of horse chestnut seed could find application in the cosmetic and pharmaceutical industry in the treatment of chronic venous insufficiency, varicose veins, haemorrhoids, post-operative edemas, burns, epidermis abrasion, skin inflammations and frostbites.⁵

Takahashi *et al.* showed that horse chestnut seed, especially the outer theca (seed shell), has strong antibacterial properties toward *Staphylococcus aureus*, *Escherichia coli* and *Streptococcus mutans*.³ Furthermore, the polyphenol content of the outer theca was around three times higher than that of “sarcocarp and endodermis”. The good antioxidant properties are probably the reason why the theca possess high antibacterial properties. The outer theca also showed high deodorizing activity against basic and acidic odors. Moreover, Kimura *et al.* showed that Japanese horse chestnut seed shell contains highly polymerized proanthocyanidins that possess strong antiobesity effects.⁶

In this research subcritical water was used for the extraction of different parts of horse chestnut (seeds, bark, seed shells and leaves). No comparable study could be found in the literature. This method was used because generally, compared to conventional extraction techniques, subcritical water shows high extraction efficiency, the process needs shorter extraction time and it is a clean and non-toxic method.

EXPERIMENTAL

Materials

Seeds, bark, seed shell and leaves of horse chestnut (*Aesculus hippocastanum*) were collected in Serbia in June 2018. All parts of the horse chestnut were air-dried and ground before the extraction. Furfural (purity 99%) and 5-HMF (purity 98 %) were purchased from Acros Organics (Geel, Belgium). Chlorogenic acid (purity 98 %), neochlorogenic acid (purity 98 %), gallic acid, escin, esculin hydrate and fraxin were purchased from Sigma–Aldrich (Steinheim, Germany).

Subcritical water extraction

The subcritical water extraction was performed in a 75 mL Parr batch reactor (series 4740 stainless steel, Parr instruments, Moline, IL, USA) at temperatures of 150, 200 and 250 °C and extraction times of 5, 15 and 30 min using a material–solvent ratio of 1 g in 20 mL. The procedure of the extraction was described in a previous work.⁷ Nitrogen was used to remove the oxygen present and to control the pressure. The mixture was stirred at 600 rpm. The reactor was heated by electrical wire. The reaction time was measured when the reactor reached the desired temperature. After the reaction, the reactor was rapidly cooled. The reactor content was filtrated and washed with water.

The extraction yield was calculated by Eq. (1):

$$Y_i = 100 \frac{m_e}{m_0} \quad (1)$$

where Y_i – the extraction yield; m_e – the mass of the extract; m_0 – the initial mass of material.

Total phenol content

The total phenol content in the extracts was determined using the Folin–Ciocalteu method, as described in a previous work.⁷ Extract (0.5 mL) was mixed with 2.5 mL of Folin–Ciocalteu reagent (diluted 1:10 with water) and 2 mL of Na_2CO_3 solution (75 g L^{-1}). The sample was heated at a temperature of $50 \text{ }^\circ\text{C}$ for 5 min in a water bath and then cooled to room temperature. After 30 min, the absorbance was measured at 760 nm using a UV-Vis spectrophotometer. Results are expressed as mg of gallic acid per g of material.

Total carbohydrate content

The total carbohydrates in the extracts was determined with the phenol–sulfuric colorimetric method explained in a previous work.⁸ Extract (1 mL) was mixed with 0.5 mL of 5 % aqueous solution of phenol and 2.5 mL of concentrated sulfuric acid. The sample was placed in an ultrasonic bath for a 10 min and then kept at room temperature for 20 min for color development. The absorbance was measured at 490 nm using a UV-Vis spectrophotometer. All measurements were performed in triplicate. The results are expressed in mg g^{-1} of material.

Antioxidant activity

The antioxidant activity of the extracts obtained by subcritical water extraction was determined by the DPPH method, as explained in a previous work.⁷ The extract (77 μL) (concentration 1 mg mL^{-1}) was mixed with 3 mL of DPPH solution. The mixture was incubated in a dark room for 15 min. The absorbance of the sample at 515 nm was measured using a UV-Vis spectrophotometer. The antioxidant activity is expressed in %.

HPLC methods

The HPLC method for detection of esculin, fraxin, 5-HMF, furfural and 5-MF is described in the literature.⁹ The extracts were analyzed using an Agilent 1100 Series HPLC system (Agilent Technologies, Waldbronn, Germany) equipped with a binary pump, an auto-sampler, a column heater, a variable wavelength detector (VWD) and an Agilent Zorbax Eclipse XDB C18 (4.6 mm \times 150 mm, 3.5 μm) column. The column temperature was $25 \text{ }^\circ\text{C}$. The mobile phase consisted of two solvents: methanol (solvent A) and water + 0.1 % trifluoroacetic acid (solvent B). The flow rate was 1 mL min^{-1} . The following gradient was set: 0 min 90 % B, 18 min 65 % B, 20 min 90 % B. The injection volume was 10 μL . Detection of the compounds was achieved at 254 nm for esculin and fraxin and 280 nm for 5-HMF, furfural, 5-MF.

The escins were determined by the HPLC method as described in the literature¹⁰ with minor modifications. The same HPLC system was used with a C18 column (150 mm \times 4.6 mm, 3.5 μm) heated to $30 \text{ }^\circ\text{C}$. The method was isocratic and the mobile phase was a mixture of acetonitrile and 0.1 % orthophosphoric acid (39:61 volume ratio). The flow rate was 1 mL min^{-1} , while the injection volume was set to 10 μL . The escins were detected at 210 nm. The quantifications were performed using standard calibration curves.

RESULTS AND DISCUSSION

Extraction yield

The yields of the extractions performed under different operating conditions are presented in Table I. The highest yields were obtained in the case of seeds, *i.e.*, 82.66 % at 150 °C and 15 min and 82.22 % at 200 °C and 5 min. The extraction yield in the case of seeds was much higher than in the case of the other materials (shell, bark and leaves) because seeds contain much higher amounts of compounds that are soluble in subcritical water (carbohydrates and especially fats). Kapusta *et al.* obtained a significantly lower extraction yield (25.2 %) using 80 % ethanol as extraction solvent at room temperature and extraction time of 72 h.¹¹

TABLE I. The extraction yields of seed (Y_{SE}), bark (Y_{BE}), seed shell (Y_{ShE}) and leaf (Y_{LE})

$T / ^\circ\text{C}$	t / min	$Y_{SE} / \%$	$Y_{BE} / \%$	$Y_{ShE} / \%$	$Y_{LE} / \%$
150	5	69.01	23.91	26.91	31.64
150	15	82.66	29.37	36.51	32.21
150	30	75.92	30.91	34.00	32.67
200	5	82.22	38.43	24.45	36.96
200	15	69.63	43.59	27.14	31.90
200	30	64.82	26.32	27.02	31.82
250	5	32.13	23.04	11.63	34.41
250	15	25.23	23.54	14.39	34.41
250	30	24.97	16.40	13.74	30.39

Total phenols, total carbohydrates and antioxidant activity

The amounts of total phenols and carbohydrates extracted from different parts of chestnut are given in Table II. The highest amounts of total phenols isolated from seeds and leaves were obtained at 250 °C and 5 min and were 26.01 and 24.48 mg g⁻¹, respectively, while the maximal amount of total phenols from seed shell and bark were obtained at 200 °C and 15 min and were 50.99 mg g⁻¹ and 33.29 mg mL⁻¹, respectively.

TABLE II. The amount (mg g⁻¹) of total phenols (Y_{TP}) and total carbohydrates (Y_{TC}) extracted from seeds (S), bark (B), seed shell (Sh) and leaves (L)

$T / ^\circ\text{C}$	t / min	Parameter							
		Y_{TPS}	Y_{TPB}	Y_{TPSh}	Y_{TPL}	Y_{TCS}	Y_{TCB}	Y_{TCSh}	Y_{TCL}
150	5	6.46	20.18	36.06	7.81	198.12	49.49	57.76	36.54
150	15	5.63	22.32	39.87	11.87	227.91	60.85	57.78	36.30
150	30	6.47	22.78	35.55	9.47	260.99	76.37	57.75	46.13
200	5	17.32	29.40	33.10	18.98	252.40	77.76	59.39	44.56
200	15	20.98	33.29	50.99	21.28	253.30	85.25	87.22	37.36
200	30	21.58	28.57	22.16	19.95	244.12	81.78	38.65	21.20
250	5	26.01	29.21	25.96	24.48	139.58	48.29	28.17	13.40
250	15	23.73	25.77	24.72	20.86	91.24	37.23	25.72	7.48
250	30	22.70	24.29	25.60	17.63	82.40	30.87	13.16	5.83

The effect of temperature on the amount of carbohydrates obtained from each material was similar. In the case of seeds, seed shell and leaves at extraction times of 5 and 15 min, on increasing the temperature from 150 to 200 °C, the amount of carbohydrate increased and then decreased on further increasing of the temperature, while at 30 min it decreased on increasing the temperature over the whole temperature range. The exception was horse chestnut bark, where the carbohydrate amount increases at temperatures from 150 to 200 °C and then decreases at 250 °C.

The highest amount of total carbohydrates extracted from seed and leaves were 260.99 mg g⁻¹ material and 46.13 mg g⁻¹ material obtained at 150 °C and 30 min, respectively, while the maximal amount of total carbohydrates from seed shell and bark obtained at 200 °C and 15 min were 87.22 and 85.25 mg g⁻¹, respectively.

The antioxidant activities of the horse chestnut extracts are presented in Table III. The antioxidant activity of seed extracts was the lowest compared to the other materials and it increased with extraction temperature and time, reaching the maximal value of 54.15 % at 250 °C and 30 min.

TABLE III. Antioxidant activity of seed (AA_S), bark (AA_B), seed shell (AA_{Sh}) and leaf (AA_L) extracts

$T/^\circ\text{C}$	t/min	$AA_S/\%$	$AA_B/\%$	$AA_{Sh}/\%$	$AA_L/\%$
150	5	3.34	67.79	89.20	18.35
150	15	2.45	61.01	90.47	25.22
150	30	3.52	57.08	90.06	21.33
200	5	9.30	55.42	89.46	32.89
200	15	15.10	60.05	87.89	42.86
200	30	16.51	83.51	84.90	41.29
250	5	47.34	92.05	89.57	57.87
250	15	53.04	88.98	88.86	47.02
250	30	54.15	91.34	90.54	40.39

The highest antioxidant activity in the case of leaf extracts was 57.87 % obtained at 250 °C and 5 min. The bark and seed shell extracts show the highest antioxidant activities (around 90 %), which could be probably attributed to higher total phenol content in extracts of these materials (in the range from 73.71 to 148.11 mg g⁻¹ of extract and from 82.0 to 223.25 mg g⁻¹ of extract, respectively) compared to seeds and leaves (in the range from 6.81 to 94.06 mg g⁻¹ of extract and from 24.68 to 71.14 mg g⁻¹ of extract, respectively). Otajagić *et al.* determined total phenolic content and antioxidant activity of ethanolic extracts of different parts of *Aesculus hippocastanum* (bark of young twigs (BT) and fruits (BF), bark of fruit with pulp (BF+P) and pulp itself (P)).¹² The highest amounts of total phenolics were detected in the BF and BT extracts, 158–202 mg GAE g⁻¹ and 178–216.97 mg GAE g⁻¹, respectively, and the antioxidant activities of these

extracts were around 90 %. These results are in agreement with the presented results for seed shell and bark, but in present work, where subcritical water was used as extraction medium, the total phenol content and antioxidant activity of seed extract was 94.06 mg g⁻¹ of extract and 53.04 %, respectively, at 250 °C and 15 min, which is much higher than in the case of ethanol extraction (8.80–12.36 mg GAE g⁻¹ and 15–25 %, respectively). Probably, at higher temperatures (200 and 250 °C), the hydrolysis of phenolic glycosides occurred and phenolic aglycones, which possess higher antioxidant activity than phenolic glycosides, were formed in the extracts. Kimura *et al.* studied the antioxidant activities and content of flavonol *O*-glycosides of whole seeds, peeled seeds and seed shells from Japanese horse chestnut (*Aesculus turbinata*) extracts, obtained with an acetone–water–acetic acid mixture (70:29.5:0.5 volume ratio).¹³ The results indicate that the peeled seeds are a good source of flavonol *O*-glycosides serving as antioxidants to be used as food additives and dietary supplements. They obtained lower content of polyphenols (5.71 mg g⁻¹ of seed extract and 68 mg g⁻¹ of seed shell extract) compared to results obtained using subcritical water extraction.

Triterpene saponins, coumarin glycosides, phenolic acids and furfurals

The amount of escins, esculin and fraxin extracted from seed, seed shell, bark and leaf of horse chestnut are presented in Table IV. The escins were detected only in seed extracts. From the results, it could be observed that at 150 °C, the amount of escins decreases with increasing extraction time, while at 200 °C after 5 min, they are completely degraded. At 150 °C and 5 min, the amount of escins extracted from seeds was 33.11 mg g⁻¹ of material, which shows that the amount of escins in seed extracts obtained by subcritical water extraction was almost the same as that obtained by extraction with methanol (34.9 mg g⁻¹ for the year of 2014) published by Abudayeh *et al.*¹⁰. Chen *et al.* determined four main saponins (escin Ia, escin Ib, isoescin Ia, isoescin Ib) from a different variety of horse chestnut (*Aesculus chinensis*) using accelerated solvent extraction.¹⁴ The solvents used were *n*-butanol, 70 % methanol, methanol, 30 % ethanol, 50 % ethanol and 80 % ethanol with 0.5 % of acetic acid. The quantities of these compounds extracted by 70 % methanol were the highest (average content of escins in different chestnut samples were 42.8 mg g⁻¹ of extract), which is similar to the results obtained by subcritical water extraction.

Esculin and fraxin were the dominant compounds in bark extracts, but they were also found in other extracts. The amounts of both esculin and fraxin isolated from bark decrease with extraction time and temperature, except at 150 °C when the esculin amount increased from 5 min to 15 min. In the case of bark extracts, esculin was not detected anymore at the conditions of 250 °C and 15 min, while fraxin was no longer present already at 200 °C and 15 min. Similar amounts of esculin and fraxin in horse chestnut bark were obtained by Stanić *et al.*,¹⁵ where

methanol was used as the extraction solvent and the highest amounts obtained in bark samples (branch diameter of 5 cm) were in the range from 36 to 59.6 mg g⁻¹ of material for esculin and from 15.3 to 26.2 mg g⁻¹ of material for fraxin. Thus, subcritical water as non-toxic and environmentally friendly medium could be good replacement for organic extraction solvents for the extraction of these compounds. In the case of other materials (seeds, seed shell and leaves), esculin and fraxin were detected in the extracts obtained at 200 °C, while above 250 °C at an extraction of 5 min, they were no longer present in the extracts.

TABLE IV. The amount (mg g⁻¹) of escins (Y_{Escin}), esculin (Y_{Escul}) and fraxin (Y_{Frax}) extracted from seed (S), bark (B), seed shell (Sh) and leaves (L)

$T/^\circ\text{C}$	t/min	Parameter								
		Y_{EscinS}	Y_{EsculS}	Y_{EsculB}	$Y_{EsculSh}$	Y_{EsculL}	Y_{FraxS}	Y_{FraxB}	Y_{FraxSh}	Y_{FraxL}
150	5	33.11	n.d.	41.63	n.d.	2.26	n.d.	20.38	n.d.	1.79
150	15	29.85	n.d.	46.18	n.d.	2.33	n.d.	18.01	n.d.	1.67
150	30	26.02	n.d.	44.19	n.d.	2.23	n.d.	n.d.	n.d.	1.79
200	5	17.08	n.d.	32.21	1.87	2.33	2.69	4.06	2.08	n.d.
200	15	n.d.	2.12	21.76	1.88	n.d.	1.74	n.d.	2.09	n.d.
200	30	n.d.	3.09	9.98	1.87	n.d.	1.74	n.d.	2.02	n.d.
250	5	n.d.	2.95	1.71	n.d.	1.92	2.75	n.d.	n.d.	1.67
250	15	n.d.	n.d.	n.d.	n.d.	n.d.	n.d.	n.d.	n.d.	n.d.
250	30	n.d.	n.d.	n.d.	n.d.	n.d.	n.d.	n.d.	n.d.	n.d.

Typical chromatograms are shown in Fig. 1 of the escin mixture standard (A) and chestnut seed extract treated with water at a temperature of 150 °C and an extraction time of 5 min (B). As can be seen from the chromatograms, the detected peaks represent escins, such as escin Ia (1), escin Ib (2), isoescin Ia (3) and isoescin Ib (4). The peaks were identified based on the data published by Abudayeh *et al.*¹⁰

The amounts of chlorogenic acid, neochlorogenic acid and gallic acid extracted from different parts of horse chestnut are presented in Table V. Chlorogenic acid was detected in higher amounts only in extracts from bark, while in extracts from other chestnut parts, it was present only in trace amounts. The results obtained for bark at 150 and 200 °C show that the amount of chlorogenic acid decreases with increasing temperature and time, while at 250 °C it was no longer present in the extract. Furthermore, the highest amount of neochlorogenic acid was detected in seed shell extracts. In the cases of seed shell, bark and leaf, the amount of neochlorogenic acid increases with increasing extraction time at 150 °C and reaches the highest value at 200 °C and 5 min. However, in the case of seeds, the amount of neochlorogenic acid increases with increasing time and temperature and reaches the highest value at 200 °C and 30 min, while at 250 °C, it was no longer present in the extracts. Oszmaiański *et al.* extracted leaves of horse chestnut with methanol acidified with 1 % acetic acid for 20 min under

sonication.¹⁶ They found different phenolic compounds (neochlorogenic acid, epicatechin, proanthocyanidins and quercetin and kaempferol derivatives) in the extracts of white and red horse chestnut leaves. The content of neochlorogenic acid found in the literature was 1.26 mg g^{-1} of leaf extracts, while in the present work, the highest content of neochlorogenic acid was 2.41 mg g^{-1} of leaf extract at $200 \text{ }^\circ\text{C}$ and 15 min. Gallic acid was detected only in leaf extracts and at $150 \text{ }^\circ\text{C}$, the amount decreased with increasing extraction time, while after $200 \text{ }^\circ\text{C}$ and 5 min, it was no longer present in the extracts. Postoyuk *et al.* identified various components in leaf extracts: 1) different phenolic compounds among which the dominant were gallic acid, hyperoside, epigallocatechin-gallate, luteolin-7-glucoside and cichoric acid; 2) organic acids such as citric, tartaric, malic, ascorbic, oxalic and lactic acid; 3) sugars such as glucose and fructose; 4) escin.¹⁷ They obtained an amount of gallic acid of 146 mg g^{-1} of leaf extract, while in the case of subcritical water extraction, this value was 4.96 mg g^{-1} of leaf extract at $150 \text{ }^\circ\text{C}$ and 5 min, probably because hydrolysis of gallic acid occurred.

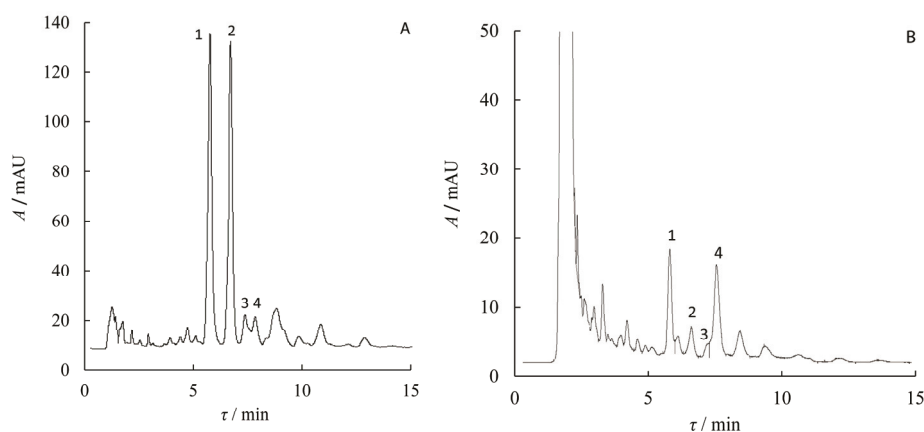


Fig. 1. Typical chromatogram of :A) escin mixture standard and B) chestnut seed extract treated with water at a temperature of $150 \text{ }^\circ\text{C}$ and an extraction time of 5 min. Identified peaks: 1 – escin Ia, 2 – escin Ib, 3 – isoescin Ia, 4 – isoescin Ib.

The extracted amounts of 5-HMF, furfural and 5-MF are presented in Table VI. Furfurals are the main sugar degradation products. Baraldi *et al.* studied chemical composition of seed samples (pure and hybrid) of *Aesculus hippocastanum* found in Italy and they obtained a glucose concentration of 6.8 % and a fructose concentration of 8.4 % in pure seed sample.¹⁸ As can be seen from Table VI, the highest amounts of 5-HMF and furfural were obtained in seed extracts, which is a consequence of higher content of total carbohydrates in seeds than in the other materials. The furfurals are in negligible low content or even not found in the extracts obtained at $150 \text{ }^\circ\text{C}$. The amounts started to increase by inc-

raising the temperature to 200 °C and by increasing the extraction time. At 250 °C, the amounts of 5-HMF and furfural started to decrease with increasing extraction time. For all materials, the amount of 5-HMF reached the maximal value at 250 °C and 5 min (42.60 mg g⁻¹ for seed, 4.52 mg g⁻¹ for bark and 2.90 mg g⁻¹ for seed shell and 0.143 mg g⁻¹ for leaf). In the case of seed, the maximal amount of furfural was 6.34 mg g⁻¹ at 250 °C and 5 min, while in the cases of bark, seed shell and leaf, the amount of furfural reached the maximum at 200 °C and 30 min (7.42, 3.22 and 0.496 mg g⁻¹, respectively). The leaf extracts contained the lowest amount of total carbohydrates and thus they contained significantly lower amounts of 5-HMF and furfural than the other parts of chestnut. 5-Methylfurfural was detected in seed, bark and seed shell extracts. In the case of seed, the amount of 5-methylfurfural increased with extraction temperature and time, while in the case of bark and seed shell, it reached the maximal values at 200 °C and 30 min and then started to decrease at 250 °C.

TABLE V. The amount (mg g⁻¹) of chlorogenic (Y_{Ch}), neochlorogenic (Y_{NCh}) and gallic (Y_{GA}) acids extracted from seed (S), bark (B), seed shell (Sh) and leaves (L)

$T/^\circ\text{C}$	t/min	Parameter					
		Y_{ChB}	Y_{NChS}	Y_{NChB}	Y_{NChSh}	Y_{NChL}	Y_{GAL}
150	5	0.69	0.27	0.34	0.91	0.48	1.57
150	15	0.68	0.30	0.45	1.21	0.55	1.56
150	30	0.61	0.38	0.52	1.36	0.65	1.34
200	5	0.49	0.45	0.88	2.19	0.79	1.10
200	15	0.48	0.53	0.85	2.10	0.77	n.d.
200	30	n.d.	0.56	0.62	1.51	0.54	n.d.
250	5	n.d.	n.d.	0.37	0.58	0.31	n.d.
250	15	n.d.	n.d.	n.d.	0.40	n.d.	n.d.
250	30	n.d.	n.d.	n.d.	n.d.	n.d.	n.d.

TABLE VI. The amount (mg g⁻¹) of extracted 5-HMF (Y_{HMF}), furfural (Y_F) and 5-methylfurfural (Y_{MF}) from seed (S), bark (B), seed shell (Sh) and leaves (L)

$T/^\circ\text{C}$	t/min	Parameter										
		Y_{5-HMFS}	Y_{5-HMFB}	$Y_{5-HMFSh}$	Y_{5-HMFL}	Y_{FS}	Y_{FB}	Y_{FSh}	Y_{FL}	Y_{MFS}	Y_{MFB}	Y_{MFSh}
150	5	n.d.	n.d.	n.d.	n.d.	n.d.	n.d.	n.d.	n.d.	n.d.	n.d.	n.d.
150	15	n.d.	n.d.	n.d.	n.d.	n.d.	n.d.	n.d.	n.d.	n.d.	n.d.	n.d.
150	30	0.16	0.11	n.d.	n.d.	0.41	0.41	n.d.	n.d.	n.d.	n.d.	n.d.
200	5	3.10	0.62	0.24	0.11	0.79	1.03	0.94	0.42	0.42	0.56	0.52
200	15	13.82	1.90	0.69	0.12	2.85	3.48	2.11	0.47	0.72	0.61	0.78
200	30	33.45	4.05	1.95	0.13	5.09	7.42	3.22	0.50	0.83	1.66	0.92
250	5	42.60	4.52	2.90	0.14	6.34	4.31	2.07	0.43	1.11	1.09	0.80
250	15	31.32	3.88	1.96	0.14	4.64	3.36	1.33	0.43	1.30	1.03	0.68
250	30	18.79	2.47	0.99	0.14	3.25	1.95	0.76	0.43	1.38	0.82	0.49

CONCLUSIONS

In the present work it was shown that subcritical water could be a suitable replacement for organic solvents and could be efficiently used as the extraction medium to extract important compounds from horse chestnut parts. Based on the results, it could be concluded that by adjusting the extraction conditions, the extraction of certain compounds could be favored. Namely, the results showed, that higher content of escins, esculin, fraxin, phenolics and carbohydrates were obtained at a lower extraction temperature (150 °C) and time, due to their degradation under rigorous conditions. On the other hand, if the desired compounds are furfurals, subcritical water extraction has to be performed at higher temperatures (200 and 250 °C) and longer times.

Acknowledgement. The authors would like to acknowledge the Slovenian Research Agency (ARRS) for financing this research within the frame of Program P2-0046 (Separation processes and production design).

ИЗВОД

ЕКСТРАКЦИЈА САСТОЈАКА ИЗ ДЕЛОВА ДИВЉЕГ КЕСТЕНА (*Aesculus hippocastanum*)
СУБКРИТИЧНОМ ВОДОМ

TANJA GAGIĆ¹, ŽELJKO KNEZ^{1,2} и MOJCA ŠKERGET¹

¹Laboratory for Separation Processes and Product Design, Faculty of Chemistry and Chemical Engineering, University of Maribor, Smetanova ulica 17, 2000 Maribor, Slovenia u ²Faculty of Medicine, University of Maribor, Taborska ulica 8, 2000 Maribor, Slovenia

Екстракција састојака из делова дивљег кестена (*Aesculus hippocastanum*), као што су плодови, омотач плода, кора и листови, субкритичном водом је изведена у шаржном реактору на температурама од 150, 200 и 250 °C и екстракцијским временима од 5, 15 и 30 min. Добијени екстракти су анализирани методом спектрофотометрије ради одређивања тоталних фенола, угљених хидрата и антиоксидативне активности. Осим тога, детектована једињења у екстрактима, као што су тритерпеноидни сапонини (ескини), кумарински гликозиди (ескулин и фраксин), фенолна једињења (хлорогенска, неохлорогенска и гална киселина) и фурфурали (5-хидрокси метилфурфурал, фурфурал, 5-метилфурфурал) су квантификовани применом HPLC. Велика количина ескина је добијена у екстрактима плода, док су највеће количине ескулина и фраксина добијене у екстрактима коре. Садржај тоталних фенола је био највећи у екстрактима омотача и коре, што имплицира да ти екстракти дају највећу антиоксидативну активност.

(Примљено 11. новембра 2020, ревидирано и прихваћено 18. фебруара 2021)

REFERENCES

1. C. R. Sirtori, *Pharmacol. Res.* **44** (2001) 183 (<http://dx.doi.org/10.1006/phrs.2001.0847>)
2. S. I. Rafiq, S. Singh, D. C. Saxena, *J. Food Meas. Charact.* **10** (2016) 302 (<http://dx.doi.org/10.1007/s11694-016-9307-2>)
3. T. Takahashi, Y. Tsurunaga, W. F. Schmidt, K. Yoshino, *J. Wood Sci.* **63** (2017) 484 (<http://dx.doi.org/10.1007/s10086-017-1649-9>)
4. P. A. De Almeida, M. C. Alves, H. C. Polonini, L. S. Dutra, M. N. Leite, N. R. B. Raposo, A. D. O. Ferreira, M. A. F. Brandão, *Lat. Am. J. Pharm.* **32** (2013) 1082 (http://www.latamjpharm.org/resumenes/32/7/LAJOP_32_7_1_19.pdf)

5. M. Dudek-Makuch, I. Matławska, *Acta Pol. Pharm. - Drug Res.* **70** (2013) 517 (<https://pubmed.ncbi.nlm.nih.gov/23757942/>)
6. H. Kimura, S. Ogawa, A. Sugiyama, M. Jisaka, T. Takeuchi, K. Yokota, *Food Res. Int.* **44** (2011) 121 (<http://dx.doi.org/10.1016/j.foodres.2010.10.052>)
7. S. Jokić, T. Gagić, E. Knez, D. Ubarić, M. Kerget, *Molecules* **23** (2018) (<http://dx.doi.org/10.3390/molecules23061408>)
8. T. Gagić, A. Perva-Uzunalić, Ž. Knez, M. Škerget, *Ind. Eng. Chem. Res.* **57** (2018) (<http://dx.doi.org/10.1021/acs.iecr.8b00332>)
9. S. Jokić, T. Gagić, Ž. Knez, M. Banožić, M. Škerget, *J. Supercrit. Fluids* **153** (2019) 104593 (<http://dx.doi.org/10.1016/j.supflu.2019.104593>)
10. Z. H. M. Abudayeh, K. M. Al Azzam, A. Naddaf, U. V. Karpiuk, V. S. Kislichenko, *Adv. Pharm. Bull.* **5** (2015) 587 (<http://dx.doi.org/10.15171/apb.2015.079>)
11. I. Kapusta, B. Janda, B. Szajwaj, A. Stochmal, S. Piacente, C. Pizza, F. Franceschi, C. Franz, W. Oleszek, *J. Agric. Food Chem.* **55** (2007) 8485 (<http://dx.doi.org/10.1021/jf071709t>)
12. M. Otajagić, S., Pinjić, Dž., Čavar, S. Vidic, D. Maksimović, *Bull. Chem. Technol. Bosnia Herzegovina* (2012) 35 (<https://www.semanticscholar.org/paper/Total-phenolic-content-and-antioxidant-activity-of-Otajagi%C4%87-Pinji%C4%87/71221e61f9b6c99ae23b0d91b3719d32d650f6c8>)
13. H. Kimura, S. Ogawa, T. Ishihara, M. Maruoka, S. Tokuyama-Nakai, M. Jisaka, K. Yokota, *Food Chem.* **228** (2017) 348 (<http://dx.doi.org/10.1016/j.foodchem.2017.01.084>)
14. J. Chen, W. Li, B. Yang, X. Guo, F. S. C. Lee, X. Wang, *Anal. Chim. Acta* **596** (2007) 273 (<http://dx.doi.org/10.1016/j.aca.2007.06.011>)
15. G. Stanić, B. Jurišić, D. Brkić, *Croat. Chem. Acta* **72** (1999) 827 (<https://hrcak.srce.hr/132302>)
16. J. Oszmiański, S. Kalisz, W. Aneta, *Molecules* **19** (2014) 14625 (<http://dx.doi.org/10.3390/molecules190914625>)
17. N. A. Postoyuk, A. A. Markaryan, T. D. Dargaeva, *Glob. J. Pharmacol.* **7** (2013) 321 (<http://dx.doi.org/10.5829/jidosi.gjp.2013.7.3.1109>)
18. C. Baraldi, L. M. Bodecchi, M. Cocchi, C. Durante, G. Ferrari, G. Foca, M. Grandi, A. Marchetti, L. Tassi, A. Ulrici, *Food Chem.* **104** (2007) 229 (<http://dx.doi.org/10.1016/j.foodchem.2006.11.032>)



J. Serb. Chem. Soc. 86 (6) 615–624 (2021)
JSCS–5448

CO oxidation over alumina monolith impregnated with oxides of copper and manganese

THIEN HUU PHAM^{1*}, VIET BANG BUI¹ and HA AN QUOC THAN^{1,2}

¹*Institute of Applied Materials Science, Vietnam Academy of Science and Technology, No 1A TL 29, Thanh Loc Ward, District 12, Ho Chi Minh 700000, Vietnam;* ²*Graduate University of Science and Technology, Vietnam Academy of Science and Technology, 18 Hoang Quoc Viet, Cau Giay, Ha Noi 10072, Vietnam*

(Received 9 May 2020, revised 10 January, accepted 15 January 2021)

Abstract: In this work, simple methods for the preparation of highly efficient heterogeneous nanocatalysts for the low-temperature oxidation of CO are described. The main advantages of the reaction are high yields. The catalysts based on oxides of copper and manganese supported on alumina monoliths were prepared by different methods: plasma corona discharge and wet impregnation. Structure and physical properties of catalysts were characterized by FT-IR, XRD, TEM, EDX and TG/DTA. The results showed that the use of a plasma corona discharge at atmospheric pressure for the preparation of the catalysts resulted in smaller particle size and uniform dispersion when compared with the catalysts prepared by wet impregnation methods. The catalytic activities of these catalysts were investigated for complete oxidation of carbon monoxide (3000 ppm) to carbon dioxide in the air at atmospheric pressure. On a single oxide catalyst, 10CuO/monolith was better than 10MnO₂/monolith under the same experimental conditions. With multi-oxide catalysts, all catalyst samples are more active than a single-oxide catalyst with the same impregnated content. In particular, the catalyst prepared by plasma corona discharge indicates the best oxidation capacity of carbon monoxide.

Keywords: oxidation of carbon monoxide; single-oxide catalysts; multi-oxide catalysts; corona discharge; alumina monolith; wet-impregnation.

INTRODUCTION

Carbon monoxide (CO) is a common contaminant of indoor and outdoor environments. Along with volatile organic compounds (VOCs) and nitrogen oxides (NO_x), CO is one of the main causes of air pollution and affects human health.^{1,2} Therefore, it is especially important to find a solution to CO removal from the air. At present, an effective solution for CO removal is to use a catalytic oxidation technique. In this method, the catalyst plays a key role in the treatment

*Corresponding author. E-mail: thieniams@gmail.com
<https://doi.org/10.2298/JSC200509004P>

efficiency as well as a change in the temperature of the oxidation reaction. Catalysts based on noble metals (Pd, Pt, Rh) exhibit a high activity for CO oxidation.^{3–5} However, the steady increase of noble metal prices, their tendency to sinter and deactivation by carbon formation pushes the development of alternative catalytic technologies and catalytic materials. Recently, studies have turned to catalysts based on transition metals (Cu, Mn, Co, Fe,...). Many studies have shown that catalysts based on Cu, Co and Mn are very efficient for CO oxidation at low temperatures.⁶

A multi-oxide catalyst on a transition metal base has recently been studied and found to be effective for the treatment of VOC and CO emissions.⁷ In these studies, oxidation is affected by the interaction between the active phases of transition metals due to the formation of strange phases during the preparation process. Morales⁸ studied the effect of the copper content in manganese on complete oxidation of ethanol and propane, showing that the addition of a small amount of copper helped prevent manganese oxide from entering the crystal structure, increases the formation of voids and the presence of $\text{Cu}_{1.5}\text{Mn}_{1.5}\text{O}_4$ phase and increases their reduction ability, thus achieving better catalytic performance in ethanol combustion.

Many factors influence the properties of the catalyst, of which one of the most important is the catalyst preparation method. With this in mind, various methods, such as wet-impregnation (WI),⁹ deposition-precipitation (DP)¹⁰ and atmospheric plasma discharge, have been investigated.^{11–13} Recently, one of the current catalytic preparation methods of interest has been corona plasma discharge at atmospheric pressure. Many reports show that the use of a plasma helps affect a significant rise in catalytic activity and a small particle size-dispersion is achieved compared to the other conventional methods.

This work was aimed at examining the influence of different preparation methods on the catalyst performance based on alumina monoliths impregnated with oxides of copper and manganese. Furthermore, the catalytic activities of these catalysts were investigated for complete oxidation of carbon monoxide in the air at atmospheric pressure.

EXPERIMENTAL

Chemicals

$\text{Cu}(\text{NO}_3)_2 \cdot 3\text{H}_2\text{O}$ (>99.5 %, Sigma Aldrich), $\text{Mn}(\text{NO}_3)_2$ (99 %, Sigma Aldrich), and alumina monoliths with a cell density of 62 cells cm^{-2} – Nanxiang-Jiangxi, China. All the chemicals were used without further purification.

Catalysts preparation

The catalysts with 10 wt. % metal loading (5 wt. % Cu and 5 wt. % Mn) were prepared by different methods: wet-impregnation (WI) and non-thermal plasma (NTP).

WI method. The alumina monoliths was the first impregnated with a solution of $\text{Cu}(\text{NO}_3)_2 \cdot 3\text{H}_2\text{O}$ and/or $\text{Mn}(\text{NO}_3)_2$. After evaporating under vacuum at 353 K, the sample

was dried at 383 K for 12 h and heated at 773 K for 5 h in air with a heating rate of 276 K min^{-1} . These samples were denoted as 10CuO/Monolith, 10MnO₂/Monolith and 5CuO–5MnO₂/Monolith, respectively.

NTP method. The non-thermal plasma technique used for this preparation was corona discharge as Fig. 1. This process is similar to the WI method. However, after evaporating under vacuum at 353 K, the sample was dried at 383 K for 12 h. The precursor was placed in the corona plasma discharge region using a cylindrical quartz tube located and centered on the holder base plate, which consisted of a continuous flow air supplying the system. The corona plasma discharge reactor was powered by a homemade high voltage direct current generator: 18 kV and 1.5 kHz. The sample was denoted as 5CuO–5MnO₂/Monolith (Plasma).

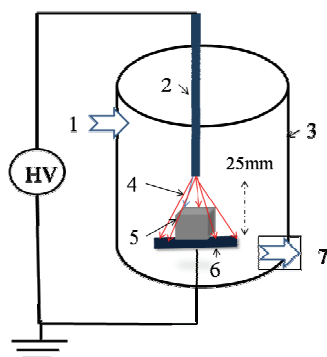


Fig. 1. The schematic diagram of the corona plasma discharge system; 1 – feed-gas system; 2 – needle electrodes; 3 – quartz tube; 4 – corona plasma discharge region; 5 – catalyst samples; 6 – plate electrode; 7 – air outlet (gas-outlet).

Catalyst characterization

Physicochemical characterization of the prepared catalyst was performed by different modern techniques such as Fourier transform infrared (FT-IR), X-ray diffraction (XRD), transmission electron microscopy (TEM), energy-dispersive X-ray (EDX) and thermogravimetric and differential thermal analysis (TG/DTA). In particular, the FT-IR spectra were measured at spectral resolution 4 cm^{-1} between 4000–400 cm^{-1} range using a Perkin Elmer Frontier 1600 series spectroscope. XRD patterns of the catalyst materials were recorded with D8 Advance-Bruker D5005 diffractometer using monochromatic high-intensity CuK α radiation ($\lambda = 0.15418$ nm) at the scanning rate of 0.03° s^{-1} in the scanning range from 20 to 80°. TEM images were taken with a JEOL JEM-1010 (Japan) at an acceleration voltage of 200 kV. The EDX analysis with 20 kV accelerated voltage was realized with EDX-8000. Finally, the simultaneous thermal analysis (TG/DTA) of the after dried samples was performed in a Q500 TA-Instruments apparatus under atmospheric pressure at a heating rate of 283 K min^{-1} , from 303 to 1073 K under a dynamic (50 mL/min) nitrogen atmosphere.

Catalytic performance

Catalytic properties of the studied samples for CO total oxidation in air were tested under the following conditions: The total flow was 450 mL min^{-1} at a volume rate (GVSH) of 5000 h^{-1} . The initial concentration of CO was fixed at 3000 ppm. The CO concentration in the reaction was analyzed *in situ* by Testo 320 LX (0563 6032 72 (Germany) and then re-analyzed by GC Clarus device (USA), a column packed with ZV-95, length 3 m, diameter 5.8 mm.

RESULTS AND DISCUSSION

X-Ray diffraction diagram (XRD)

The X-ray diffraction (XRD) patterns of the catalysts are shown in Fig. 2.

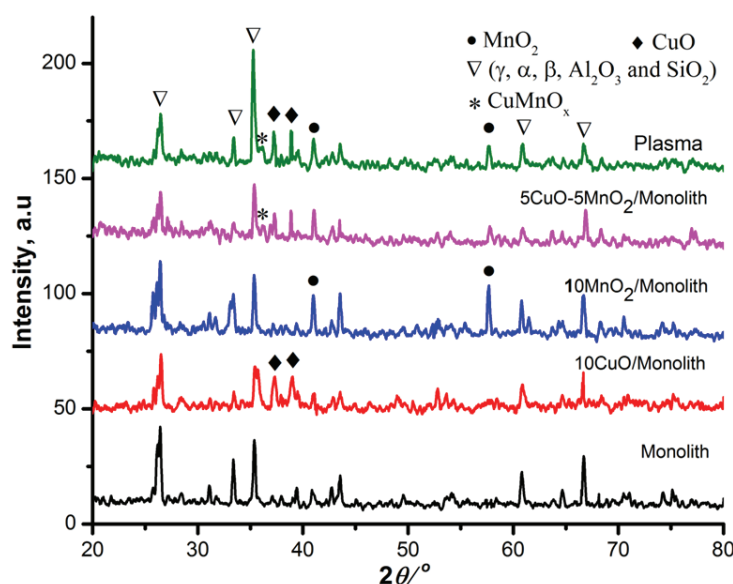


Fig. 2. The X-ray diffraction (XRD) patterns of the catalysts.

As indicated in Fig. 2, the main components of the alumina monolith substrate were α -Al₂O₃, β -Al₂O₃, γ -Al₂O₃ and SiO₂ with specific diffraction signals at 2θ 25.9, 33.6 and 36.1°. On the single-oxide catalysts, the copper-based catalysts have typical diffraction signals of the CuO phase (2θ 35.7 and 38.8°, JCPDS 80-1268). On the manganese-based catalyst, the characteristic diffraction signals are those of the MnO₂ phase (2θ 41.1, 44.7 and 57.7°, JCPDS 44-0141). On multi-oxide catalysts, besides the diffraction signals of CuO and MnO₂ phases, on the X-ray diffraction diagram also appear a diffraction signal of weak intensity of the CuMnO_x phase (2θ = 37.2°). These results are similar to those of Dey.¹⁴ Compared with the catalysts prepared by the wet-impregnation method, in the diffraction pattern of 5CuO–5MnO₂/Monolith-corona (Plasma) appeared narrow high intensity peaks of CuO and MnO₂. This difference could be explained by the interaction of the reactive species produced by plasma discharges, such as O[•], N[•], NO[•], OH[•], O₃ and H₂O₂, with the catalyst sample in the preparation process led to changes in the phase structure properties.

Fourier transform infrared spectrum (FT-IR)

The FT-IR spectra of the samples are shown in Fig. 3.

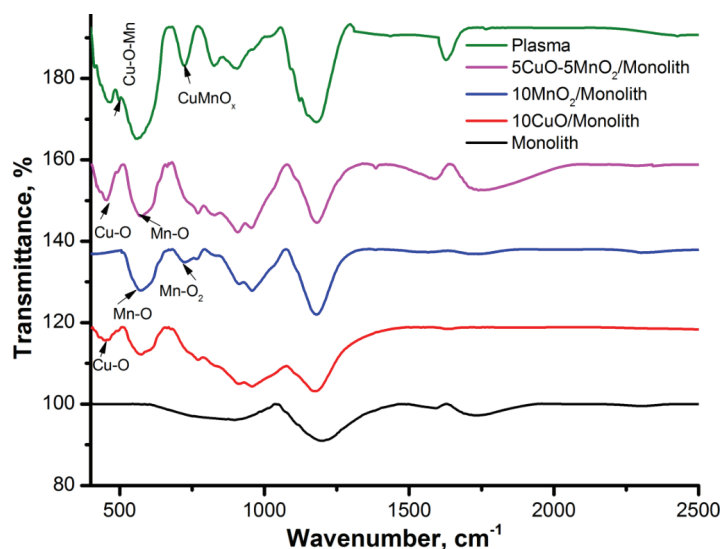


Fig. 3. FT-IR spectra of the catalysts.

According to the results in Fig. 3, the absorption peaks due to Cu–O bonds in the CuO phase structure are found in the region 420 to 500 cm^{-1} for $10\text{CuO}/\text{Monolith}$ catalyst. This result is similar to the studies by Dubal *et al.*¹⁵ This shows that the CuO phase was successfully impregnated on alumina monolith. In the spectra of the $10\text{MnO}_2/\text{Monolith}$ catalyst, characteristic vibrations of Mn–O bonds are found at 535 and 690 cm^{-1} for the MnO_2 phase. This result is also in agreement with the studies of Aghazadeh.¹⁶ In multi-oxide catalysts case, all catalysts also indicated typical vibrations of CuO and MnO_2 phases impregnated on alumina monolith.

Transmission electron microscopy (TEM)

Typical TEM results for the catalysts are shown in Fig. 4.

According to the TEM images, both catalysts possessed spherical morphology ($<50\text{ nm}$). Fig. 4a and b show the presence of CuO and MnO_2 phases impregnated on the alumina monolith for both single-oxide catalysts with particle sizes ranging from 30 – 50 nm . In addition, the results also show a fairly even dispersion of these active phases on the supports. On a multi-oxide catalyst (Fig. 4c), the size of the active phase and the dispersion are similar to the single-oxide catalyst. However, with multi-oxide catalysts prepared by plasma discharge technique indicate a different surface morphology. High dispersion and small active particle size (10 – 20 nm) were found for this catalyst (Fig. 4d). This suggests that the use of plasma discharges during the preparation process drastically changed the catalytic properties leading to increased catalytic oxidation.

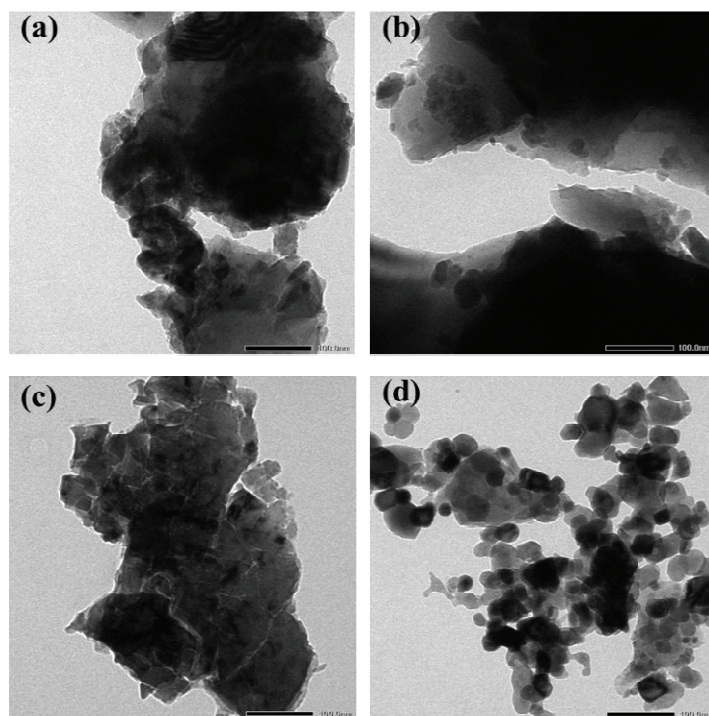


Fig. 4. TEM images of 10CuO/Monolith (a), 10MnO₂/monolith (b), 5CuO–5MnO₂/Monolith (c) and 5CuO–5MnO₂/Monolith (Plasma) (d).

Besides, to test the impregnation of Cu and Mn metals onto monolith, EDX analysis method used to determine metal content in the monolith (Fig. 5 and Table I). The results indicated the presence of elemental Cu and Mn in the 5CuO–5MnO₂/Monolith (Plasma). It could be concluded that the impregnation of the active phase on support by the non-thermal plasma technique was successful.

Thermogravimetric and differential thermal analysis (TG/DTA)

The TG/DTA analysis of the samples showed a major mass loss of about 11 % in the range of 303 to 1073 K, which was due to the elimination of the majority of the nitrate compounds (Fig b). The first mass loss step in the TGA plot occurred between 273–393 K, corresponding to the weak endothermic peak in the DTA curve at 343 K, which was caused by dehydration. In the last mass loss step, a drastic weight loss at 473–573 K resulted from the combustion of nitrate compounds and NO_x formation *via* the decomposition of nitrate compounds as suggested by the exothermic peak around 508 and 528 K in the DTA curve. No further mass loss occurred above 573 K, indicating completion of combustion and the formation of the expected oxide CuO–MnO₂ phase.

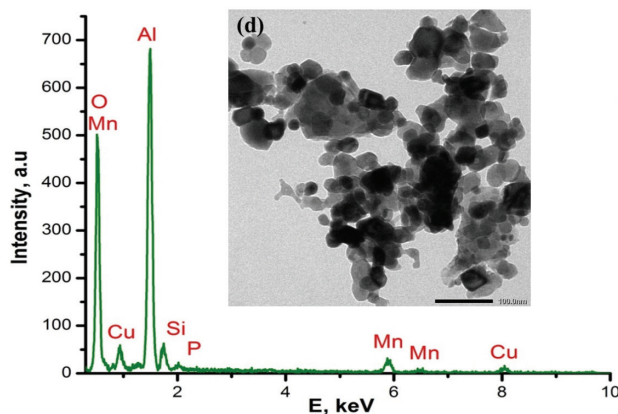


Fig. 5. EDX analysis of the 5CuO–5MnO₂/Monolith (Plasma) catalyst.

TABLE I. Elemental composition analysis of 5CuO–5MnO₂/Monolith (Plasma) catalyst

Element	Amount, wt. %	Amount, at. %
O	48.34	62.28
Al	32.75	26.98
Si	4.98	5.70
P	0.59	0.39
Mn	6.29	2.36
Cu	7.05	2.29
Total	100.00	—

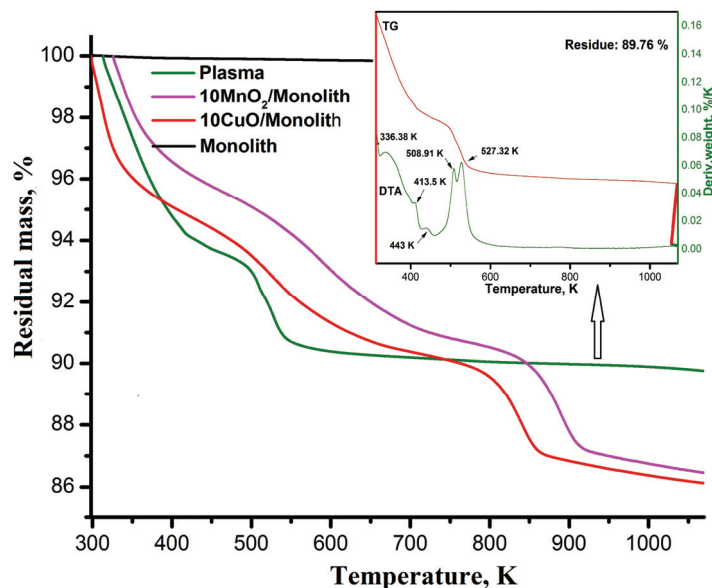


Fig. 6. TG/DTA analysis of the catalysts.

Catalytic activity for complete oxidation of CO

The complete oxidation of CO to CO₂ was performed over various catalysts according to temperature. The conversion of CO according to temperature over the catalysts is shown in Fig. 7.

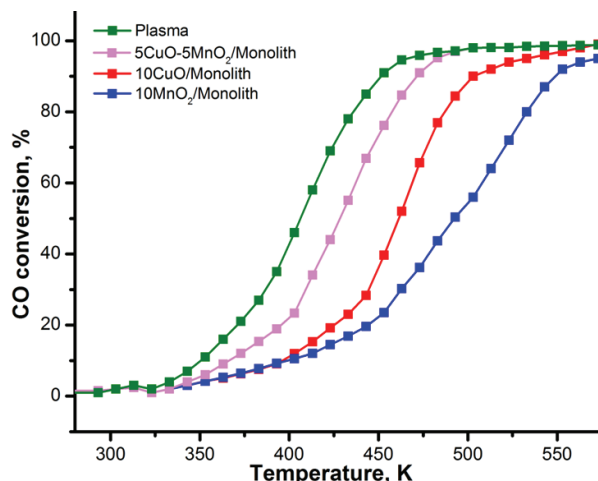


Fig. 7. CO conversion over the different catalysts according to temperature.

The results indicated that complete oxidation of CO (>98 % conversion) was achieved at temperatures above 503 K for both multi-oxide catalysts. Whereas, the conversion was only 90 % for single oxide 10CuO/Monolith catalyst and 56 % conversion for 10MnO₂/Monolith catalyst.

A comparison of the activity of the catalysts in different temperature ranges is also presented in Table II.

TABLE II. Conversion of CO (%) at different temperatures and over different catalysts

Catalyst	Temperature, K		
	373	423	573
10CuO/Monolith	6.3	19.2	99.0
10MnO ₂ /Monolith	6.4	14.5	95.0
5CuO-5MnO ₂ /Monolith	12.1	44.1	98.7
5CuO-5MnO ₂ /Monolith (Plasma)	21.2	69.3	98.8

At 373 K, the difference in CO treatment efficiency of the four catalysts is negligible. As the temperature increased, the catalyst conversion rates began to diverge. At 423 K, the 5CuO-5MnO₂/Monolith (Plasma) catalyst yielded 1.6 times higher conversion than the 5CuO-5MnO₂/Monolith catalyst, 3.6 times higher than 10CuO/Monolith and 4.8 higher than 10MnO₂/Monolith. When the reaction temperature reached 573 K, total oxidation of CO was obtained for all

catalysts. These results could be explained by the 5CuO–5MnO₂/Monolith (Plasma) catalyst treated by the plasma discharge caused CuO–MnO₂ particles to disperse highly and evenly on the surface of the alumina monolith as nanoparticles. This would increase the interaction with CO in the reaction. Besides, the increase in activity is also due to the appearance of a new active phase CuMnO_x from the interaction between the oxides of copper and manganese.

The catalytic activity for CO oxidation is shown in the following order: 5CuO–5MnO₂/Monolith (Plasma) catalyst > 5CuO–5MnO₂/Monolith catalyst > 10CuO/Monolith > 10MnO₂/Monolith.

In general, the intervention of plasma discharge during the preparation process changed the catalytic properties leading to high treatment efficiency for CO removal. In summary, the 5CuO–5MnO₂/Monolith (Plasma) catalyst shows an efficient oxidation of CO at lower temperatures than the other studied cases.

CONCLUSIONS

First, single-oxide and multi-oxide catalysts based on copper and manganese-impregnated on alumina monolith were successfully prepared by two different methods. The results indicate that the differences in the preparation methods play an important role in the determination of the physicochemical properties as well as the oxidative activities of the catalysts. Secondly, on a single oxide catalyst, the 10CuO/Monolith sample was better than a 10MnO₂/Monolith sample. With multi-oxide catalysts, all catalyst samples are more active than single-oxide catalysts at the same impregnated content. Finally, the catalyst prepared by the plasma discharge method showed the best oxidation of CO capacity when compared with the catalysts prepared by the wet-impregnation method under the same experimental conditions.

Acknowledgment. This research was funded by the Vietnam National Foundation for Science and Technology Development (NAFOSTED, Grant No. 103.99-2016.67).

ИЗВОД

ОКСИДАЦИЈА УГЉЕН-МОНОКСИДА НА МОНОЛИТИМА ГЛИНИЦЕ ИМПРЕГНИСАНИМ ОКСИДИМА БАКРА И МАНГАНА

THIEN HUU PHAM¹, VIET BANG BUI¹ и НА AN QUOC THAN^{1,2}

¹*Institute of Applied Materials Science, Vietnam Academy of Science and Technology, No 1A TL 29, Thanh Loc Ward, District 12, Ho Chi Minh 700000, Vietnam* и ²*Graduate University of Science and Technology, Vietnam Academy of Science and Technology, 18 Hoang Quoc Viet, Cau Giay, Ha Noi 10072, Vietnam*

У овом раду описани су припрема и перформансе катализатора, користећи једноставну методу и високо ефикасан хетерогени нанокатализатор. Главна предност реакције су високи приноси оксидације СО на ниској температури. Катализатори на бази оксида бакра и мангана на монолитној глиници као носачу припремљени су различитим методама: корона пражењем у плазми и мокром импрегнацијом. Структура и физичка својства катализатора окарактерисани су FT-IR, XRD, TEM, EDX и TG/DTA методама. Резултати су показали да коришћење корона пражења у плазми, при атмосферском притиску, у процесу припреме катализатора даје мању величину честица и равномер-

нију дисперзију у поређењу са катализаторима припремљеним методама влажне импрегнације. Каталитичке активности ових катализатора су испитане за потпуну оксидацију угљен-моноксида (3000 ppm) у угљен-диоксид у ваздуху, при атмосферском притиску. При поређењу појединачних оксидних катализатора, 10CuO/монолит је био ефикаснији од 10MnO₂/монолита у при истим експерименталним условима. Код мултиоксидних катализатора, сви узорци катализатора су активнији од монооксидног катализатора у истом импрегнираном садржају. Конкретно, катализатор припремљен корона пражњењем у плазми показује најбољи оксидациони капацитет угљен-моноксида (CO).

(Примљено 9. маја 2020, ревидирано 10. јануара, прихваћено 15. јануара 2021)

REFERENCES

1. H. Kinoshita, H. Türkan, S. Vucinic, S. Naqvi, R. Bedair, R. Rezaee, A. Tsatsakis, *Toxicol. Rep.* **7** (2020) 169 (<https://doi.org/10.1016/j.toxrep.2020.01.005>)
2. R. J. Levy, *Neurotoxicol. Teratol.* **49** (2015) 31 (<https://doi.org/10.1016/j.ntt.2015.03.001>)
3. J. Xu, T. White, P. Li, C. He, J. Yu, W. Yuan. Y.-F. Han, *J. Am. Chem. Soc.* **132** (2010) 10398 (<https://doi.org/10.1021/ja102617r>)
4. A. S. Ivanova, E. M. Slavinskaya, R. V. Gulyaev, V. I. Zaikovskii, O. A. Stonkus, I. G. Danilova, L. M. Plyasova, I. A. Polukhin, A. I. Boronin, *Appl. Catal. B: Environ.* **97** (2010) 57 (<https://doi.org/10.1016/j.apcatb.2010.03.024>)
5. H. Huang, D. Y. C. Leung, D. Ye, *J. Mater. Chem.* **21** (2011) 9647 (<https://doi.org/10.1039/C1JM10413F>)
6. Y. Lang, J. Zhang, Z. Feng, X. Liu, Y. Zhu, T. Zeng, Y. Zhao, R. Chen, B. Shan, *Catal. Sci. Technol.* **8** (2018) 5490 (<https://doi.org/10.1039/C8CY01263F>)
7. D. A. Aguilera, A. Perez, R. Molina, S. Moreno, *Appl. Catal., B* **104** (2011) 144 (<https://doi.org/10.1016/j.apcatb.2011.02.019>)
8. M. R. Morales, B. P. Barbero, L. E. Cadús, *Fuel* **87** (2008) 1177 (<https://doi.org/10.1016/j.fuel.2007.07.015>)
9. P. W. Park, J. S. Ledford, *Appl. Catal., B* **15** (1998) 221 ([https://doi.org/10.1016/S0926-3373\(98\)80008-8](https://doi.org/10.1016/S0926-3373(98)80008-8))
10. K. Y. Koo, U. H. Jung, W. L. Yoon, *Int. J. Hydrogen Energy* **39** (2014) 5696 (<https://doi.org/10.1016/j.ijhydene.2014.01.128>)
11. Z.-H. Li, S.-H. Tian, H.-T. Wan, H.-B. Tian, *J. Mol. Catal., A* **211** (2004) 149 (<https://doi.org/10.1016/j.molcata.2003.10.003>)
12. W. Hua, L. Jin, X. He, J. Liu, H. Hu, *Catal. Commun.* **11** (2010) 968 (<https://doi.org/10.1016/j.catcom.2010.04.007>)
13. M. H. Chen, W. Chu, X. Y. Dai, X. W. Zhang, *Catal. Today* **89** (2004) 201 (<https://doi.org/10.1016/j.cattod.2003.11.027>)
14. S. Dey, G. C. Dhal, D. Mohan, R. Prasad, *Bull. Chem. React. Eng. Catal.* **12** (2017) 437 (<https://doi.org/10.9767/bcrec.12.3.900.437-451>)
15. D. P. Dubal, G. S. Gund, C. D. Lokhande, R. Holze, *Mat. Res. Bull.* **48** (2013) 923 (<https://doi.org/10.1016/j.materresbull.2012.11.081>)
16. M. Aghazadeh, M. Asadi, M. G. Maragheh, M. R. Ganjali, P. Norouzi, F. Faridbod, *App. Surf. Sci.* **364** (2016) 726 (<https://doi.org/10.1016/j.apsusc.2015.12.227>).